# SPECTROSCOPIC INVESTIGATION OF COPPER-CONTAINING ENZYMES USING LIGANDS THAT BIND TO THE CU(I) STATE OF THE METAL CENTERS

Francis C. Rhames
B.A., Kalamazoo College, 1992

A dissertation submitted to the faculty of the
Oregon Graduate Institute of Science and Technology
in partial fulfillment of the
requirements for the degree
Doctor of Philosophy
in
Biochemistry and Molecular Biology

February 2001

The dissertation "Spectroscopic Investigation of Copper-Containing Enzymes Using Ligands That Bind to the Cu(I) State of the Metal Centers" by Francis C. Rhames has been examined and approved by the following Examination Committee:

Ninian J. Blackburn, Advisor
Professor

Thomas M. Loehr
Professor

James W. Whittaker
Associate Professor

Svetlana Lutsenko
Assistant Professor
Oregon Health Sciences University

## ACKNOWLEDGMENTS

There are many people to thank who have helped me in completing my doctorate degree. I would like to start by thanking my advisor, Ninian Blackburn, who was centermost in guiding me through my exodus. He allowed me to explore my capabilities through independent trials and errors. Furthermore, by working under him, I was able to tap into some of the immense fundamental knowledge of enzyme structure and function that he had to offer. I would also like to thank everyone with whom I have had the opportunity to work, including (but not limited to) Martina Ralle, Shula Jaron, Jay Stasser, John Boswell, and Kaitlin Grammer. I would also like to thank Thomas Loehr, Jim Whittaker, and Svetlana Lutsenko for serving on my thesis committee. Also, special thanks go out to Joann Sanders-Loehr and Thomas Loehr for inviting me to attend OGI and learn what the department had to offer. I would also like to extend thanks to Ed Green for giving me some diversions during my studies there. The final people at OGI to whom I owe thanks are Nancy Christie and Terrie Hadfield, whose administrative assistance and thesis formatting guidance has helped me not to become lost on the way to completion of my final product.

Finally, I would like to express my gratitude to my family and especially to my wife, Jody, who has been there from the beginning, many years ago.

## TABLE OF CONTENTS

ACKNOWLEDGMENTS . . . . . iii
TABLE OF CONTENTS . . . . . iv
LIST OF TABLES . . . . . viii
LIST OF FIGURES . . . . . ix
LIST OF SCHEMES . . . . . xii
ABSTRACT . . . . . xiii

**CHAPTER 1:** AN INTRODUCTION TO COPPER-CONTAINING ENZYMES . 1
1.1 Oxygen Chemistry . . . . . 1
1.2 Metalloproteins . . . . . 2
1.2.1 Copper Proteins . . . . . 3
1.2.2 T1 Copper Centers . . . . . 3
1.2.3 T2 Copper Proteins . . . . . 5
1.2.4 T3 Copper Proteins . . . . . 5
1.2.5 Hemocyanin . . . . . 8
1.2.6 Deoxyhemocyanin . . . . . 8
1.2.7 Oxyhemocyanin Structure . . . . . 10
1.3 Peptidylglycine $\alpha$-Amidating Monooxygenase . . . . . 10
1.4 Background on Dopamine $\beta$-Monooxygenase . . . . . 22
1.5 Homology between PHM and D$\beta$M . . . . . 33
1.6 Goals . . . . . 35

**CHAPTER 2:** METHODS FOR SPECTROSCOPY, ENZYME EXPRESSION, GROWTH, PURIFICATION, AND COPPER RECONSTITUTION . . . . . 37
2.1 Spectroscopic Methods . . . . . 37

2.1.1 Infrared Spectroscopy . . . . . 37
2.1.2 Electron Paramagnetic Spectroscopy (EPR) . . . . . 37
2.1.3 X-ray Absorption Spectroscopy (XAS) . . . . . 39
2.2 Cell Growth . . . . . 42
2.2.1 Preparation of Medium for Cell Culture . . . . . 42
2.2.2 Cell Lines and Cell Growth . . . . . 42
2.3 Purification Protocol for PHMcc . . . . . 43
2.3.1 Chromatography . . . . . 43
2.3.2 Enzyme Assay . . . . . 47
2.3.3 Determination of Copper and Protein Concentrations . . . . . 48
2.4 Copper Reconstitution . . . . . 48
2.4.1 Gel Filtration . . . . . 49
2.4.2 EPR Analysis of Copper Reconstitution . . . . . 52
2.4.3 EPR Titrations of Copper Binding . . . . . 57
2.5 Conclusions . . . . . 59

**CHAPTER 3:** ISOCYANIDE BINDING TO WILD-TYPE PHMcc . . . . . 60
3.1 Introduction . . . . . 60
3.2 Experimental Methods . . . . . 61
3.2.1 Cell Growth/Enzyme Isolation/Activity Measurement/Copper Reconstitution . . . . . 61
3.2.2 Isocyanide Titration . . . . . 61
3.2.3 Fourier Transform Infrared (FTIR) Measurements . . . . . 61
3.2.4 X-ray Absorption (XAS) Sample Preparation . . . . . 63
3.2.5 XAS Data Collection and Analysis . . . . . 63
3.3 Results . . . . . 65
3.3.1 DIMPI Binding to Wild-type Enzyme . . . . . 65
3.3.2 Isopropyl Isocyanide Binding to Copper . . . . . 65
3.3.3 XAS Analysis of DIMPI Bound to PHMcc . . . . . 71
3.4 Discussion . . . . . 74
3.5 Conclusions . . . . . 81

**CHAPTER 4:** ISOCYANIDE LIGATION TO MUTANT FORMS OF PHMcc . 82
4.1 Introduction . . . . . 82
4.2 Experimental Methods . . . . . 83
4.2.1 Cell Growth/Enzyme Isolation . . . . . 83
4.2.2 Isocyanide Titration . . . . . 83
4.2.3 Fourier Transform Infrared (FTIR) Measurements . . . . . 84
4.3 Results . . . . . 84
4.3.1 Copper Reconstitution . . . . . 84
4.3.2 EPR Spectra of Each Mutant . . . . . 86
4.3.3 FTIR of $Cu_A$ Active Site Mutants . . . . . 86
4.3.4 FTIR of $Cu_B$ Active Site Mutants . . . . . 97
4.4 Discussion . . . . . 103
4.4.1 Copper Binding to the Mutants in the Oxidized and Reduced State 103
4.4.2 Analysis of His107/108Ala Isocyanide Complexes . . . . . 110
4.4.3 Analysis of the $Cu_B$ Depleted Mutants with Isocyanide Present . . 112
4.4.4 FTIR Analysis of Bound Isocyanide to His172Ala . . . . . 116
4.5 Conclusions . . . . . 118

**CHAPTER 5:** CARBON MONOXIDE BINDING TO HEMOCYANIN . . . . . 119
5.1 Introduction . . . . . 119
5.2 Experimental Methods . . . . . 120
5.2.1 Isolation of Hemocyanin . . . . . 120
5.2.2 Determination of Copper and Protein Concentrations . . . . . 121
5.2.3 Preparation of Half-Apo Hemocyanin . . . . . 121
5.2.4 Preparation of Carbonylated Species . . . . . 122
5.2.5 Data Collection and Analysis . . . . . 122
5.3 Results/Discussion . . . . . 122
5.3.1 Measurement of the Amount of Copper Removed via $CN^-$ Dialysis 122
5.3.2 Fully Metallated CO-Hc . . . . . 123
5.3.3 Characterization of Half-Apo $^{12}$CO-Hc . . . . . 128
5.3.4 Half-Apo $^{13}$CO-Hc IR Spectrum . . . . . 128

5.3.5 Peak Heights and Half-Widths . . . . . 128
5.3.6 Half-Apo $^{13}$CO–Hc IR Spectrum . . . . . 133
5.4 Conclusions . . . . . 133

**CHAPTER 6:** CONCLUSIONS . . . . . 134

LITERATURE CITED . . . . . 136
BIOGRAPHICAL SKETCH . . . . . 144

## LIST OF TABLES


1.1 Metal-to-Ligand Distances in DβM and PHMcc . . . . . 36

3.1 Peak Frequencies and Widths for DIMPI and IPI Bound to PHMcc . . . . . 68

3.2 Parameters Used to Simulate the EXAFS and Fourier Transform of Reduced PHMcc Reacted with 0.5 mol Equivalents of DIMPI per Copper . . . . . 73

4.1 Copper-to-Protein Ratios for Each Mutant . . . . . 85

4.2 DIMPI-Cu(I) Frequencies for Each Mutant . . . . . 92

4.3 IPI-Cu(I) Frequencies for Each Mutant . . . . . 93

5.1 Carbon Monoxide Stretching Frequencies and Peak Widths for the Hemocyanin Complexes . . . . . 125

## LIST OF FIGURES


1.1 Comparison of spectral features for T1 and T2 copper proteins . . . . . 4

1.2 Active site crystal structure for poplar plastocyanin T1 copper center showing the amino acid residues ligated to the copper atom . . . . . 6

1.3 Active site crystal structure for galactose oxidase . . . . . 7

1.4 Crystal structure of *Limulus polyphemus* subunit II showing all three domains . . . . . 9

1.5 Crystal structure of deoxyhemocyanin and oxyhemocyanin active site structure . . . . . 11

1.6 Reaction catalyzed by the bifunctional enzyme PAM and the reactions catalyzed by the two enzymes that comprise PAM . . . . . 13

1.7 Molecular forms of PAM showing different cleavage points . . . . . 14

1.8 Crystal structure of PHMcc showing the location of the active site pocket . 16

1.9 Crystal structure of the active site of Cu(II) form of PHMcc . . . . . 18

1.10 PHMcc structure with peptide bound . . . . . 19

1.11 D$\beta$M catalyzed reaction . . . . . 23

1.12 Proposed active site structures for the oxidized and reduced D$\beta$M . . . . . 24

1.13 General kinetic mechanism for D$\beta$M . . . . . 26

1.14 Steady-state kinetic mechanism for D$\beta$M . . . . . 27

1.15 The structure of 2,6-dimethylphenyl isocyanide (DIMPI) . . . . . 29

1.16 IR absorbance of DIMPI bound to D$\beta$M, showing the progression of mono-isocyanide complex conversion to the tris-isocyanide complex as the dialysis time increased . . . . . 30

1.17 Titration of D$\beta$M with stoichiometric amounts of DIMPI . . . . . 31

1.18 The titration of DIMPI against hemocyanin showing the conversion of the 2148 $cm^{-1}$ band into the 2160 $cm^{-1}$ species as the concentration of DIMPI increased . . . . . 32

1.19 IR titration of model complex with DIMPI; spectrum of tris-DIMPI Cu(I) perchlorate; Raman titration of model compound with DIMPI . . . . 34
2.1 Infrared energy diagram . . . . . 38
2.2 EPR energy diagram . . . . . 40
2.3 An example of an XAS spectrum . . . . . 41
2.4 A typical gel filtration chromatogram for PHMcc . . . . . 45
2.5 A typical HIC chromatogram for PHMcc . . . . . 46
2.6 Plot of the Cu/PHMcc ratio versus the amount of background $Cu^{2+}$ added to the phosphate buffer used in the reconstitution by gel chromatography . . . . . 50
2.7 Plot of the Cu/PHMcc ratio versus the amount of background $Cu^{2+}$ added to the phosphate buffer used in the Amicon reconstitution study . . . 51
2.8 Plot of the Cu/PHMcc ratio versus the amount of background $Cu^{2+}$ added to the phosphate buffer used in the dialysis reconstitution study . . . 53
2.9 EPR spectrum of PHMcc reconstituted to 1.6 Cu/protein via gel chromatography . . . . . 54
2.10 EPR spectrum of PHMcc reconstituted to 1.6 Cu/protein via dialysis . . . . 55
2.11 Comparison of the EPR signals generated by three different reconstitution methods . . . . . 56
2.12 EPR spectrum of PHMcc titrated with $^{63}Cu^{2+}$ . . . . . 58
3.1 The structures of 2,6-dimethylphenyl isocyanide (DIMPI) and isopropyl isocyanide (IPI) . . . . . 62
3.2 IR spectra of the titration of DIMPI with PHMcc . . . . . 66
3.3 Spectral fitting of the titration of DIMPI to Cu(I) . . . . . 67
3.4 IR spectra of the titration of IPI with PHMcc . . . . . 69
3.5 Spectral simulation of the IR spectra of the titration of IPI with PHMcc . . 70
3.6 Fourier transform and EXAFS of DIMPI bound to PHMcc . . . . . 72
3.7 Modeling of DIMPI bound to the active site of PHMcc . . . . . 78
3.8 Modeling of IPI bound to the active site of PHMcc . . . . . 80
4.1 EPR of mutants and wild-type PHMcc after reconstitution by dialysis . . . 87
4.2 Comparison of the EPR signal from His107/108Ala and wild-type PHMcc 88

4.3 IR spectrum of the titration of DIMPI with His172Ala . . . . . 89
4.4 Spectral simulation of the IR spectrum from the titration of DIMPI with His172Ala . . . . . 91
4.5 IR spectrum of the titration of IPI with His172Ala . . . . . 94
4.6 IR spectra of the titration of DIMPI against His107/108Ala . . . . . 95
4.7 Spectral simulation of the IR spectrum from the titration of DIMPI with His107/108Ala . . . . . 96
4.8 IR spectra of the titration of IPI against His107/108Ala . . . . . 98
4.9 Spectral simulation of the IR spectrum from the titration of IPI with His107/108Ala . . . . . 99
4.10 IR spectra of the titration of DIMPI against His242Ala . . . . . 100
4.11 Spectral simulation of the IR spectrum from the titration of DIMPI with His242Ala . . . . . 101
4.12 IR spectra of the titration of DIMPI against Met314Ile . . . . . 102
4.13 Spectral simulation of the IR spectrum from the titration of DIMPI with Met314Ile . . . . . 104
4.14 IR spectra of the titration of IPI against Met314Ile . . . . . 105
4.15 Spectral simulation of the IR spectrum from the titration of IPI with Met314Ile . . . . . 106
4.16 IR spectra of the titration of IPI against His242Ala . . . . . 107
4.17 Spectral simulation of the IR spectrum from the titration of IPI with His242Ala . . . . . 108
5.1 IR spectra of $^{12}$CO-Hc complex (A). Spectral simulation of $^{12}$CO-Hc (B) 124
5.2 IR spectra of $^{13}$CO-Hc complex (A). Spectral simulation of $^{13}$CO-Hc (B) 126
5.3 Difference spectrum of $^{12}$CO-Hc subtracted from $^{13}$CO-Hc . . . . . 127
5.4 IR spectra of $^{12}$CO-Hc complex (A). Spectrum of the half-apo $^{12}$CO-Hc complex (B). Spectral simulation of the half-apo $^{12}$CO-Hc complex (C) . 129
5.5 IR spectra of $^{13}$CO-Hc complex (A). Spectrum of the half-apo $^{13}$CO-Hc complex (B). Spectral simulation of the half-apo $^{13}$CO-Hc complex (C) . 130

## LIST OF SCHEMES


1.1 Proposed mechanism for monooxygenation by PHMcc . . . . . 20

3.1 Proposed ligation of isocyanide to PHMcc . . . . . 76

4.1 Predicted isocyanide ligation to His107/108Ala . . . . . 111

4.2 Predicted isocyanide ligation to His242Ala . . . . . 114

4.3 Predicted isocyanide ligation to Met314Ile . . . . . 115

4.4 Predicted isocyanide ligation to His172Ala . . . . . 117

5.1 Proposed ligation of CO to Hc before and after cyanide dialysis . . . . . 132

# Abstract

**Spectroscopic Investigation of Copper-Containing Enzymes Using Ligands That Bind to the Cu(I) State of the Metal Centers**

Francis C. Rhames

Ph.D., Oregon Graduate Institute of Science and Technology

February 2001

Thesis Advisor: Dr. Ninian J. Blackburn

The use of ligands directed towards the reduced copper centers in PHMcc and hemocyanin has provided valuable spectroscopic information concerning these two proteins. Ligation of isocyanides to the Cu(I) center in PHMcc has shown that there exist significant differences between the binding properties of the two Cu(I) metal centers. Titration of isocyanides led to binding of the ligand to the $Cu_B$ center with infrared frequencies indicative of both a mono or a tris isocyanide–Cu(I) complex. However, two mutant forms of PHMcc that did not contain a $Cu_B$ center (His242Ala and Met314Ile), but did contain the $Cu_A$ center, were shown to ligate the isocyanide ligand with a $\nu$(CNR) for a bis isocyanide–Cu(I) complex. Furthermore, mutations affecting the ligands to the $Cu_A$ center (His107/108Ala) changed the ability of the $Cu_B$ center to ligate isocyanides to the $Cu_B$ center. The $Cu_B$ center was now able to form three different isocyanide–Cu(I) complexes; a mono, bis, and tris-isocyanide–Cu(I) complex were observed. Finally, investigation of the His172Ala protein showed that this mutant retained both copper centers and could ligate isocyanides, with ligation possibly occurring at both centers simultaneously. Therefore, it appears that by either

removing one of the copper centers in PHMcc or altering the geometry of the centers affects the binding properties of the active site copper centers.

Carbon monoxide (CO) ligation to the binuclear Cu(I) center in Hc was also revisited. Here we report evidence that the mode of CO ligation is not to a single Cu(I) atom, but rather as a bridging complex between the two centers. Removal of one of the copper atoms in Hc, to form a half-apo species, results in an upshift in the observed $\nu$(CO) for Hc, from 2063 $cm^{-1}$ to 2072 $cm^{-1}$. This upshift of the half-apo CO–Hc complex is more consistent with the frequency observed for small model compounds, where CO is bound terminally to a copper center that contains three heterocyclic nitrogen ligands.

# CHAPTER 1
# AN INTRODUCTION TO COPPER-CONTAINING ENZYMES

## 1.1 OXYGEN CHEMISTRY

Life on earth has evolved from a time in which living organisms did not derive their cellular energy from the metabolism of molecular oxygen to a time in which oxygen has become necessary for the survival of the majority of species in existence today. Interestingly, the percentage of $O_2$ in the environment today is toxic to the earlier life forms. Ninety percent of the oxygen consumed today is used to produce energy for cellular life [Sawyer, 1991]. This conversion of $O_2$ to energy proceeds via a four-electron reduction of oxygen to water. The remainder of oxygen consumed by aerobic organisms is used for the biosynthesis or biodegradation of compounds by cellular oxidases, monooxygenases, or dioxygenases.

Nonmediated four-electron reduction of $O_2$ is very rare, usually occurring as a series of one or two electron reductions, even though the reduction of $O_2$ to $H_2O$ has a potential of +0.815 V versus the normal hydrogen electrode, indicating that the reaction is thermodynamically favorable [Ho et al., 1995]. One crucial aspect of $O_2$ reduction involves the first one electron reduction step. With a reduction potential of -0.33 V, the initial one electron reduction of $O_2$ to superoxide is both rate limiting and thermodynamically unfavored. This allows the cell to control the consumption of $O_2$ and to prevent random $O_2$ reactions from occurring and possibly damaging the organism. A second kinetic barrier to $O_2$ reduction is that dioxygen has two unpaired electrons with parallel spin, resulting in a triplet ground state. This gives rise to a spin restriction barrier that must also be overcome for activation of $O_2$. However, within the cell, all that is needed to activate $O_2$ is a strong reducing agent such as reduced flavins.

Direct, uncatalyzed oxygenation of organic substrates by $O_2$ is not a major reaction pathway. In a cell, for oxygenation to occur at appreciable rates, the majority of these reactions require enzymes for catalysis. This requirement allows the living cell to control when and where $O_2$ is used. Most oxygenase enzymes that have been characterized contain transition metal ions as essential cofactors. The interaction of the metal ion with the $O_2$ or the substrate is the critical aspect in activating oxygen for further incorporation into a substrate. $O_2$ activation requires prior $O_2$ binding to a metal center. Copper cofactors in proteins are one type of metal atoms that have the ability to both reversibly bind and activate oxygen for further insertion into a substrate. Outlined in upcoming sections are examples of copper containing proteins that bind $O_2$ and utilize oxygen for specific cellular functions.

## 1.2 METALLOPROTEINS

Enzymes containing one or more of the elements from the first transition series (Mn, Fe, Co, Ni, Cu, and Zn) are prevalent in practically every organism living today. One recent review of the literature suggested that a third of all enzymes purified required a metal center for activity [Holm et al., 1996]. Metal containing proteins can be divided into five different classes of metalloenzymes: (i) metals that are required for protein folding and structure; (ii) enzymes that are involved in the regulation of free metals in the cell; (iii) metalloenzymes that are involved in electron transfer; (iv) $O_2$ binding and transporter metalloproteins; and (v) metalloenzymes that are involved in catalysis.

No eukaryotes and only a few prokaryotes are able to survive without copper and iron metalloproteins. This is due to the central role these two metals play in these organisms as the primary oxidases, oxygenases and oxygen carriers in animal cells [Frieden, 1981]. As transition metals, both of these elements have the capacity to form complexes with a variety of proteins and organic cofactors (e.g., porphyrins), exhibit a variety of oxidation states, and bind small molecules like oxygen. It is their ability to bind $O_2$ that has made them a requirement for aerobic life. Due to its abundance in nature and its rich chemistry, iron is probably the most commonly found

transition metal cofactor. The lower abundance of copper in the environment may be the major reason why Cu is not the paramount redox-active metal in proteins, since the diverse roles copper plays in cellular life are as numerous as iron.

### 1.2.1 Copper Proteins

Copper proteins occur widely in nature and are responsible for performing a diverse array of functions [Adman, 1991]. The classification of copper centers found in enzymes is based on the spectroscopic properties of the center. There are presently four types of copper centers: Type 1 (T1) copper centers (blue copper) are normally involved in electron transport; type 2 (T2) centers are termed "normal" copper centers because of their typical EPR spectra that resemble inorganic Cu(II) complexes; type 3 (T3) centers are EPR silent, owing to the magnetic coupling of their binuclear copper ions in the oxidized state; as in hemocyanin, tyrosinase, and catechol oxidase. The fourth class is the multicopper containing enzymes that usually contain all three types of copper centers.

### 1.2.2 T1 Copper Centers

Blue copper proteins are important electron transfer proteins with an intense absorption near 600 nm resulting in their blue color. This absorption is due to an intense Cys · S→Cu(II) charge transfer band that typically has an $\epsilon \sim 5000\ M^{-1}\ cm^{-1}$ (Figure 1.1B). Their Cu(II) EPR hyperfine splitting ($A_{\|}$) is usually half the value typically observed in normal Cu(II) complexes (Figure 1.1A). These spectral features are associated with a cysteine residue bound to the Cu(II) in a distorted tetrahedral geometry with an unusually short Cu–S(Cys) bond. The T1 centers exhibit relatively high reduction potentials. This high potential is attributed to a combination of the distorted tetrahedral geometry of the copper center, and the poor donor interaction of a long thioether–Cu(II) bond. The latter contribution has the effect of destabilizing Cu(II) relative to Cu(I) and leads to an increase in potential [Guckert et al., 1995].

One example of a blue copper protein is poplar plastocyanin. Plastocyanins are found in nearly all chloroplast containing organisms where they function as membrane-bound electron transport proteins in the photosynthetic pathway. High-

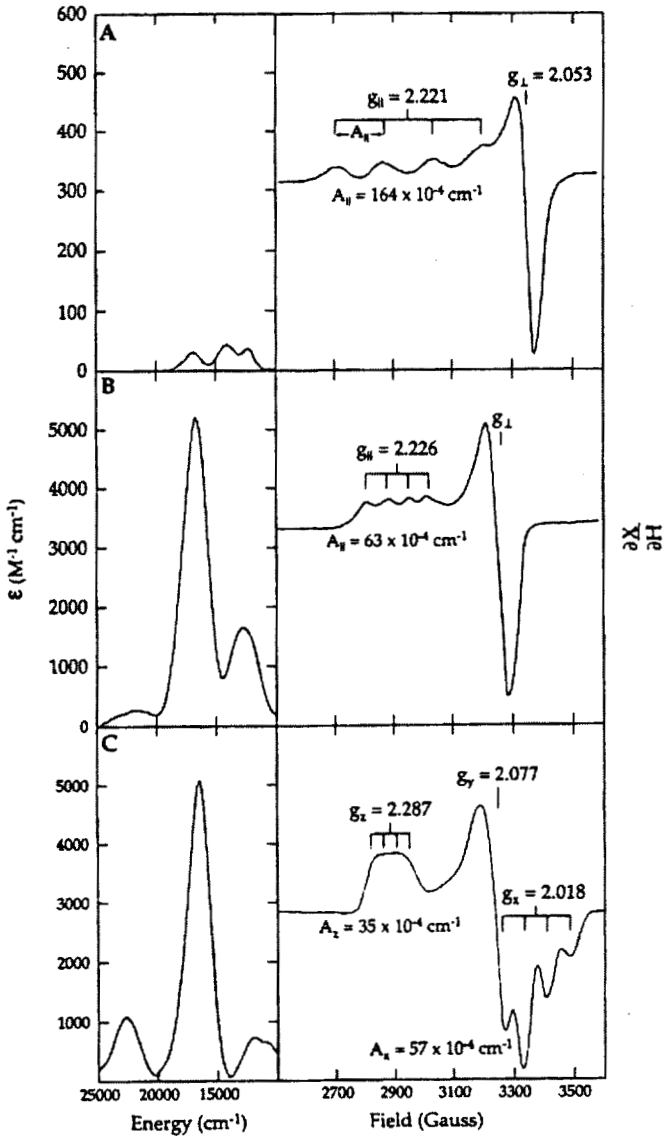


**Figure 1.1** Comparison of spectral features for T1 and T2 copper proteins. Low-temperature UV/Vis absorption (left) and electron paramagnetic resonance spectra (right) for normal tetragonal copper complex (A), poplar plastocyanin (B), and stellacyanin (C).

Originally published as Figure 5 in:
Holm, R. H., Kennepohl, P., and Solomon, E. I. (1996) Structural and functional aspects of metal sites in biology. *Chem. Rev.* 96, 2239-2314.

resolution X-ray crystal structures are available for this protein (Figure 1.2) [Colman et al., 1977; Guss and Freeman, 1983]. The center can be described as highly distorted tetrahedral with the copper coordinated by two nitrogens (derived from histidine residues 37 and 87) at a distance of 2.04 and 2.10 Å, respectively, one short Cu–S(Cys 84) bond of 2.10 Å, and one long Cu–S(Met 92) at 2.90 Å.

### 1.2.3 T2 Copper Proteins

With the noted exception of galactose oxidase, the T2 copper proteins usually do not have intense absorbance in the visible region. Superoxide dismutase, galactose oxidase, amine oxidase along with peptidylglycine $\alpha$-amidating monooxygenase and dopamine $\beta$-monooxygenase all belong to this class. Typical spectral characteristics of T2 centers are weak absorption spectra and EPR parameters resembling simple tetragonal copper complexes (Figure 1.1A). Unlike the T1 class of copper centers, T2 proteins have a wide variety of redox potentials. Furthermore, the copper atom is usually ligated by nitrogens and oxygens. A more in-depth analysis of a T2 enzyme will occur in an upcoming section.

Galactose oxidase (GO) is a 68 kD single polypeptide fungal protein that contains a T2 copper center. GO catalyzes the conversion of primary alcohols to aldehydes with the associated two-electron reduction of $O_2$ to peroxide [Klinman, 1996]. A crystal structure is available for GO at low pH showing that the copper center is 5-coordinate and in a square pyramidal geometry (Figure 1.3) [Ito et al., 1991]. Forming the base of the pyramid are His496 (2.11 Å), His581 (2.15 Å), Tyr272 (1.94 Å), and an acetate ion (not shown, 2.69 Å). The axial ligand is derived from a second tyrosine residue 495. At neutral pH, the acetate ligand is replaced by a solvent water molecule.

### 1.2.4 T3 Copper Proteins

Hemocyanin (Hc), tyrosinase, and catechol oxidase contain a coupled binuclear (T3) copper center. All three proteins contain two copper atoms that are antiferromagnetically coupled in the Cu(II) state. The ground state of oxygenated Hc is EPR silent due to a strong antiferromagnetic coupling of the two Cu(II) ions by an

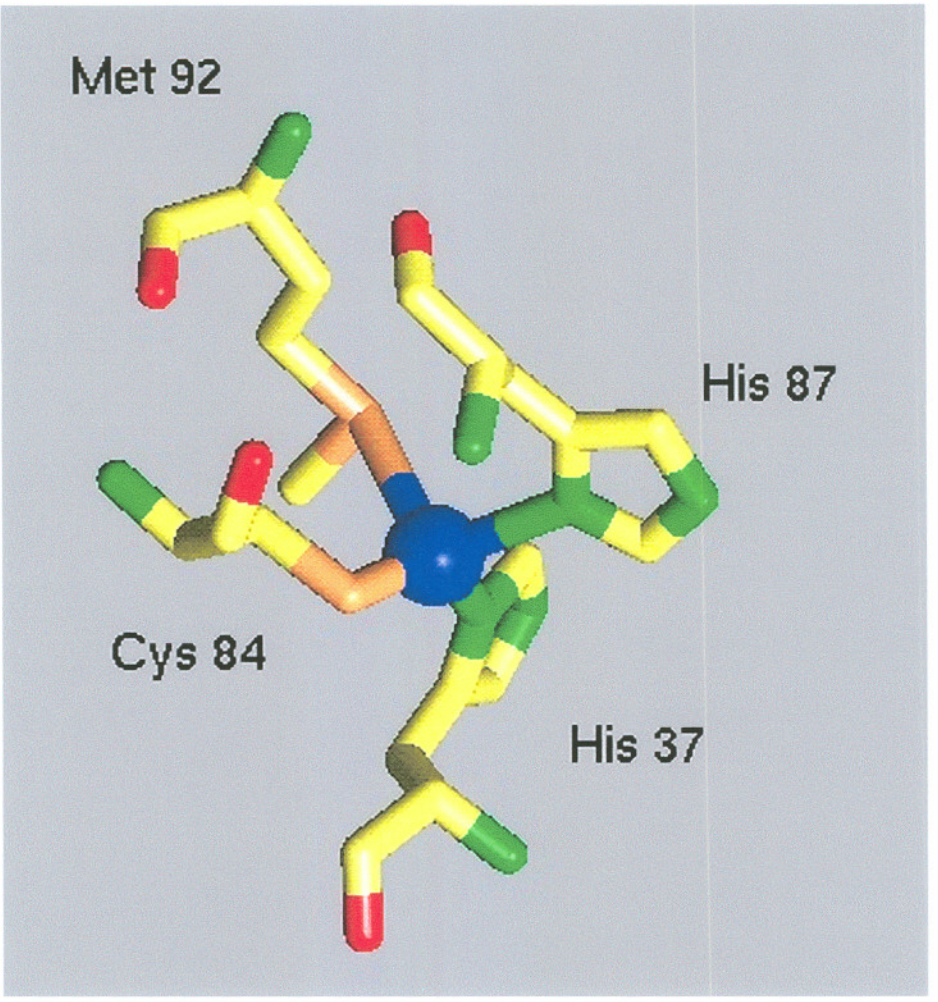


**Figure 1.2** Active site crystal structure for poplar plastocyanin T1 copper center showing the amino acid residues ligated to the copper atom. Cu = blue, S = orange, N = green, C = yellow, O= red.

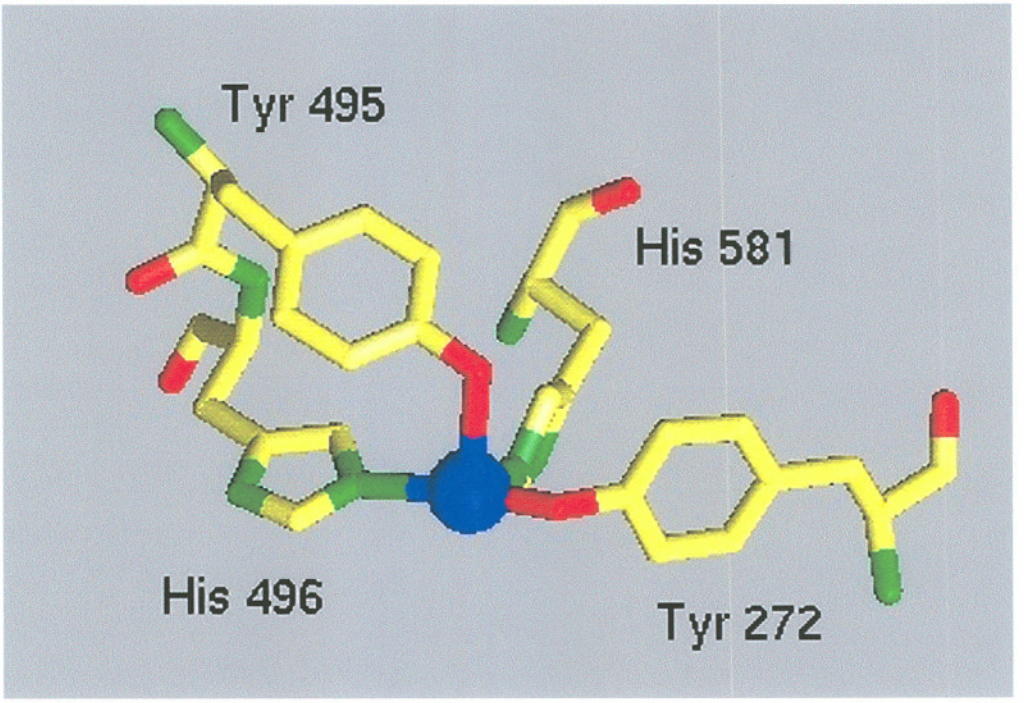


**Figure 1.3** Active site crystal structure for galactose oxidase. Acetate/water ligand not shown. Cu = blue, O = red, N = green, C= yellow.

endogenous ligand that bridges the two metal centers [Solomon et al., 1976; Dooley et al., 1978]. This Cu–Cu interaction results in strong exchange coupling of the unpaired electron. T3 proteins exhibit a relativity intense LMCT band centered near 350 $nm^{-1}$, derived from peroxide to Cu(II) charge transfer of the bound $O_2$.

### 1.2.5 Hemocyanin

Hemocyanins are very large (up to 9 MDa) $O_2$-transporting proteins in mollusks and arthropods [Eickman et al., 1979]. Hc contain two Cu atoms at its active site, termed $Cu_A$ and $Cu_B$. The amino acid sequence surrounding the $Cu_A$ center of molluscan Hc is similar to that of tyrosinase but not to arthropodal hemocyanins [Ling et al., 1994]. Interestingly, one of the His ligands to the $Cu_A$ center is modified by a thioether linkage to a nearby Cys residue in only molluscan Hc and some tyrosinases but not arthropodal Hc [Lerch et al., 1982]. In contrast to the $Cu_A$ center, the amino acid sequence involved in binding of the $Cu_B$ atom appears to be conserved in all hemocyanins and tyrosinases. Hc reversibly binds $O_2$. In oxyHc, the $O_2$ has been reduced to peroxide and is bound in a $\mu$-$\eta^2$:$\eta^2$ configuration between the two copper centers [Kitajima et al., 1992a,b; Magnus et al., 1994]. Deoxygenated Hc with reduced Cu(I) Cu(I) is colorless reflecting the $3d^{10}$ dicopper(I) state. X-ray crystal structures exist for the Hcs of the arthropods spiny lobster (*Panulirus interruptus*) and horseshoe crab (*Limulus polyphemus*), and the molluscan octopus (*Octopus dofleini)* [Volbeda and Hol, 1989; Hazes et al., 1993; Magnus et al., 1994; Cuff et al., 1998].

### 1.2.6 Deoxyhemocyanin

The crystal structure for the deoxygenated *Limulus polyphemus* subunit II hexamer is available at a resolution of 2.18 Å [Hazes et al., 1993]. The overall structure shows a subunit that is comprised of three domains (Figure 1.4). Domain 1 is mainly $\alpha$-helical with one $\beta$-strand that interacts with domain 3. Domain 2 is also predominately $\alpha$-helical in nature and is packed between domain 1 and 3. Domain 2 also contains the T3 copper center with all the histidine ligands to the copper centers

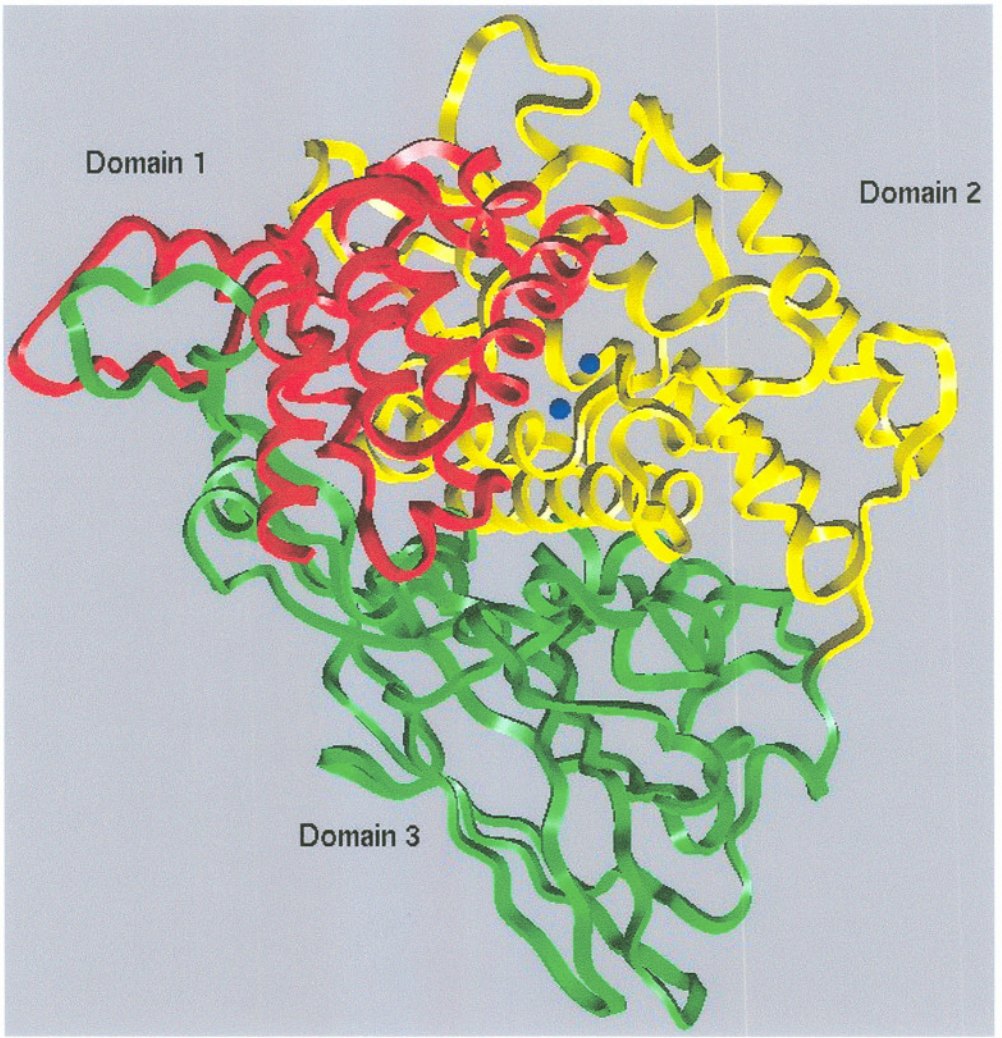


**Figure 1.4** Crystal structure of *Limulus polyphemus* subunit II showing all three domains. The copper atoms are in blue.

coming from within the domain. Domain 3 contains a seven-stranded $\beta$-barrel, and interacts with both domain 1 and 2.

The active site copper center was determined to be nearly coplanar with respect to its three ligating $N^{\epsilon}$-histidine nitrogens (Figure 1.5A). Each copper can be described as distorted trigonal planar with $Cu_A$ best resembling an ideal trigonal coordination. The nitrogen to copper distances for $Cu_A$ fall between 2.1 and 1.9 Å. The distances for $Cu_B$ are slightly larger at 2.2 and 1.9 Å giving this center a more distorted trigonal geometry. The Cu–Cu distance was determined to be unexpectedly large at 4.6 Å which differed from the expected distance of 3.6 Å seen by EXAFS and in the crystal structure for *Panulirus* [Brown et al., 1980; Woolery et al., 1984]. Interestingly, no bridging ligand could be observed between the two copper centers, as previously speculated to be present and responsible for the coupling of the two metal centers [McKee et al., 1981; Volbeda and Hol, 1989].

### 1.2.7 Oxyhemocyanin Structure

A crystal structure of *Limulus polyphemus* subunit II with $O_2$ bound to the binuclear copper center is available at a resolution of 2.4 Å [Magnus et al., 1994]. The overall protein structure closely resembles what was seen in the deoxygenated Hc structure. However, upon oxygenation, the two copper atoms move significantly closer to each other, and are now only 3.6 Å apart (Figure 1.5B). The oxygen is symmetrically bound between the two coppers in an $\mu$-$\eta^2$:$\eta^2$ configuration. The geometry of the copper atoms can be described as square planar to both of the oxygen molecules and two of the three histidine ligands. Above and below the plane lie His204 and His328. Interestingly, the crystal structure of the oxy form of octopus Hc shows a dramatically similar active site coordination of the Cu atoms and the oxygen compared to that of the *Limulus* structure [Cuff et al., 1998].

## 1.3 PEPTIDYLGLYCINE $\alpha$-AMIDATING MONOOXYGENASE

$\alpha$-amidation is an important biological process that activates many neuropeptides by enabling them to bind to their respective receptors with much

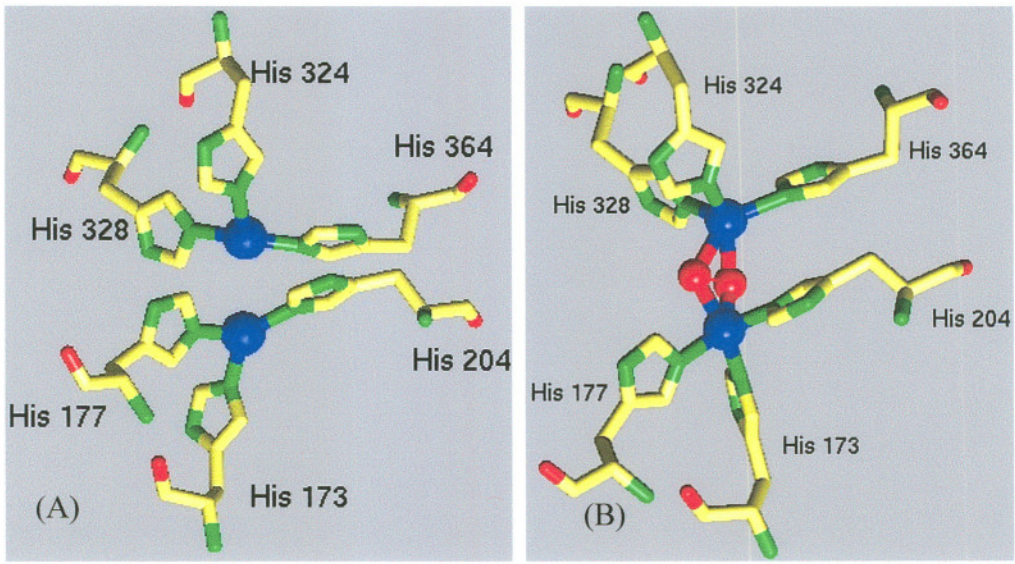


**Figure 1.5** Crystal structure of deoxyhemocyanin (A) and oxyhemocyanin (B) active site structure. Cu = blue, O = red, N = green, C = yellow.

greater affinities. This enzymatic process involves the conversion of the free carboxylic acid into a nonionizable α-amide [Eipper et al., 1992b]. The amidation reaction is a two step process that is accomplished through the interaction of the neuropeptide with the bifunctional enzyme peptidylglycine α-amidating monooxygenase (PAM, EC 1.14.17.3) (Figure 1.6). Early research into this reaction revealed that the amide moiety was derived from the glycine residue and not from exogenous nitrogen [Bradbury et al., 1982]. Further studies demonstrated that the $O_2$ is derived from molecular oxygen and not from $H_2O$ [Zabriskie et al., 1991]. Kinetic isotope data indicate an equilibrium ordered mechanism with substrate binding occurring first, followed by $O_2$ ligation [Francisco et al., 1998]. The first step, formation of the intermediate peptidyl α-hydroxylglycine, occurs when the α-carbon of the terminal glycine residue becomes hydroxylated, and takes place in the peptidyl α-hydroxylglycine monooxygenase (PHM) domain. The second step is cleavage of the N–C bond to produce the amidated peptide and glyoxalate and occurs in the α-amidating lyase (PAL) domain.

A single gene encodes both activities of the PAM enzyme. However, various forms of the enzyme can be produced through tissue specific alternative splicing and endoproteolytic processing (Figure 1.7) [Ouafik et al., 1984; Stoffers et al., 1989; Eipper et al., 1991; Milgram et al., 1992]. For example, in the rat atrium, a full length mRNA encodes a 120-kD protein that is comprised of an $NH_2$-terminal PHM domain, a PAL domain, a hydrophobic transmembrane section, and a cytoplasmic tail (rPAM-1). Furthermore, mRNAs have been isolated that encode a second membrane bound protein that is only 105 kD (rPAM-2). Both of these bifunctional enzymes are identical, but differ in that rPAM-2 does not contain the 315 base pairs that comprise the optional exon A [Eipper et al., 1991, 1992a; Husten and Eipper, 1991; Stoffers et al., 1991; Husten et al., 1993]. This exon encodes a potential endoproteolytic cleavage site that has been shown to be susceptible to digestion with endoproteases [Husten and Eipper, 1991]. Cleavage at this site can give rise to a separation of the bifunctionality of the enzyme where the PHM and the PAL functions are now separated. mRNA found in the neurointermediate pituitary and the brain lack the optional exon B. Exon B codes for the hydrophobic transmembrane anchor (rPAM-3)

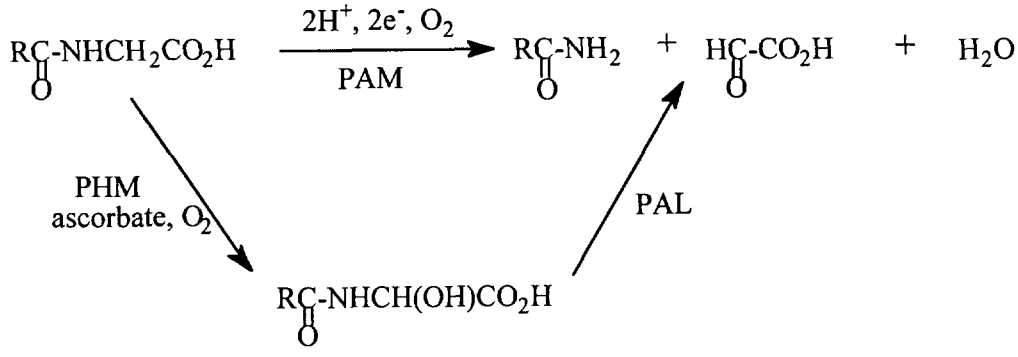


**Figure 1.6** Reaction catalyzed by the bifunctional enzyme PAM and the reactions catalyzed by the two enzymes that comprise PAM.

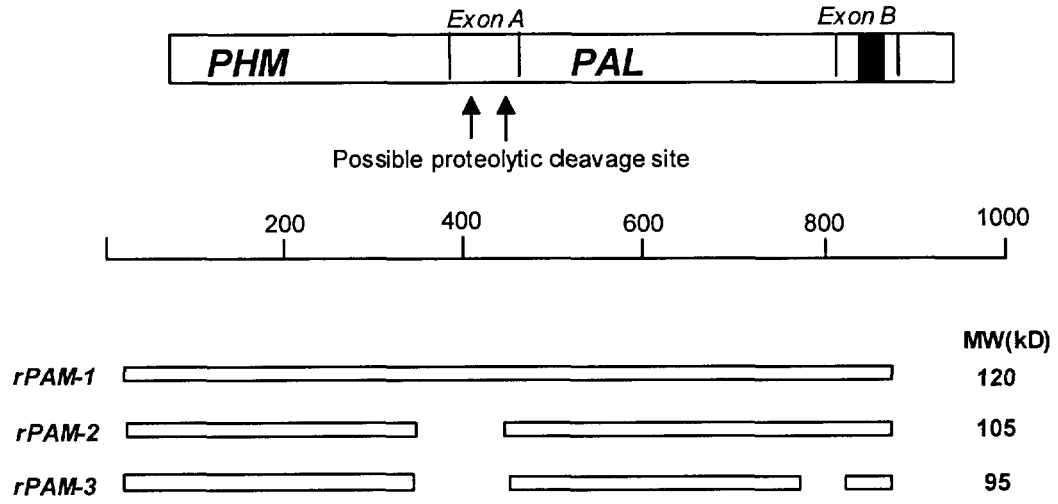


**Figure 1.7** Molecular forms of PAM showing different cleavage points.

[Husten and Eipper, 1991]. Therefore, expressed enzymes lacking this exon are soluble.

Another area of intense focus centered on elucidation of the overall structure of PHM. One aspect of this research dealt with determining the necessary length of protein needed for full enzymatic activity. Initial studies on truncated PHM demonstrated that a sequence of amino acids from 36–359 were sufficient for activity [Eipper et al., 1995]. However, further truncation led to a fully active fragment that contained only amino acid residues 42–356, termed PHMcc [Kolhekar et al., 1997].

Further structural studies on the PHMcc domain revealed that 10 cysteine residues are present and involved in making 5 disulfide linkages [Kolhekar et al., 1997]. Determining where these linkages occur in the protein was facilitated by the discovery that PHMcc contains a linker region that separates the N and C termini that was susceptible to proteolytic cleavage. This linkage also contains a novel endoproteolytic cleavage site that allows the enzyme to be separated into two domains of 18.5 kD (N-terminus) and 16.5 kD (C-terminus) in size. Three of the disulfide bridges occur in the N-terminal domain and the remaining two are in the C-terminal domain [Kolhekar et al., 1997]. It is interesting to note that there are no disulfide bridges linking the two domains. Sequence analysis of the N-terminus determined that the three conserved histidine residues associated with $Cu_A$ binding occur here, whereas, the C-terminus contains the ligands (2 histidines, 1 methionine) associated with $Cu_B$ ligation [Kolhekar et al., 1997].

The crystal structure of the oxidized form of PHMcc has recently been solved [Prigge et al., 1997]. The structure showed that each domain is about 150 amino acids in length. Both are comprised mainly of nine $\beta$-strands forming a $\beta$-sandwich structure (Figure 1.8). The interchain linker region is highly hydrophobic and limits the interdomain space to 8 $Å^2$ of solvent accessible space. The ligand structure surrounding the two copper centers is found to correspond closely to previous models predicted from earlier spectroscopic and chemical methods [Southan and Kruse, 1989; Eipper et al., 1995; Kolhekar et al., 1997]. The two Cu(II) ions are located on different domains and are approximately 11 Å apart. Both are fully solvent accessible. The $Cu_A$ is ligated by three histidines (amino acids 107, 108, and 172).

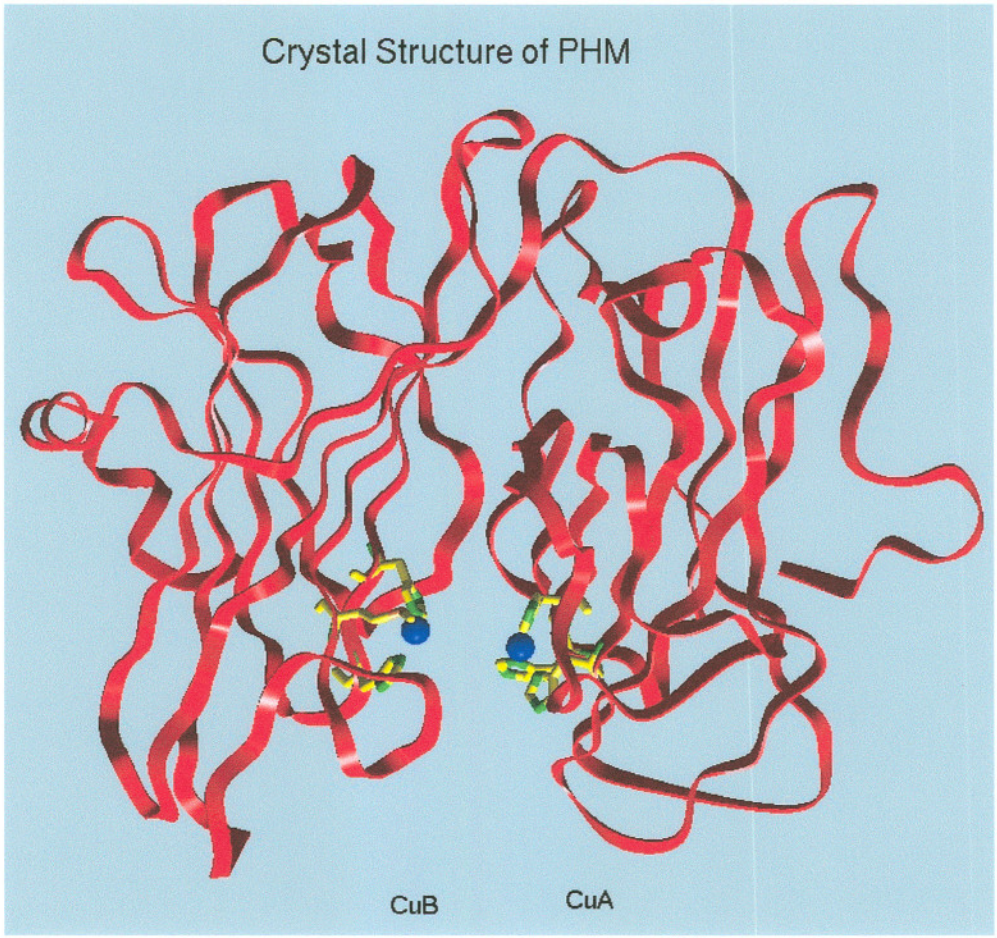


**Figure 1.8** Crystal structure of PHMcc showing the location of the active site pocket. Cu = blue, S = orange, N = green.

The $Cu_B$ site is ligated by two histidines (242 and 244), a distant methionine (314), and one water (Figure 1.9). $Cu_A$ appears to be in a square pyramidal configuration with the $\delta$-nitrogens forming the ligand interaction with the copper. $Cu_B$ is of tetrahedral geometry with the $\epsilon$-nitrogens ligating the copper and the solvent molecule lying near the methionine residue.

The interaction of a substrate analog (N-$\alpha$-acetyl-3,5-diiodotyrosylglycine) bound to PHMcc was also investigated in this study [Prigge et al., 1997]. The peptide inside the active site pocket is anchored through a series of H-bonds with amino acid residues Arg240, Tyr318, Asn316 and one structural water (Figure 1.10). Furthermore, the hydroxyl group on the tyrosine peptide H-bonds with the carbonyl oxygen of Ala135. Also helping secure the substrate in the active site cleft are several hydrophobic contacts between the peptide backbone and the enzyme, including a contact with Met314. These interactions appear to orientate the pro-*S* hydrogen so that it is pointing toward the $Cu_B$. Studies previously demonstrated the importance of the peptide interaction between Tyr318 and Met314. Replacement of Tyr318 with phenylalanine resulted in an increase in $K_m$ of about 7-fold but did not effect $V_{max}$ [Kolhekar et al., 1997]. Replacement of Met314 with isoleucine results in both an inactive enzyme and one that binds substrate less tightly than wild type [Eipper et al., 1995].

What the crystal structure fails to unravel is how electrons are passed from one copper site to the other. Scheme 1.1 depicts a proposed hydroxylation mechanism for PHMcc that can be subdivided into a separate reductive and oxidative cycle. In the reduction cycle, both cupric atoms are one electron reduced by ascorbate. This is followed by substrate binding to the active site near the $Cu_B$ center and $O_2$ incorporation in an equilibrium ordered fashion. At this stage, all current experimental data suggest that the $O_2$ binds to the $Cu_B$ center where it becomes reduced by an electron from each copper center to form a peroxide intermediate bound to the $Cu_B$ site. Homolytic 0–0 bond cleavage and H-atom abstraction from the substrate by peroxide produces two radicals, one oxygen radical at $Cu_B$, and a radical on the substrate, and the release of water. Radical recombination forms the final product of an alkoxide bound to the $Cu_B$ center, the rate limiting step being the

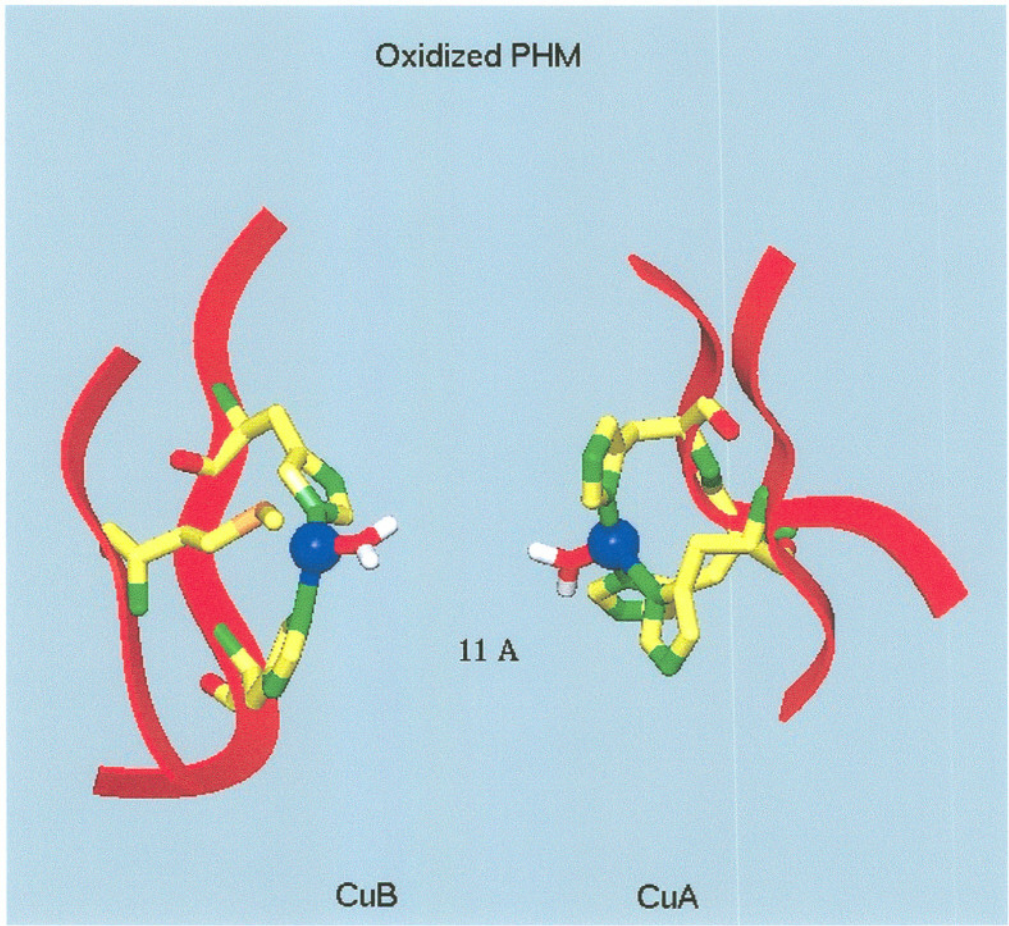


**Figure 1.9** Crystal structure of the active site of Cu(II) form of PHMcc. Cu = blue, S = orange, N = green, C= yellow, O= red.

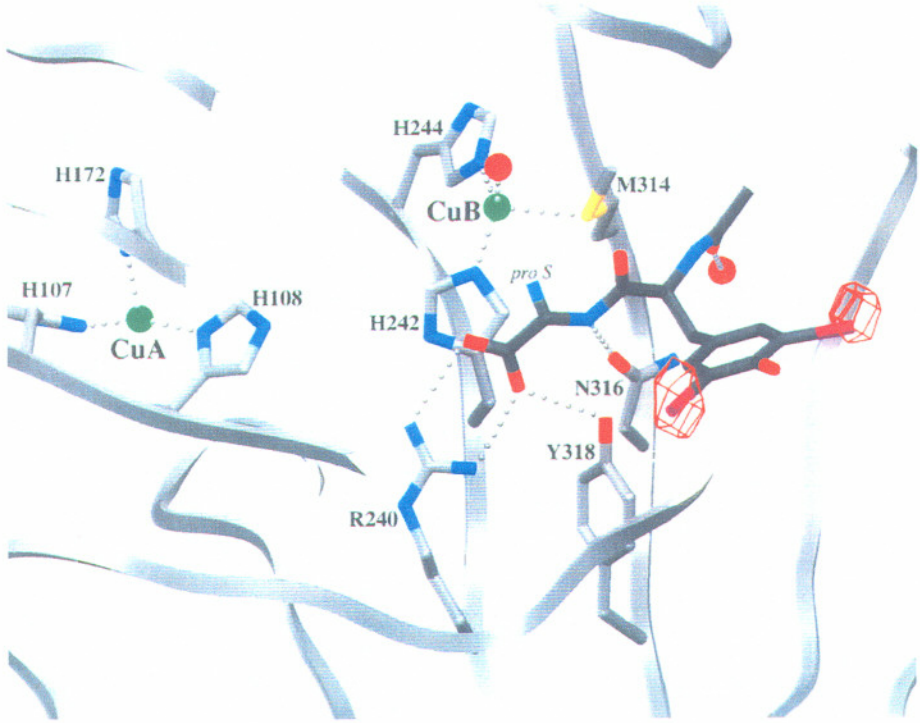


**Figure 1.10** PHMcc structure with peptide bound.

Originally published as Figure 4a in:
Prigge, S. T., Kolhekar, A. S., Eipper, B. A., Mains, R. E., and Amzel, L. M. (1997) Amidation of bioactive peptides: the structure of peptidylglycine α-hydroxilating monooxygenase. *Science* **278,** 1300-1305.
Used here with permission of Science.

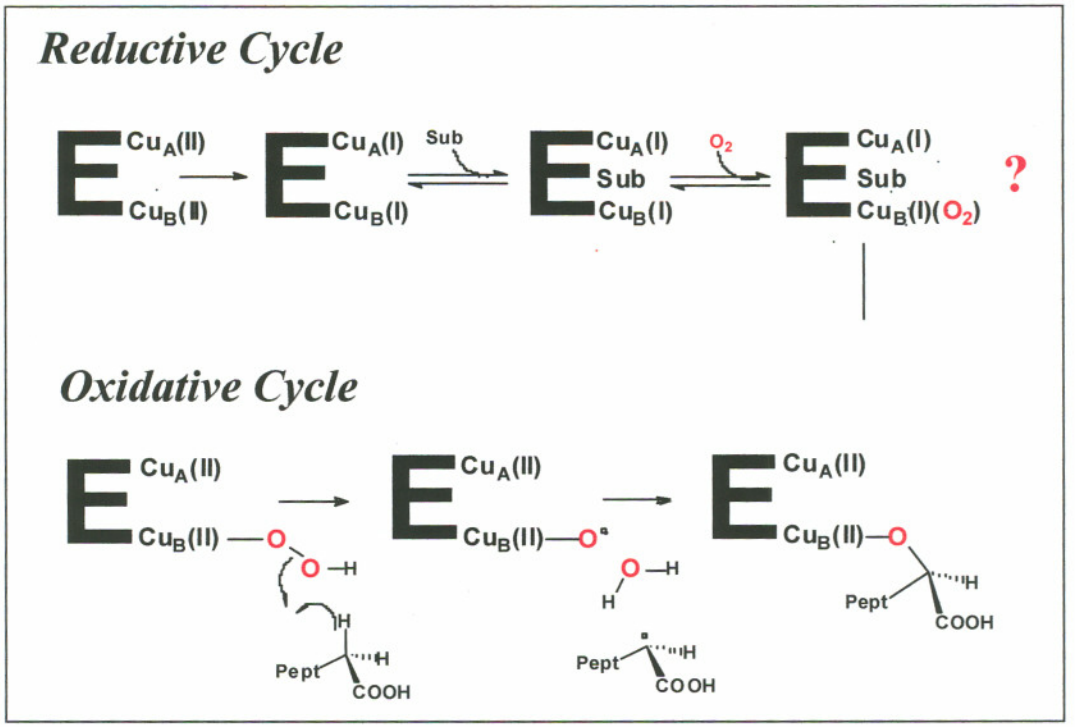


**Scheme 1.1** Proposed mechanism for monooxygenation by PHMcc

dissociation of this alkoxide from the active site. As stated previously, the two copper centers are 11 Å apart from each other and no short range through-bond pathway exists for electrons to travel from one center to the other. There are several theories on how the electrons are passed from one center to the other. The possibility of domain motion upon peptide binding and thus bringing the two copper centers closer and forming a pseudo-T3 center has been investigated. This could then facilitate electron transfer between the two centers via a bridged $O_2$ mechanism. However, when a comparison of the peptide bound structure to the unligated structure was made, no domain closing was observed [Prigge et al., 1997]. The structure does indicate that when peptide binds, the geometry surrounding the $Cu_B$ center would allow the peptide backbone to move almost 0.4 Å closer to the copper [Prigge et al., 1997]. Modeling of domain motion of reduced PHMcc was also explored. The results showed that the two domains could not move closer in reduced PHMcc because the His108 ligand to the $Cu_A$ center would collide with the substrate glycine residue [Prigge et al., 1997]. The crystal structure does not rule out the possibility of electron transfer occurring through the interactions of structured water in the active site of PHMcc. A third possibility is that $O_2$ may first bind at the $Cu_A$ center becoming one electron reduced to superoxide forming a Cu(II)–$O_2\cdot$ intermediate [Jaron and Blackburn, 2000]. The superoxide intermediate then acquires a proton and migrates from the $Cu_A$ center to the $Cu_B$ center, where it accepts a second electron from the $Cu_B$ atom forming the peroxide intermediate. The advantages of this mechanism are 2-fold. First, the transfer of electrons between the two distant Cu centers is occurring through the $O_2$ substrate. Furthermore, the pH maximum for this enzyme is in the 5.5–5.7 range. However, there is not a suitable active site base with a pKa in this range that could act as a proton donor. However, the pKa of superoxide is reported to be 4.78 suggesting that a neutral protonated superoxide may also be responsible for the hydrogen transfer along with the electron transfer between the two metal centers.

## 1.4 BACKGROUND ON DOPAMINE β-MONOOXYGENASE

Many of the experiments set forward in this thesis were designed to spectroscopically study the copper centers of PHM. The design of these experiments are based on PHM's similarities to another dinuclear copper containing monooxygenase, dopamine β-monooxygenase (DβM, EC 1.14.17.1). DβM, isolated from bovine adrenal medulla, is a glycoprotein of 290 kD that can exist in either a soluble or membrane-bound form [Stewart and Klinman, 1988]. DβM catalyzes the physiologically important conversion of dopamine to norepinephrine (Figure 1.11) [Villafranca, 1981; Stewart and Klinman, 1988]. Over the past three decades, much research has been directed at elucidating the structure and function of this enzyme. An early study involving rapid freeze quench kinetics determined that there are 2 mol of copper per mole of subunit and both coppers are required for activity [Klinman et al., 1984]. Spectroscopic studies centering on the active site copper atoms have led to the development of a "spectroscopically effective" model of the ligand sets bound to these copper atoms. Research utilizing EPR and ESEEM methods have suggested that the most probable ligands to the copper atoms are histidines [Blackburn et al., 1984, 1988; McCracken et al., 1992].

X-ray absorption fine structure spectroscopy (EXAFS) and kinetic studies have shown that there are differences not only between the two copper centers, but also between the reduced and oxidized forms of the enzyme [Stewart and Klinman, 1987; Blumberg et al., 1989; Brenner and Klinman, 1989; Brenner et al., 1989]. Figure 1.12 depicts the expected copper ligands surrounding the two T2 copper centers. In the oxidized state, the $Cu_A$ center appears to be ligated by three histidine ligands at a distance of 1.99 Å and one water at 1.94 Å; whereas, the $Cu_B$ center is ligated by two histidines (1.99 Å) and two waters (1.94 Å). Upon reduction of the coppers, the solvent derived oxygen ligands dissociate, leaving two 3-coordinate Cu(I) ions where the $Cu_A$ center is ligated by three histidines and the $Cu_B$ center has two histidines and one methionine ligand at 2.25 Å (Figure 1.12B) [Blackburn et al., 1991]. The histidine distances in the reduced form move from 1.99 Å to 1.93 Å [Blackburn et al., 1991].

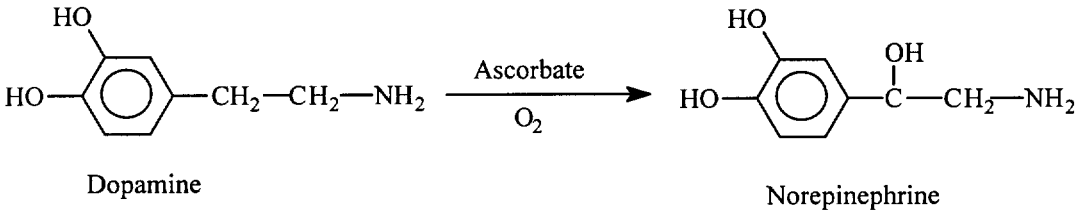


**Figure 1.11** DβM catalyzed reaction.

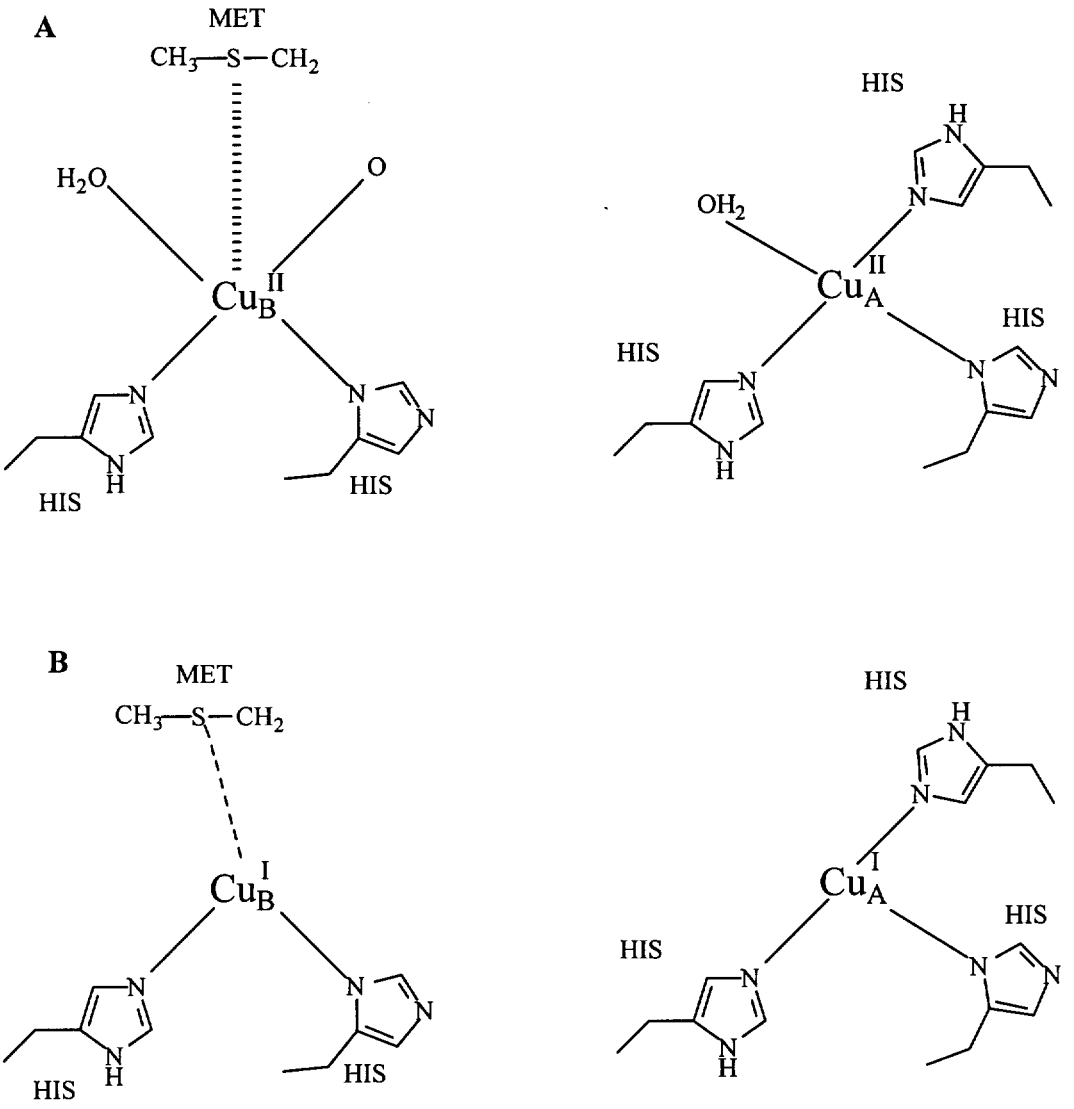


**Figure 1.12** Proposed active site structures for the oxidized (A) and reduced (B) DβM.

Steady-state kinetic isotope studies and single-turnover experiments have led to a proposed mechanism for the DβM catalyzed reaction (Figure 1.13) [Stewart and Klinman, 1988]. After ascorbate reduction, the enzyme binds both $O_2$ and substrate [Tian and Klinman, 1993]. This is followed by electron transfer from the two copper centers to the $O_2$, forming a Cu(II)-hydroperoxide at the $Cu_B$ center. This mechanism has been further refined from the findings involving novel oxygen isotope data [Tian et al., 1994]. It has been proposed that following the formation of the Cu(II)-hydroperoxide, a nearby tyrosine reacts with the cupric hydroperoxide to form a Cu(II)–O· protein radical pair (Figure 1.14). This then extracts a hydrogen from the substrate and finally, the Cu(II)–O· rebounds with the substrate to form the final product [Tian and Klinman, 1993; Tian et al., 1994].

The use of ligand probes directed to the Cu(I) centers in DβM has been helpful in gathering both structural and mechanistic details concerning the enzyme. Previous studies have shown that DβM can bind only one CO per dinuclear copper center, and that CO is inhibitory towards $O_2$ binding [Pettingill et al., 1991]. Fourier transform infrared spectroscopy (FTIR) on this CO-DβM adduct showed a stretching frequency of 2089 $cm^{-1}$. Comparison of this value with literature data revealed that most tris-histidine Cu(I)–CO complexes have $\nu_{CO}$ values significantly lower than the DβM-CO frequency [Fager and Alben, 1972; Ferrari et al., 1990]. Therefore, the observed upshift in the frequency of the CO stretch in DβM was an indication of CO bound to a copper that was less basic than a 3-coordinate His-Cu center [Pettingill et al., 1991]. Dialysis of CO-bound DßM against free cyanide leads to selective removal of the $Cu_A$ center in DβM and the formation of half-apo DβM [Reedy and Blackburn, 1994]. EXAFS analysis of this half-apo CO–DβM complex, reveals that the remaining Cu(I)–CO complex is also ligated by the Met ligand. This suggests that $Cu_B$ is the site of $O_2$ and CO binding, since $Cu_A$ does not contain the novel Met ligand [Reedy and Blackburn, 1994].

Using isocyanide as a ligand to the Cu(I) ions in DβM has provided information about both centers. Studies have shown that isocyanides bind to both copper centers with unique stretching frequencies: $Cu_A$ 2148 $cm^{-1}$, $Cu_B$ 2129 $cm^{-1}$

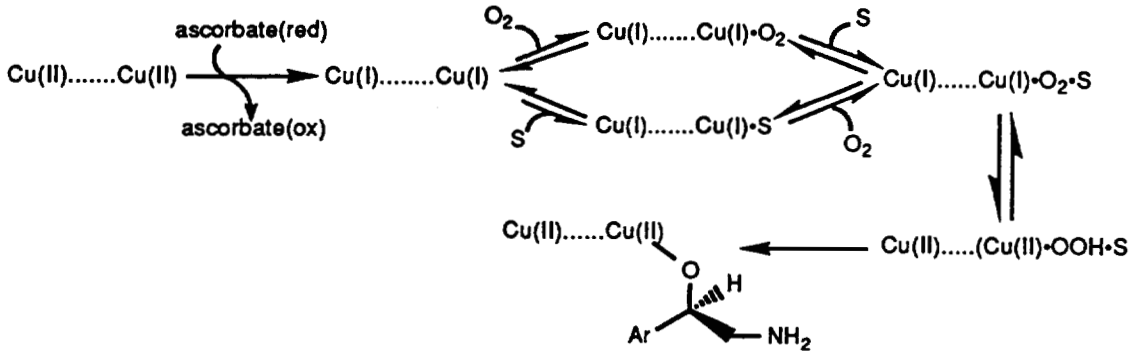


**Figure 1.13** General kinetic mechanism for DβM.

Originally published as Scheme 2 in:
Tian, G., Berry, J. A., and Klinman, J. P. (1994) Oxygen-18 kinetic isotope effects in the dopamine β-monooxygenase reaction: evidence for a new chemical mechanism in non-heme metallomonooxygenases. *Biochemistry* **33,** 226-234.

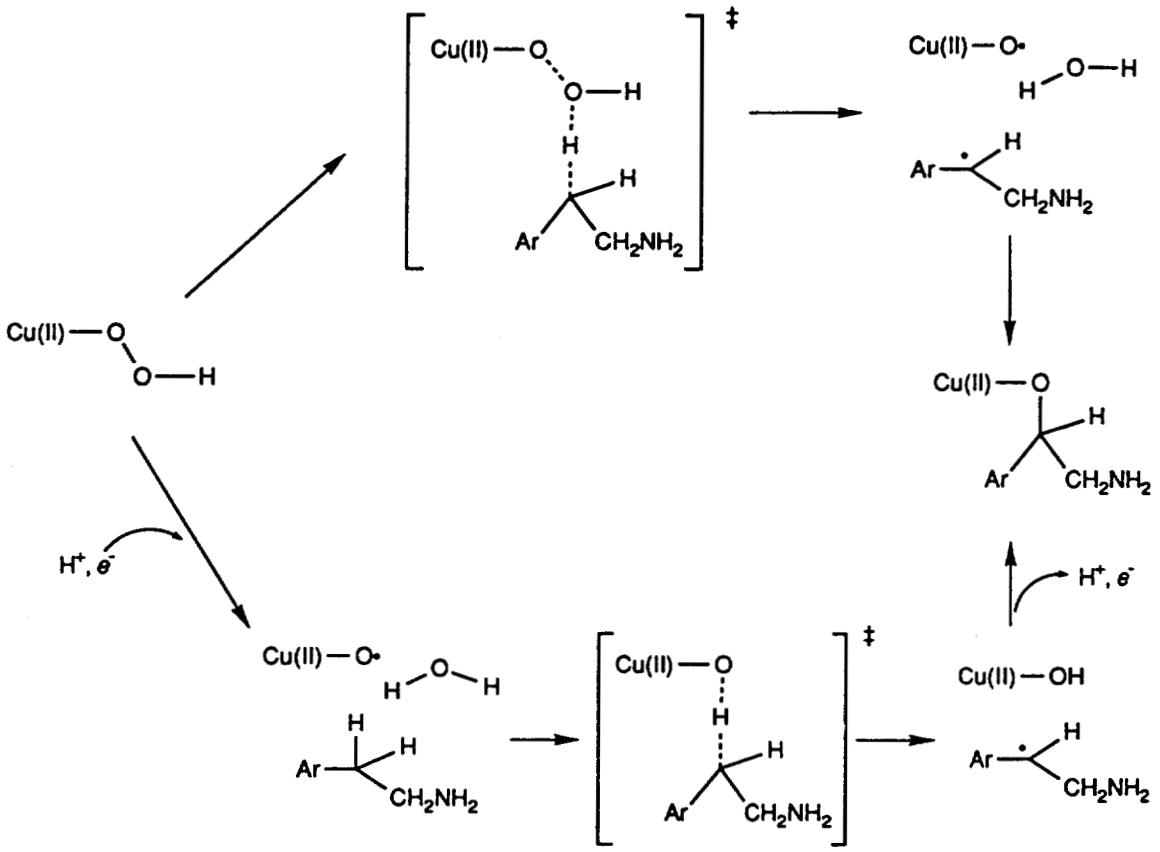


**Figure 1.14** Steady-state kinetic mechanism for DβM.

Originally published as Scheme 3 in:
Tian, G., Berry, J. A., and Klinman, J. P. (1994) Oxygen-18 kinetic isotope effects in the dopamine β-monooxygenase reaction: evidence for a new chemical mechanism in non-heme metallomonooxygenases. *Biochemistry* **33,** 226-234.

[Reedy et al., 1995]. These copper center frequencies were assigned by comparing the frequencies of D$\beta$M with that obtained from hemocyanin.

When ascorbate-reduced D$\beta$M was allowed to react (by dialysis in phosphate buffer) with low concentrations of 2,6-dimethylphenyl isocyanide (DIMPI) (Figure 1.15), three different time dependent bands were seen (Figure 1.16 A,B,C). Early in the reaction, two bands were observable. The main peak was centered at 2129 $cm^{-1}$ and a shoulder was present at 2148 $cm^{-1}$. Curve fitting of the spectra produced a third peak at 2160 $cm^{-1}$. As the reaction proceeded, the 2148 $cm^{-1}$ band increased in intensity as did the 2160 $cm^{-1}$ band. However, the 2129 $cm^{-1}$ band decreased in intensity. Finally, both the 2148 and the 2129 $cm^{-1}$ bands converted to the band at 2160 $cm^{-1}$ (Figure 1.16) [Reedy et al., 1995].

When this experiment was performed using substoichiometric amounts of DIMPI to copper, the FTIR spectra were composed mainly of the two bands at 2148 and 2129 $cm^{-1}$. Spectral deconvolution of this spectrum revealed that the two bands were of equal contribution and there was a small contribution from the peak at 2160 $cm^{-1}$ (Figure 1.17). Therefore, it was determined that the two bands at the lower frequency were from mono isocyanide species bound to each copper. Results from further studies using IR and Raman on a number of structurally characterized inorganic Cu(I) DIMPI complexes confirm that the band corresponding to the frequency at 2160 $cm^{-1}$ was from Cu(I) bound to three DIMPI ligands [Reedy et al., 1995].

In order to determine which of the lower frequencies corresponded to which copper site, the reaction of the copper centers to DIMPI was followed by using molluscan hemocyanin (Figure 1.18). Hemocyanin has a dicopper type 3 copper site with three histidines on each copper, and so one would expect only one IR band when DIMPI was bound at stoichiometric concentrations. After reacting the deoxy-hemocyanin with two mol per copper of DIMPI, a single IR band at 2148 $cm^{-1}$ is seen. As the concentration of DIMPI increases, the band at 2148 $cm^{-1}$ converts to 2160 $cm^{-1}$. Comparing the results from the hemocyanin experiments with the results from D$\beta$M suggest that the 2148 $cm^{-1}$ band is an isocyanide bound to the $Cu_A$ site of D$\beta$M, and the 2129 $cm^{-1}$ band is from the $Cu_B$ [Reedy et al., 1995].

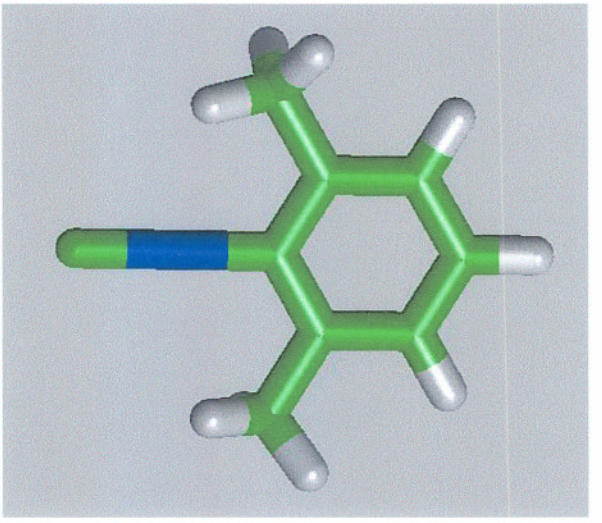

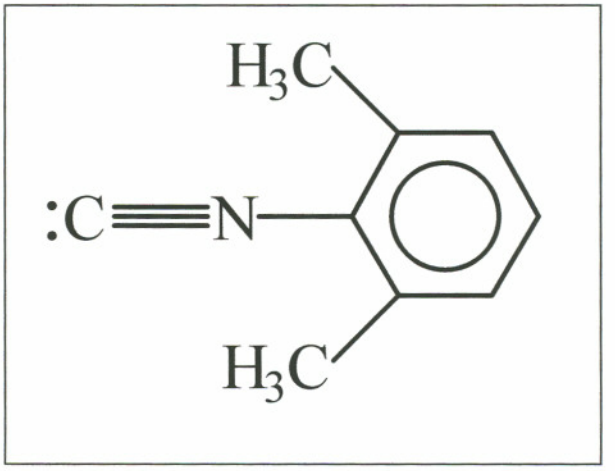


**Figure 1.15** The structure of 2,6-dimethylphenyl isocyanide (DIMPI).

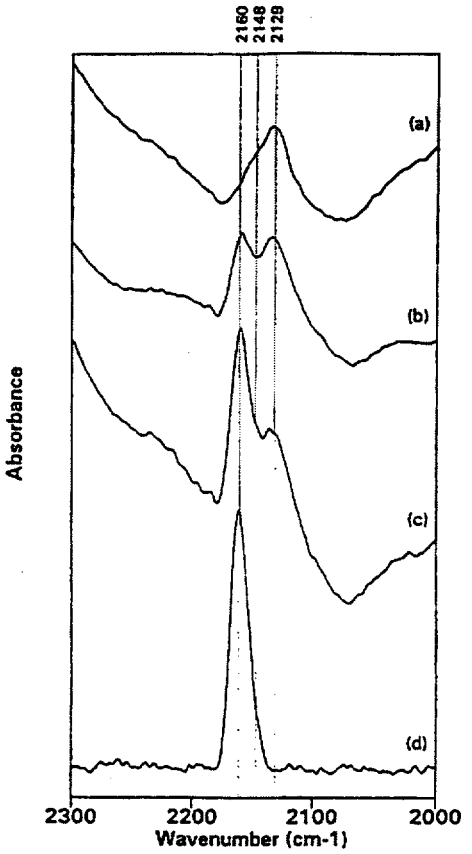


**Figure 1.16** IR absorbance of DIMPI bound to DβM, showing the progression of mono-isocyanide complex conversion to the tris-isocyanide complex as the dialysis time increased.

Originally published as Figure 1 in:
Reedy, B. J., Murthy, N. N., Karlin, K. D., and Blackburn, N. J. (1995) Isocyanides as ligand-directed indicators of Cu(I) coordination in copper proteins. Probing the inequivalence of the Cu(I) centers in reduced dopamine β-monooxygenase. *J. Am. Chem. Soc.* **117**, 9826-9831.

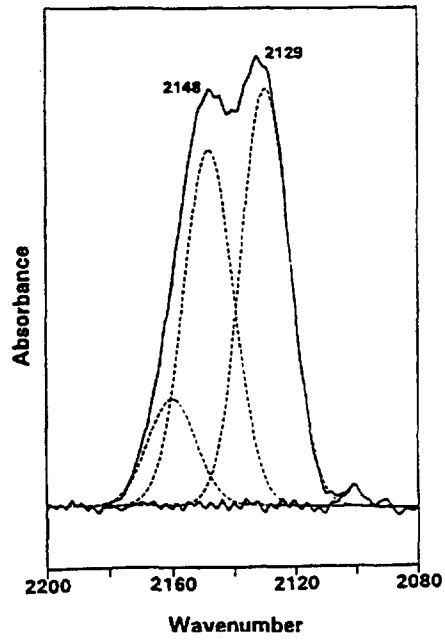


**Figure 1.17** Titration of DβM with stoichiometric amounts of DIMPI.

Originally published as Figure 2 in:
Reedy, B. J., Murthy, N. N., Karlin, K. D., and Blackburn, N. J. (1995) Isocyanides as ligand-directed indicators of Cu(I) coordination in copper proteins. Probing the inequivalence of the Cu(I) centers in reduced dopamine β-monooxygenase. *J. Am. Chem. Soc.* **117**, 9826-9831. Used here with permission of the American Chemical Society.

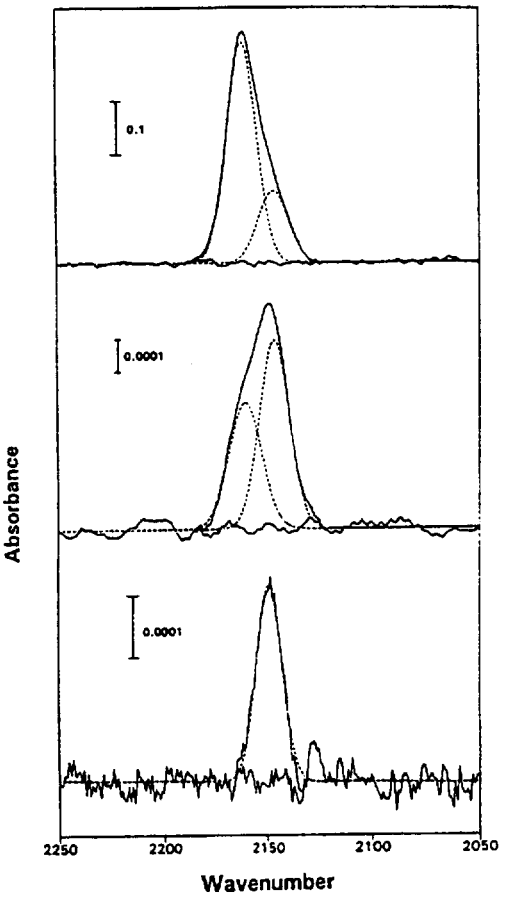


**Figure 1.18** The titration of DIMPI against hemocyanin showing the conversion of the 2148 $cm^{-1}$ band into the 2160 $cm^{-1}$ species as the concentration of DIMPI increased.

Originally published as Figure 3 in:
Reedy, B. J., Murthy, N. N., Karlin, K. D., and Blackburn, N. J. (1995) Isocyanides as ligand-directed indicators of Cu(I) coordination in copper proteins. Probing the inequivalence of the Cu(I) centers in reduced dopamine β-monooxygenase. *J. Am. Chem. Soc.* **117,** 9826-9831.

The assignment of the 2160 $cm^{-1}$ frequency was aided by comparison of the DIMPI-D$\beta$M results with results obtained when DIMPI was titrated against a 3-coordinate Cu model compound [($Cu^{I}$(MePY2)]($ClO_4$) where (MePY2) is bis(2-pyridylethyl) methylamine. Upon titration of this compound with 1 mol of DIMPI, the observed $\nu$(CNR) is coincident in the IR and Raman at 2132 $cm^{-1}$ (Figure 1.19). Upon continued addition of DIMPI, two new Raman bands appear at 2162 $cm^{-1}$ and 2183 $cm^{-1}$, indicative of a new species being formed. Assignment of this new species as a tris-isocyanide copper complex was supported by the following evidence. Firstly, a total of three equivalents of DIMPI were required to fully form this complex. Secondly, group theoretical analysis suggests that the new species has a 3-fold symmetry because a bis complex would have two bands present in both the Raman and the IR, whereas in the model compound only a single band is observed in the IR. However, if the compound is of $D_{3h}$ or $C_{3v}$ symmetry, two Raman active bands would be observable, and a single IR band would be present, which is what was observed for this compound. Finally, comparison of the data obtained for the above compound with data obtained for a tris-DIMPI-Cu perchlorate compound yielded very similar results.

## 1.5 HOMOLOGY BETWEEN PHM AND D$\beta$M

From the similarities described below, there appear to be a new family of copper containing monooxygenases emerging that require $O_2$, Cu, and ascorbate for activity. These enzymes contain inequivalent copper centers, one of which is ligated an unusual methionine ligand. Sequence alignment studies show that there exists a 28% homology throughout the catalytic domain of D$\beta$M and PHMcc. Furthermore, intrachain disulfide linkages found in D$\beta$M correspond to conserved cysteine ligands in PHM [Southan and Kruse, 1989; Robertson et al., 1994; Kolhekar et al., 1997]. D$\beta$M differs in the fact that it has two additional disulfide linkages. These two linkages crosslink separate monomers [Southan and Kruse, 1989; Robertson et al., 1994; Kolhekar et al., 1997]. The spectroscopic derived active site ligands to the coppers in D$\beta$M are believed to be the same as the active site ligands determined

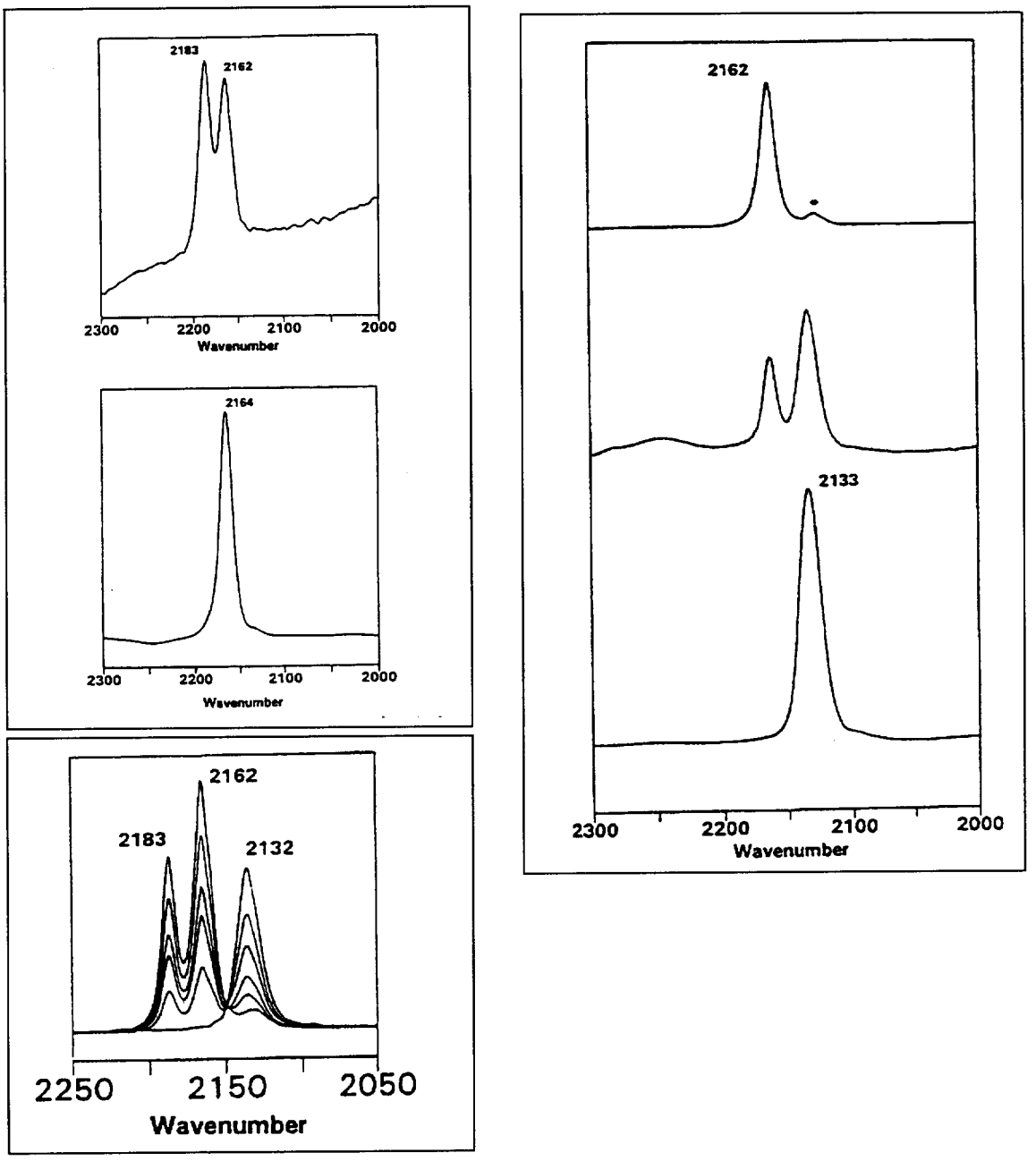


**Figure 1.19** Top right: IR titration of model complex with DIMPI (see text for further detail). Top left: Spectrum of tris-DIMPI Cu(I) perchlorate (top frame = Raman, bottom frame = IR). Bottom left: Raman titration of model compound with DIMPI.

Originally published as Figures 5, 6, and 7 in:
Reedy, B. J., Murthy, N. N., Karlin, K. D., and Blackburn, N. J. (1995) Isocyanides as ligand-directed indicators of Cu(I) coordination in copper proteins. Probing the inequivalence of the Cu(I) centers in reduced dopamine β-monooxygenase. *J. Am. Chem. Soc.* **117**, 9826-9831.

crystallographically in PHMcc. Moreover, the distances between the ligands and the copper centers determined by both EXAFS and through the crystal structure determination are quite similar (Table 1.1). Finally, the site at which hydroxylation of substrate occurs is most likely the same in both enzymes, where conversion of substrate to product takes place at the $Cu_B$ center. This finding is contrary to other T2 copper proteins where $O_2$ chemistry usually occurs at a tris-histidine ligated copper center and a sulfur ligated copper is normally an electron transfer center as seen in T1 containing proteins.

## 1.6 GOALS

Set forth in this thesis are experiments that will enable us to gain valuable knowledge on the active site structure and function of an important enzyme, peptidylglycine $\alpha$-amidating monooxygenase which is involved in the activation of many of the neural peptides found in our cells. The ability to isolate high concentrations of the monooxygenase domain of PAM and the PHMcc mutants will enable us to explore the structure and function of this enzyme without being limited to its availability. Much of the knowledge derived from the study of D$\beta$M will be beneficial in serving as a basis for experimental design.

Our current goals for this study are as follows: to investigate the uptake of copper into the active sites of the protein; to apply this information in the study of the mutants to determine whether they will bind either one or two coppers per protein; to probe, via EPR and FTIR, the two inequivalent copper sites. This will allow us to better understand their individual environments and lead to a better understanding of the catalytic mechanism of this enzyme. Lastly, to study copper depleted PHM active site mutants. This will enable us to selectively probe either the $Cu_A$ or the $Cu_B$ site of the protein, thus gaining information about each site independently from the other.

## Table 1.1

Metal-to-Ligand Distances in DβM and PHMcc

| DβM (EXAFS) | Distance Å | Coordination Number (per Cu) |
|---|---|---|
| Oxidized | | |
| His | 1.99 | 2-3 |
| Oxygen | 1.94 | 1 |
| Reduced | | |
| His | 1.93 | 2-3 |
| Sulfur | 2.25 | 0.5 |

| PHMcc (EXAFS) | Distance Å | Coordination Number (per Cu) |
|---|---|---|
| Oxidized | | |
| His | 1.97 | 2.5 |
| Oxygen | 1.97 | 1.5 |
| Reduced | | |
| His | 1.91 | 2.5 |
| Sulfur | 2.27 | 0.5 |

| Bonds | Distance (X-tal) Å |
|---|---|
| $Cu_A$-H107 | 1.92 |
| $Cu_A$-H108 | 2.07 |
| $Cu_A$-H172 | 2.07 |
| $Cu_B$-H-242 | 1.93 |
| $Cu_B$-H-244 | 2.12 |
| $Cu_B$-M312 | 2.86 |
| $Cu_B$-Solvent | 2.00 |

# CHAPTER 2
# METHODS FOR SPECTROSCOPY, ENZYME EXPRESSION, GROWTH, PURIFICATION, AND COPPER RECONSTITUTION

## 2.1 SPECTROSCOPIC METHODS

### 2.1.1 Infrared Spectroscopy

The basic principle of infrared spectroscopy is that in order to observe an absorption of energy, a molecule must undergo a net change in its dipole moment. Therefore, there must exist a permanent dipole in the molecule that is being studied. When the applied frequency matches the natural vibrational frequencies of the molecule's normal modes, the molecule then absorbs energy and increases one of its own vibrational energy by vibrating with an increased amplitude (Figure 2.1). The energy needed to cause a change from the vibrational ground state to the 1st vibrational excited state is represented by Equation 2.1.

$$E = (v + \frac{1}{2})h\nu \qquad \text{(Eq. 2.1)}$$

Where v is the vibrational quantum number, h is Plank's constant, and $\nu$ is the frequency of radiation that will bring about the observed change. The absorbed frequency depends on the molecular vibrational frequency, however the absorbed intensity depends on how effectively the IR photon energy can be transferred to the molecule and this depends on the change in the dipole moment that occurs as a result of molecular vibration.

### 2.1.2 Electron Paramagnetic Spectroscopy (EPR)

The technique of electron spin resonance spectroscopy can only be applied to species having one or more unpaired electrons. The spin of an electron and its

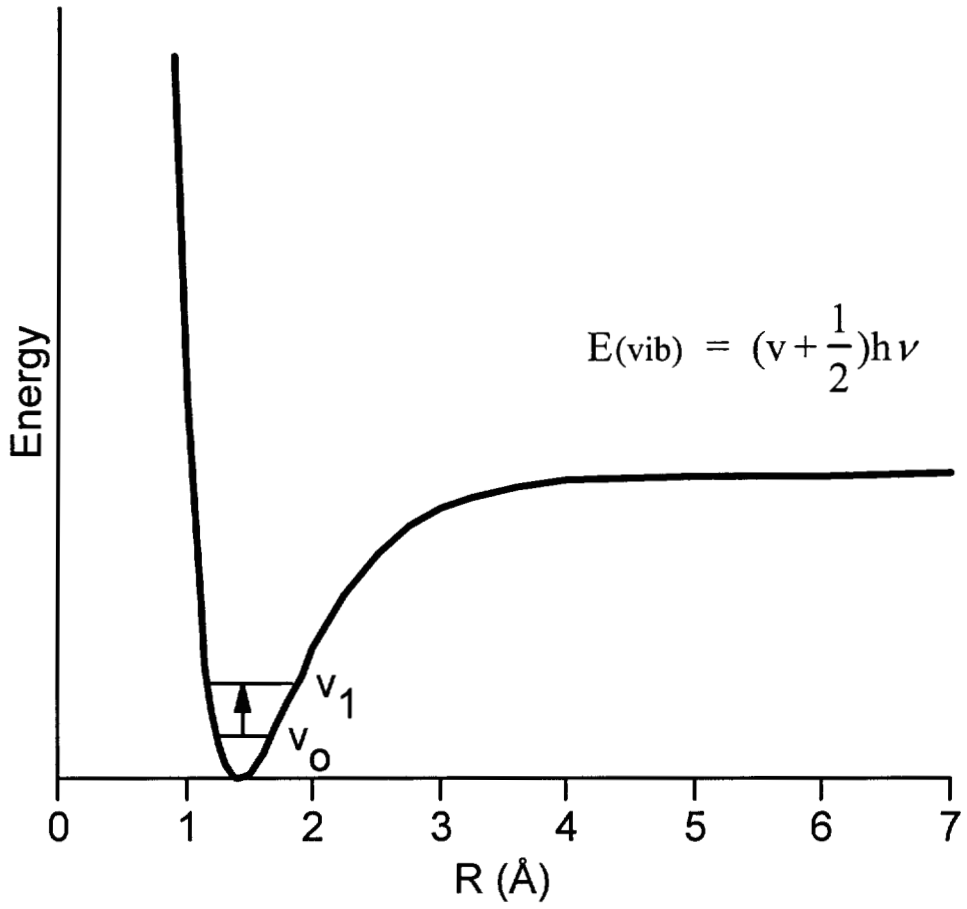


**Figure 2.1** Infrared energy diagram.

associated magnetic moment are the basis of EPR. The different energy states arise from the interaction of the unpaired electron spin moment with the magnetic field. The electron has a spin quantum number of one half and thus has two energy levels that differ slightly in energy under the influence of a strong magnetic field. Resonance is observed when the microwave quantum energy exactly equals the spacing between the levels (Figure 2.2). The energy needed to observe this resonance can be quantified by Equation 2.2,

$$E = g\beta H \qquad \text{(Eq. 2.2)}$$

where $\beta$ is equal to the Bohr magneton, g is the electron splitting factor, and H is the magnetic field strength.

### 2.1.3 X-ray Absorption Spectroscopy (XAS)

Figure 2.3 depicts an example of a spectrum obtained by XAS. This technique involves an input of energy that is sufficient to eject a core electron from the ground state into the continuum. This ejection of an electron is characterized by the sharp absorption edge that is generated upon excitation at the appropriate X-ray energy. The absorption known as K-edge is when the photoelectron originates from the 1s core level of the atom being studied. Promotion of this photoelectron into empty 3d, 4s or 4p energy levels results in spectral absorption features that can be seen in the sharp absorption edge of the spectrum. The edge region contains information about the oxidation state, covalency, site symmetry and coordination number of the system being studied.

At energies above the edge, there is an oscillation in the absorption due to the interference between the outgoing photoelectron wave and components of the wave backscattered from neighboring atoms in the molecule. This region of the spectrum is known as the extended X-ray absorption fine structure (EXAFS) and contains information about the separation between the absorbing and backscattering atoms as well as the number and identity of the backscatterer.

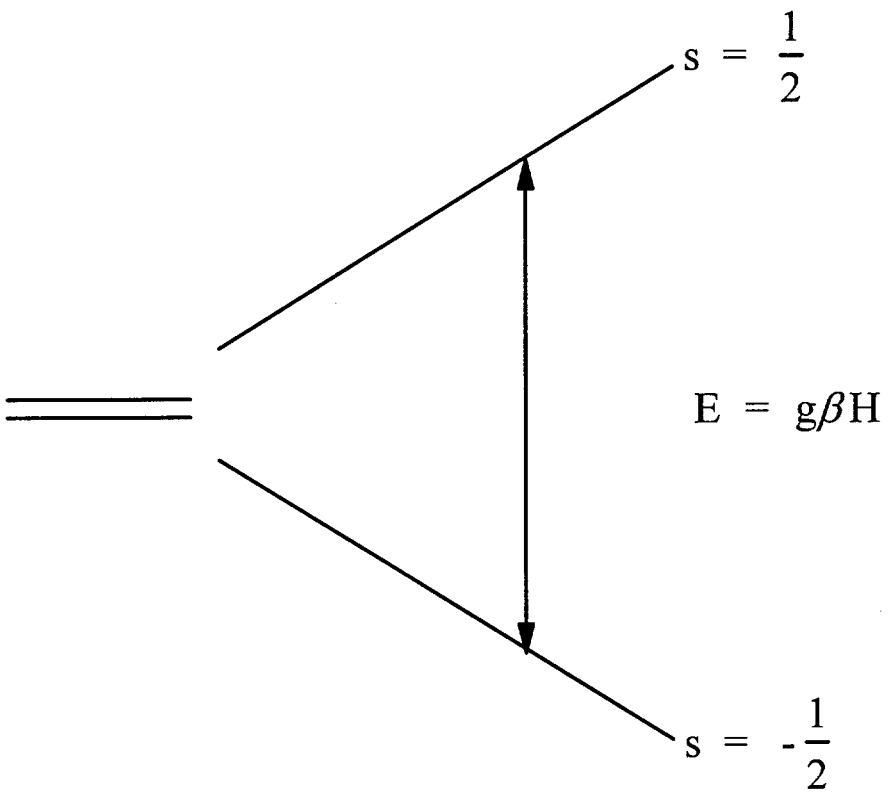


**Figure 2.2** EPR energy diagram.

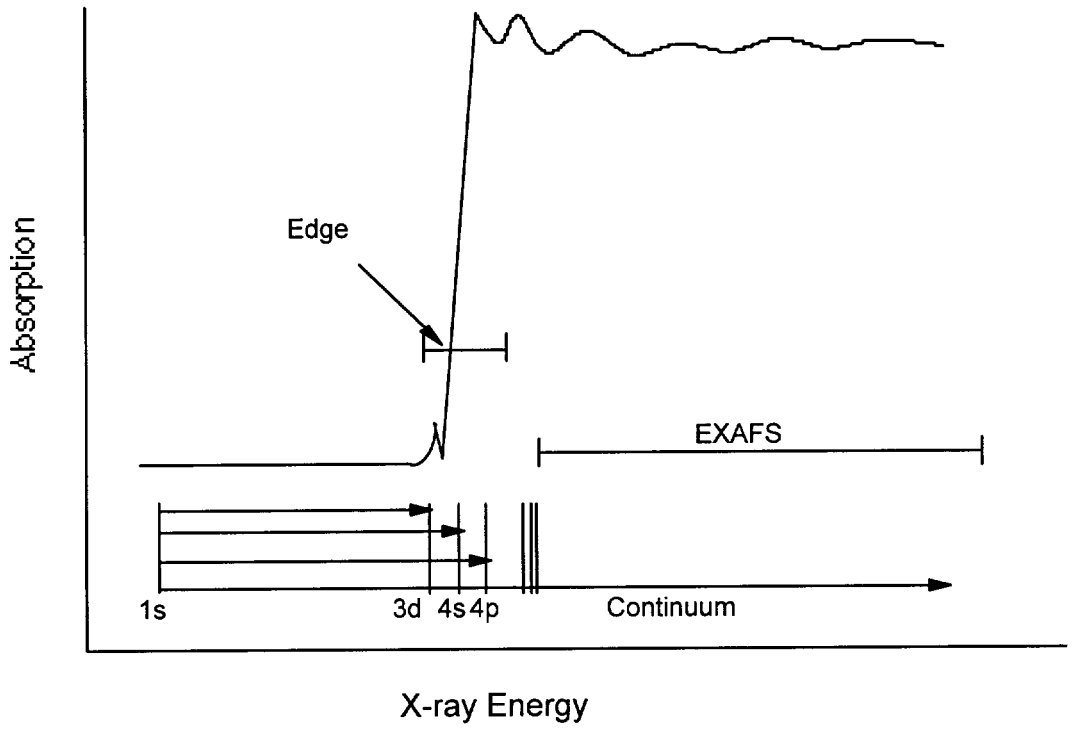


**Figure 2.3** An example of an XAS spectrum.

## 2.2 CELL GROWTH

### 2.2.1 Preparation of Medium for Cell Culture

Minimal medium was prepared as follows. To 1 L of deionized (Nano-pure) water was added 1 packet α-MEM, 1.23 g of HEPES, 1.35 g of glucose, 0.12 g of penicillin G, 0.2 g of streptomycin sulfate, and 0.6 g of glutamine. The pH was adjusted to 7.35, and the solution stirred for 30 min, after which 2.2 g of sodium bicarbonate was added. For serum-containing medium, 100 mL of dialyzed calf serum (Hyclone) was added to 900 mL of medium, and the solution was sterile filtered into 1-L glass or polycarbonate bottles. The medium was stored sterile at 4°C.

DMEM/F12 medium was prepared as above, except that a 1-L packet of DMEM/F12 was used instead of α-MEM. Serum-containing medium was prepared by adding 100 mL of fetal clone II (Hyclone) to 900 mL of medium, followed by sterile filtration into glass bottles. The medium was stored sterile at 4°C. Complete serum-free medium (CFSM) was prepared as above, except that dialyzed calf serum or fetal clone II was omitted and 2.5 mg insulin and 0.5 mg of transferrin were added per liter of medium. The solution was sterile filtered and stored at 4°C.

### 2.2.2 Cell Lines and Cell Growth

The cell lines used to express and purify PHMcc and the mutant forms of PHMcc were constructed and kindly provided by Drs. Richard E. Mains and Betty A. Eipper (Department of Neuroscience, The Johns Hopkins School of Medicine). The pCIS.PHMcc vector carrying the PHMcc gene was constructed and stably transfected into a Chinese hamster ovary (CHO) cell line DG44 (dhfr-) (created by Dr. L. A. Chasin, Columbia University). Full details are described by Eipper and coworkers [Kolhekar et al., 1997]. Frozen cells were thawed and grown initially on minimal medium (α-MEM, GIBCO), containing 10% dialyzed calf serum in order to ensure positive selection for cells that retained high copy numbers of the pCIS.PHMcc vector. After the first passage, the medium was changed to DMEM/F12 (GIBCO) containing 10% fetal clone II (Hyclone) which produced more rapid cell growth and

higher rates of division than the minimal medium. Cell mass was amplified in NUNC triple flasks until a confluent area of 0.3–0.4 $m^2$ was achieved. At this point the cells were trypsinized, resuspended in 75 mL of the DMEM/F12/fetal clone II serum-containing medium, and inoculated into a Cellmax 100 1.1 $m^2$ hollow-fiber bioreactor (Spectrum). In this system, the cell mass grows on the outside of the hollow fiber capillaries through which oxygen-rich medium flows. Since the hollow fibers have a 4-kD molecular weight cut-off, the secreted proteins, including PHMcc, concentrate in the extra capillary space and can be harvested daily.

The cell mass was grown for approximately 10 days on the serum-containing DMEM/F12/fetal clone II medium. The volume of medium circulated through the bioreactor was 1 L, and the medium was changed when the glucose level dropped below 50%, and/or the pH dropped below 6.6. At 3-day intervals, the medium within the extra capillary space (in contact with the growing cell mass) was drained, and fresh DMEM/F12/fetal clone II containing medium was introduced. After 10 days, the serum was eliminated from the medium, and the cells were switched to growth on CSFM. The extra capillary medium ($\sim$60 mL) was harvested daily, but the initial 4–5 days of harvested medium was discarded because activity levels typically rose sharply after about one week of operation. The bioreactor consumed 1 L of CSFM per day, and the average daily PHMcc production was approximately 7–10 mg.

## 2.3 PURIFICATION PROTOCOL FOR PHMcc

### 2.3.1 Chromatography

This protocol is applicable for both wild-type PHMcc and the various mutant forms of PHMcc. Typically, seven days of protein were thawed in a warm water bath and agitated manually to ensure uniform thawing. The volume of liquid was then measured and pooled together. Ammonium sulfate (AmS) was slowly added, over 15 min, to the protein to form a final solution that was 50% saturated (0.291 g/mL). This was then allowed to stir at 5°C for 1 h. The solution was then centrifuged at 9000 g for at least 40 min. The liquid was discarded and the pellet was

isolated and redissolved in a minimum volume of 50 mM potassium phosphate pH 7.4, usually requiring between 13 and 25 mL of the buffer. The redissolved solution was centrifuged again to remove any of the insoluble solids that remained.

The crude protein was then applied to a 26/60 Hiload Superdex 75 prep grade size exclusion column (Pharmacia) that had been equilibrated with two column volumes of 50 mM potassium phosphate. The column was connected to a Pharmacia FPLC chromatographic system. The injection volume was no more than 13 mL, or 1% of the column volume, and the flow rate was 2.5 mL/min. Figure 2.4 shows the typical profile of this separation process. The initial void peak eluted after 90–100 mL of buffer had flowed through the column. The fraction displaying the PHMcc protein eluted at ~170 mL and was collected until the detector absorbance returned to the baseline. This fraction was then concentrated and dialyzed overnight against 100 mM potassium phosphate containing 500 mM AmS, pH 7.4.

The dialyzed sample was then applied to a Phenyl Superose HR 10/10 (Pharmacia) hydrophobic interaction column (HIC) that had been equilibrated with two column volumes of buffer containing the same components as the dialysis buffer. The injection volume was kept between 4–6 mL and the flow rate was between 0.5 and 1.0 mL/min. Figure 2.5 shows the profile of the HIC chromatography step. The initial void peak started to elute after 5–8 mL of buffer had been applied to the column and continued to elute for another 15–20 mL. After the detector absorbance had returned to the baseline, a gradient from 0 to 100%, over 5 mL, of a second buffer containing 50 mM potassium phosphate and no AmS at pH 7.5 was employed. This essentially changed the buffer being passed through the column from one containing high amounts of AmS to one containing no AmS. After ~8 mL of the second buffer had flowed through the column, the PHMcc protein fraction started to elute. This fraction was collected and concentrated to about 3 mL for analysis and copper reconstitution. As isolated, the enzyme was 90–95% pure via SDS-PAGE electrophoresis. On average, 50 mg of pure PHMcc was obtained from a seven day bioreactor harvest.

The purification of wild-type and mutant forms of PHMcc has been developed into a protocol that is quite facile and very reproducible. Initially, this was a two step

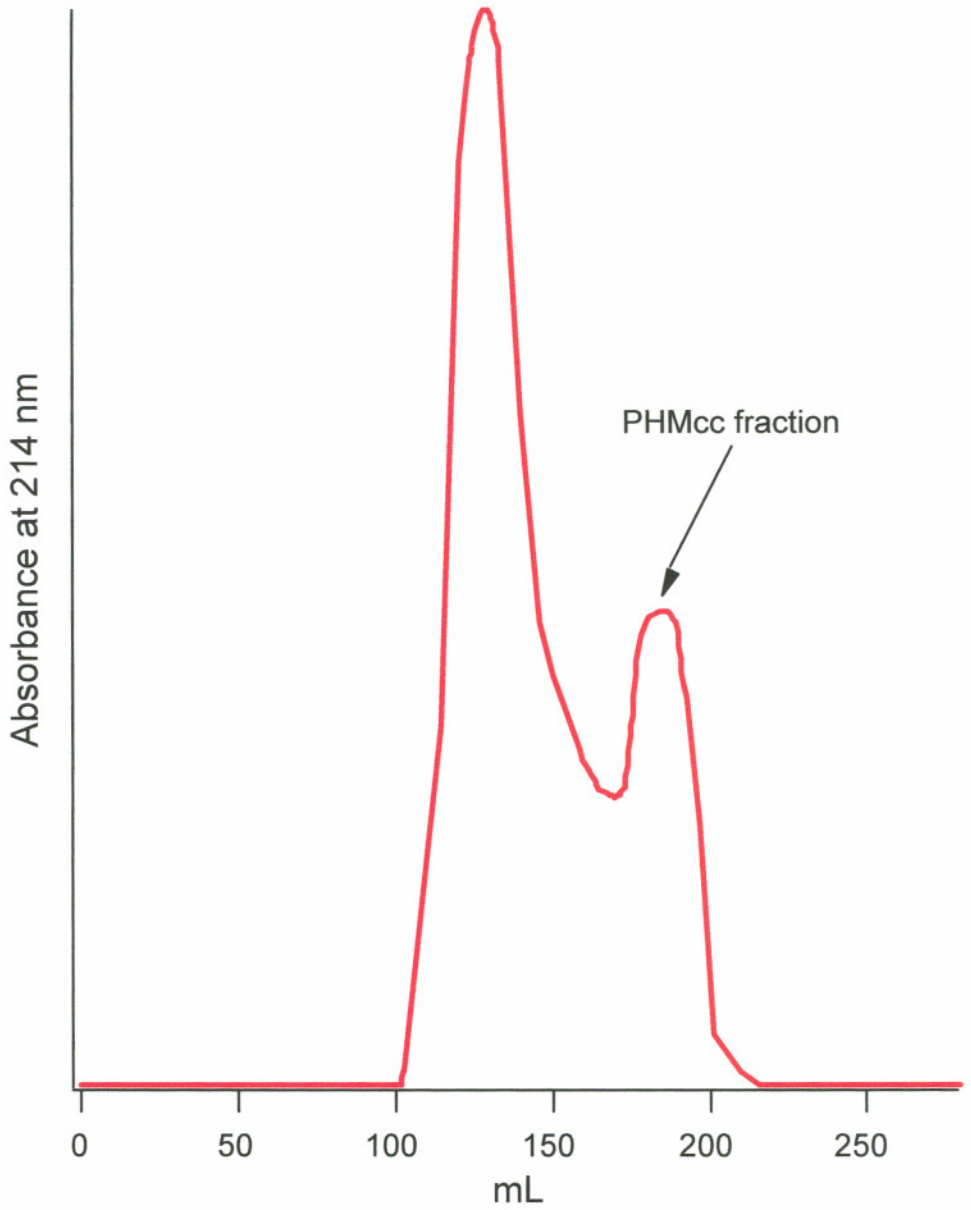


**Figure 2.4** A typical gel filtration chromatogram for PHMcc (red line).

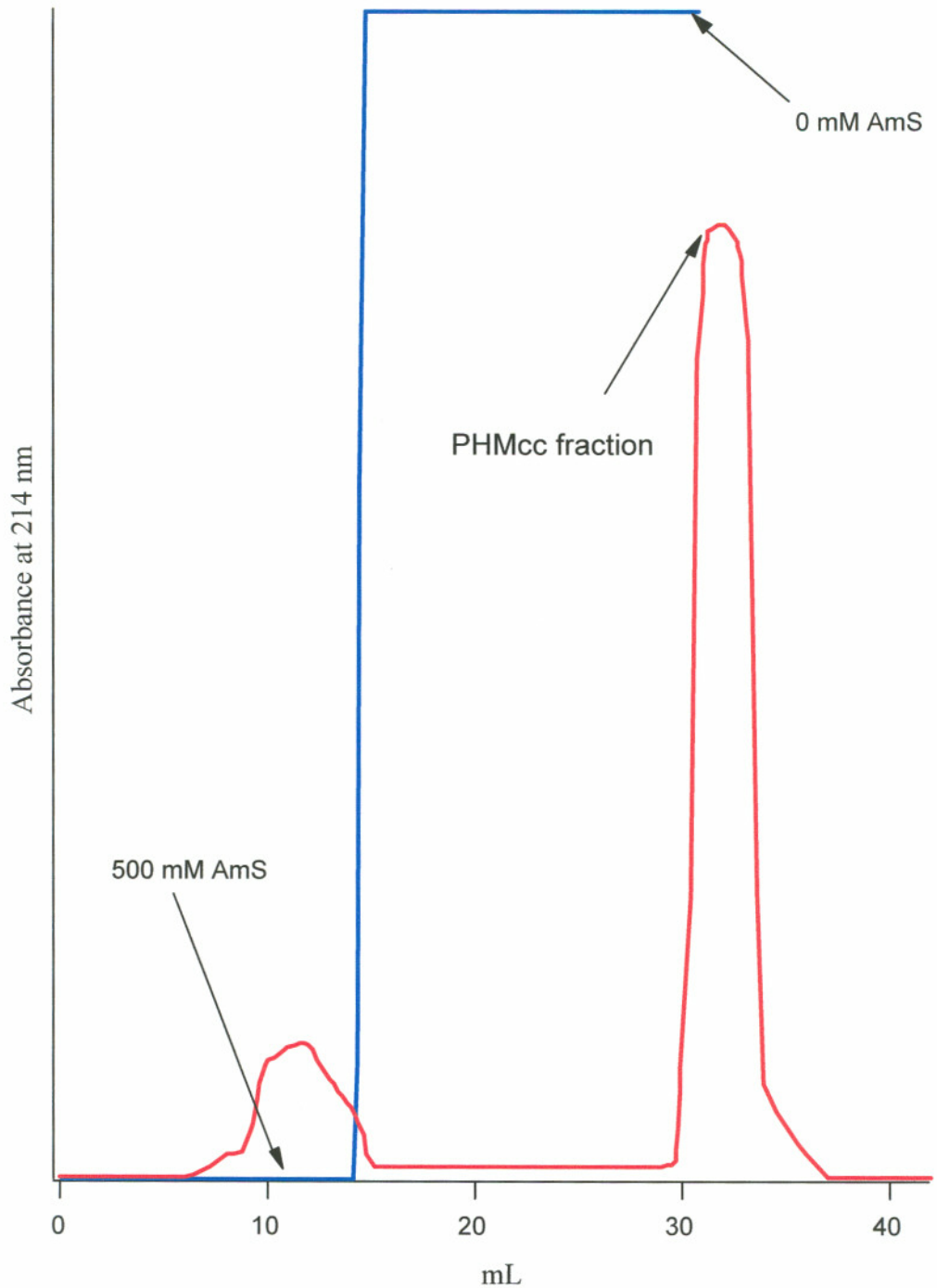


**Figure 2.5** A typical HIC chromatogram for PHMcc (red line). The blue line represents the buffer gradient applied to the column.

chromatographic process that started with crude protein that had been concentrated from ~300 mL to a volume between 13–25 mL through the use of a stirred cell concentrator. However, calculation of the total active protein present in the crude to the total active protein present after the initial gel filtration step revealed that significant (20–25%) amounts of PHMcc was being lost. Since proteins do not normally adhere to a gel filtration column, it was believed that the loss of protein was occurring during the initial concentration of the crude protein. Two possibilities can account for this loss, the first being that the PHMcc may form large aggregates at higher concentrations and thus, precipitate out of solution. The second possibility could be that the PHMcc is hydrophobic enough to adhere to the membrane being used in the stirred cell.

In overcoming this problem, it was decided that the crude protein could be concentrated by precipitation of the initial crude protein with AmS. To find the proper saturation amount of AmS needed to precipitate all of the PHMcc from the dilute crude liquid, a series of experiments were set up where increasing percentages of saturated AmS were added to the liquid until the PHMcc activity could no longer be detected via the $O_2$ electrode assay. It was determined that a 50% saturated solution of AmS was a sufficient amount needed to precipitate about 95% of the PHMcc from the crude liquid. Therefore, the initial concentration step of the purification protocol was changed from the stirred cell method to the AmS precipitation step with a resulting gain in the protein recovery of 25%.

### 2.3.2 Enzyme Assay

PHMcc activity was assayed by following the rate of oxygen uptake with an oxygen sensitive electrode. The reaction mixture was kept at a constant volume and temperature (2 mL, 37°C). The mixture was comprised of 1.66 mL MES (150 mM, pH 5.5), 200 $\mu$L catalase (1300 units, 0.1 mg/mL), 100 $\mu$l $CuSO_4$ (100 mM), 10 $\mu$L ascorbate (200 mM), 10 $\mu$l AcTyrValGly (25 mM), and 10 $\mu$l PHMcc (0.3–1.5 mg/mL). The MES, ascorbate, copper sulfate, catalase, and PHMcc were added to the stirred cell and allowed to equilibrate until a flat baseline was established. The baseline was determined to be equal to 178 $\mu$M of $O_2$ in $O_2$-saturated water at 37°C.

The reaction was initiated by the addition of the peptide substrate. The activity was calculated from the slope of the linear line corresponding to $O_2$ uptake by PHMcc. The specific activity of the enzyme ranged between 15 and 20 $\mu$M $O_2$ consumed per min per mg of PHMcc.

### 2.3.3 Determination of Copper and Protein Concentrations

Initial protein concentrations were calculated using the Bicinchoninic Acid Protein Assay Kit (Sigma). The extinction coefficient ($A_{0.1\%}$ 280 nm) was then calculated for PHMcc by using the concentration of protein determined from the protein assay. The average of six experiments led to the determination of $\epsilon$ to equal 0.98. Protein concentration for all subsequent studies were determined from the optical density at 280 nm using a Shimadzu UV/Vis spectrophotometer at room temperature. Copper concentrations were determined by flame atomic absorption on a Varian-Techtron atomic absorption spectrometer against standard copper solutions that would fall on the standard curve. All proteins measured were diluted so their measured Cu amount would correlate to the standard curve.

## 2.4 COPPER RECONSTITUTION

In order to develop a definitive laboratory protocol for reconstitution of PHMcc with Cu, three different methods were explored. The aim was to develop a method that was reproducible, time efficient, and reconstituted the protein to appropriate levels of copper. The importance of a protocol that ensures full reconstitution of the protein becomes critical when comparing the wild-type enzyme with the physical properties of the various mutant forms of PHMcc. If the conditions under which copper reconstitution that give rise to a ratio of 2 Cu/protein in the wild-type enzyme were not determined, then when examining the copper/protein ratio of the mutants, we could not positively say exactly how much copper the mutants bound, since we would not be sure whether the reconstitution conditions allowed for fully loading of the protein or the protocol was actually limiting the amount of copper available in the buffer. Once these conditions were known, then determination of the

copper binding ratio of the mutants would allow for a more conclusive comparison to the wild-type enzyme.

### 2.4.1 Gel Filtration

The first method investigated utilized a high-resolution gel filtration column to reconstitute the protein. This was performed by injecting 100 $\mu$L samples of apo enzyme onto a Superdex 75 HR 10/30 column (Pharmacia) that was equilibrated with 50 mM potassium phosphate (pH 7.4) into which varying amounts of free $Cu^{2+}$, as cupric nitrate, were added. Each copper concentration was repeated three times and the average level of Cu/PHMcc was calculated. The results from this study show that there may exist two distinct stages in reconstitution of PHMcc (Figure 2.6). Between 1 and 3 $\mu$M of free $Cu^{2+}$ in the buffer, the Cu/PHMcc was almost 1 to 1. As the amount of available $Cu^{2+}$ increased to between 4–5 $\mu$M, the ratio also increased to 1.5 to 1. Finally, when the amount of $Cu^{2+}$ in the buffer was increased to either 6 and 7 $\mu$M, the Cu/PHMcc ratio increased to 2 to 1. Higher concentration of free $Cu^{2+}$, tended to lead to adventitious binding of $Cu^{2+}$ to the protein. Copper loading by this method appeared to be linear, where the initial increase of the Cu/PHMcc ratio of 1 to 1 was followed by a plateau in the Cu/PHMcc ratio. This was subsequently followed by a second increase of the ratio to 2 to 1. However, when the percent error for each ratio was taken into consideration, the copper reconstitution profile by this method could be considered linear.

The second method explored for reconstitution was to add back copper through the use of a stirred-cell concentrator (Amicon). The protein collected from the final HIC chromatographic step was placed into a 150 mL stirred-cell that was fitted with a 10-kD cutoff membrane (YM10). The cell was filled with the phosphate buffer containing a predetermined amount of free $Cu^{2+}$, between 5 and 25 $\mu$M. Under 2.4 atm of $N_2$, the solution was concentrated to a final volume of 3 mL and both the protein and copper concentrations were measured. Figure 2.7 shows the results obtained from this study. Each trial was repeated three times and the average Cu/PHMcc ratio was calculated. The results show that this method appears to reconstitute the protein with higher Cu/PHMcc ratios achieved as the amount of free

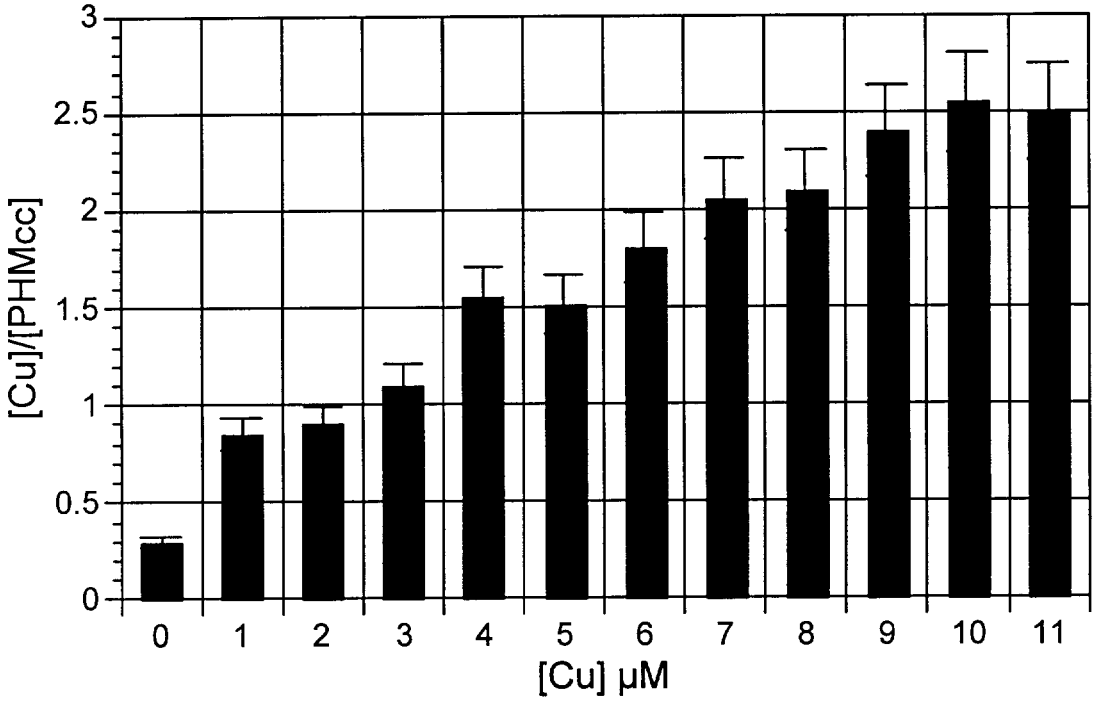


**Figure 2.6** Plot of the Cu/PHMcc ratio versus the amount of background $Cu^{2+}$ added to the phosphate buffer used in the reconstitution by gel chromatography. Each bar is an average of three trials.

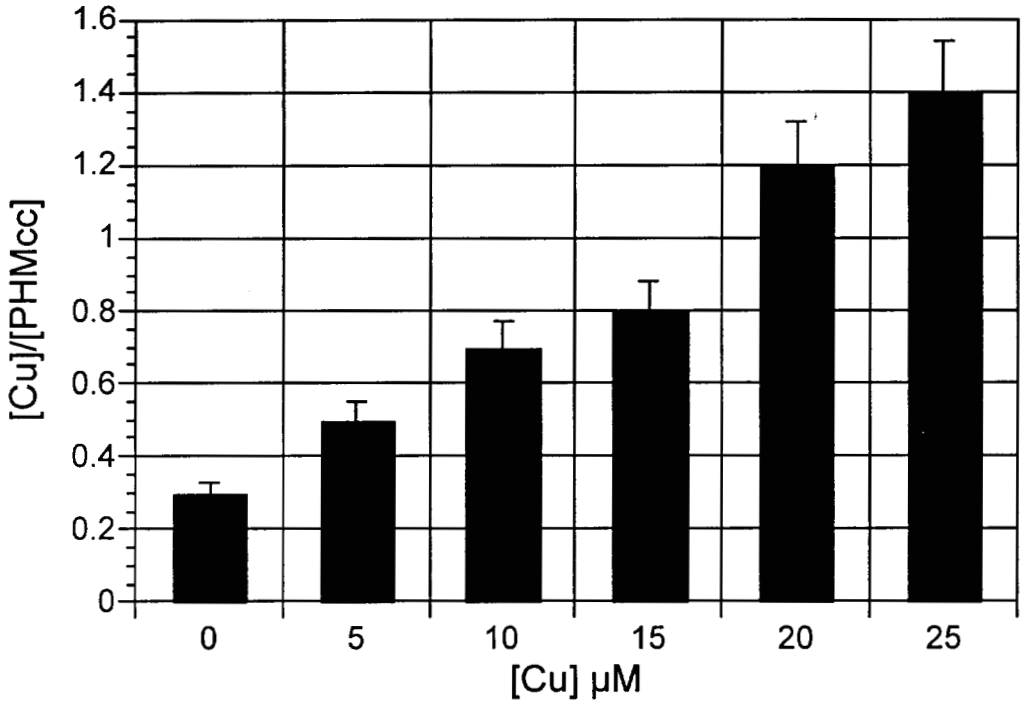


**Figure 2.7** Plot of the Cu/PHMcc ratio versus the amount of background $Cu^{2+}$ added to the phosphate buffer used in the Amicon reconstitution study. Each bar is an average of three trials.

$Cu^{2+}$ in the buffer increased. However, it also appeared that between 10-15% of the protein was lost during the reconstitution, probably due to the enzyme adhering to the membrane. Therefore, this method was not explored further.

The final reconstitution method studied was to reconstitute the protein by dialyzing PHMcc against free $Cu^{2+}$ dissolved in the phosphate buffer. To determine the amount of free $Cu^{2+}$ needed to achieve full reconstitution of the enzyme, a series of dialysis experiments were set up in which 300 $\mu$l samples of protein were dialyzed against concentrations of $Cu^{2+}$ varying between 5 and 25 $\mu$M. The samples were allowed to dialyze for two days with a buffer change after the first day. The results for this method show a linear increase of copper/PHMcc ratio as the amount of $Cu^{2+}$ in the dialysis buffer increased (Figure 2.8). The maximal Cu/PHMcc ratio of 1.8 was achieved by dialyzing the protein against 25 $\mu$M potassium phosphate for two days.

### 2.4.2 EPR Analysis of Copper Reconstitution

The copper reconstitution via gel chromatography was followed by EPR. At each free $Cu^{2+}$ concentration level, the fractions collected from the column were concentrated to 500 $\mu$L. EPR measurements were performed on a 200 $\mu$L aliquot of this sample. Figure 2.9 shows an example of an EPR signal obtained from reconstitution of the protein in this manner. The signal appeared to be comprised of copper atoms in two different species. This signal could arise from the gel column possibly unfolding the protein resulting in copper being incorporated into the protein not at the active site. Furthermore, when a direct comparison of the signal generated by reconstitution via the chromatographic method is compared to EPR signals obtained from reconstitution by dialysis, or what was previously observed [Boswell et al., 1996], it becomes apparent that the chromatographic reconstitution method is altering the spectral properties of the copper centers (Figure 2.10).

The reconstitution of PHMcc via the dialysis method was also followed by EPR. Figure 2.11 shows the results of a series of increasing ratios of Cu/PHMcc generated by this method. The spectra derived from the protein at high levels of copper coordination closely resemble the previously published spectrum for the

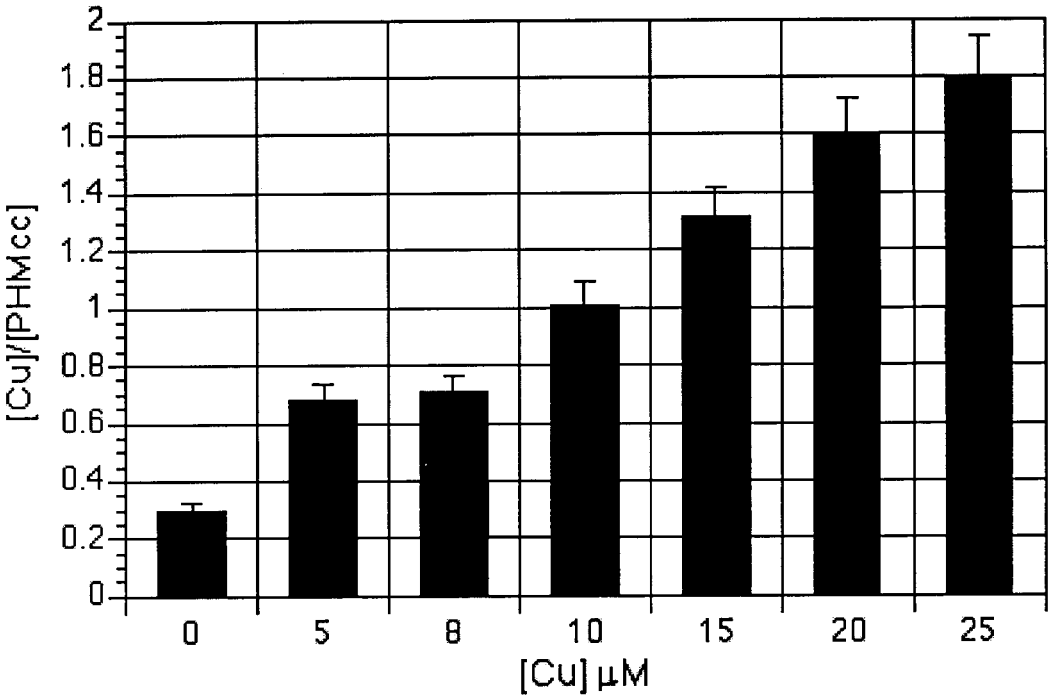


**Figure 2.8** Plot of the Cu/PHMcc ratio versus the amount of background $Cu^{2+}$ added to the phosphate buffer used in the dialysis reconstitution study. Each bar is an average of three trials.

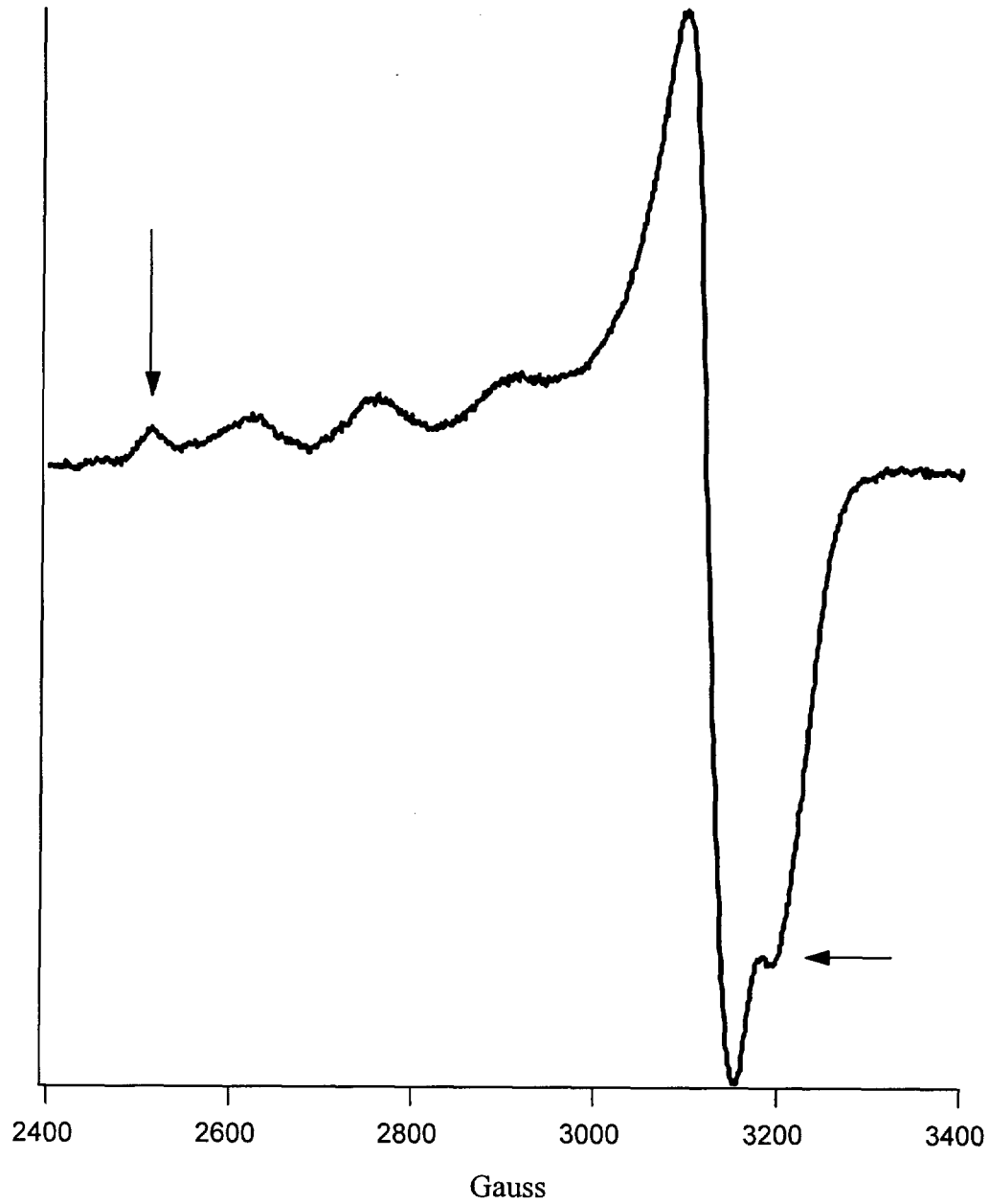


**Figure 2.9** EPR spectrum of PHMcc reconstituted to 1.6 Cu/protein via gel chromatography. The arrows highlight the atypical $Cu^{2+}$ signal.

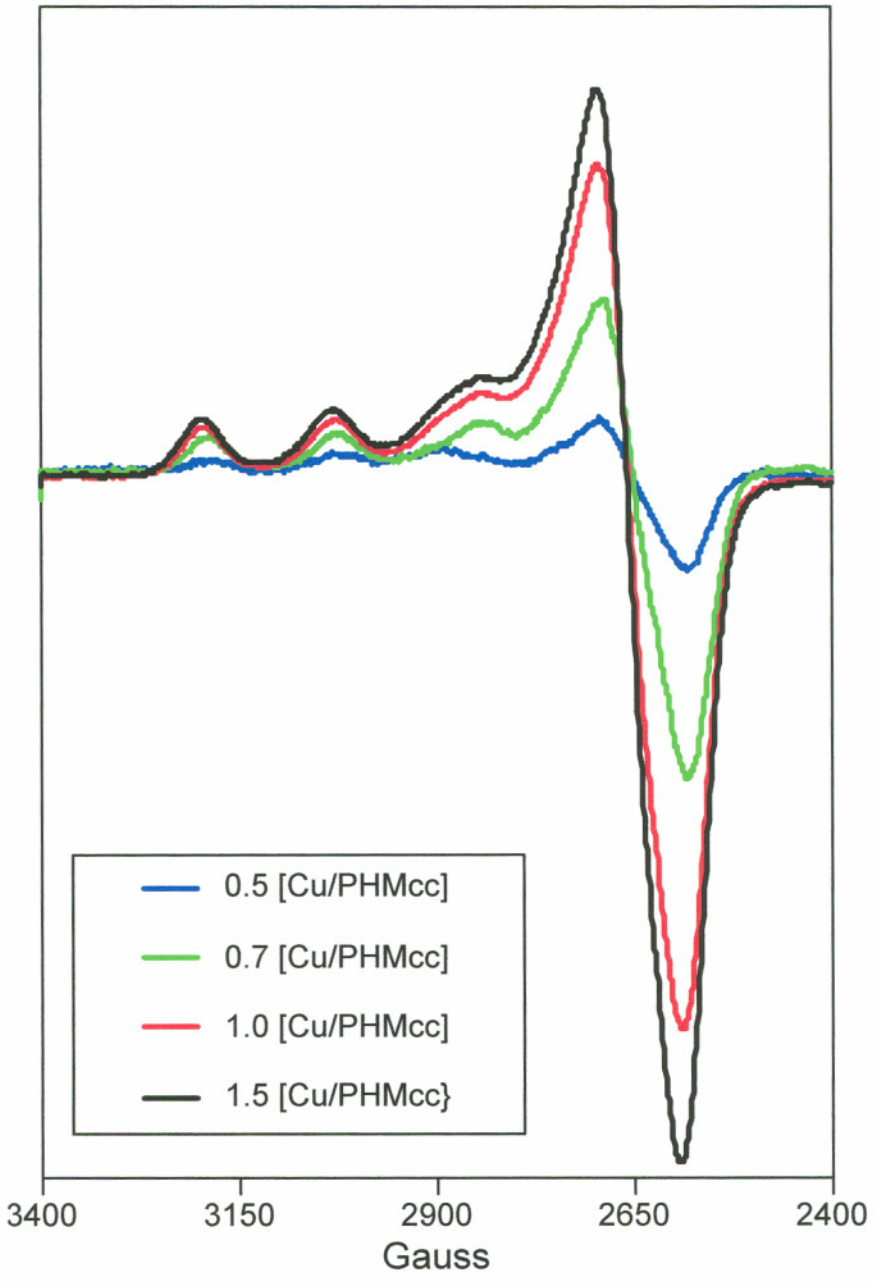


**Figure 2.10** EPR spectrum of PHMcc reconstituted to 1.6 Cu/protein via dialysis. The arrows highlight the atypical $Cu^{2+}$ signal. Labeled from lowest to highest intensity.

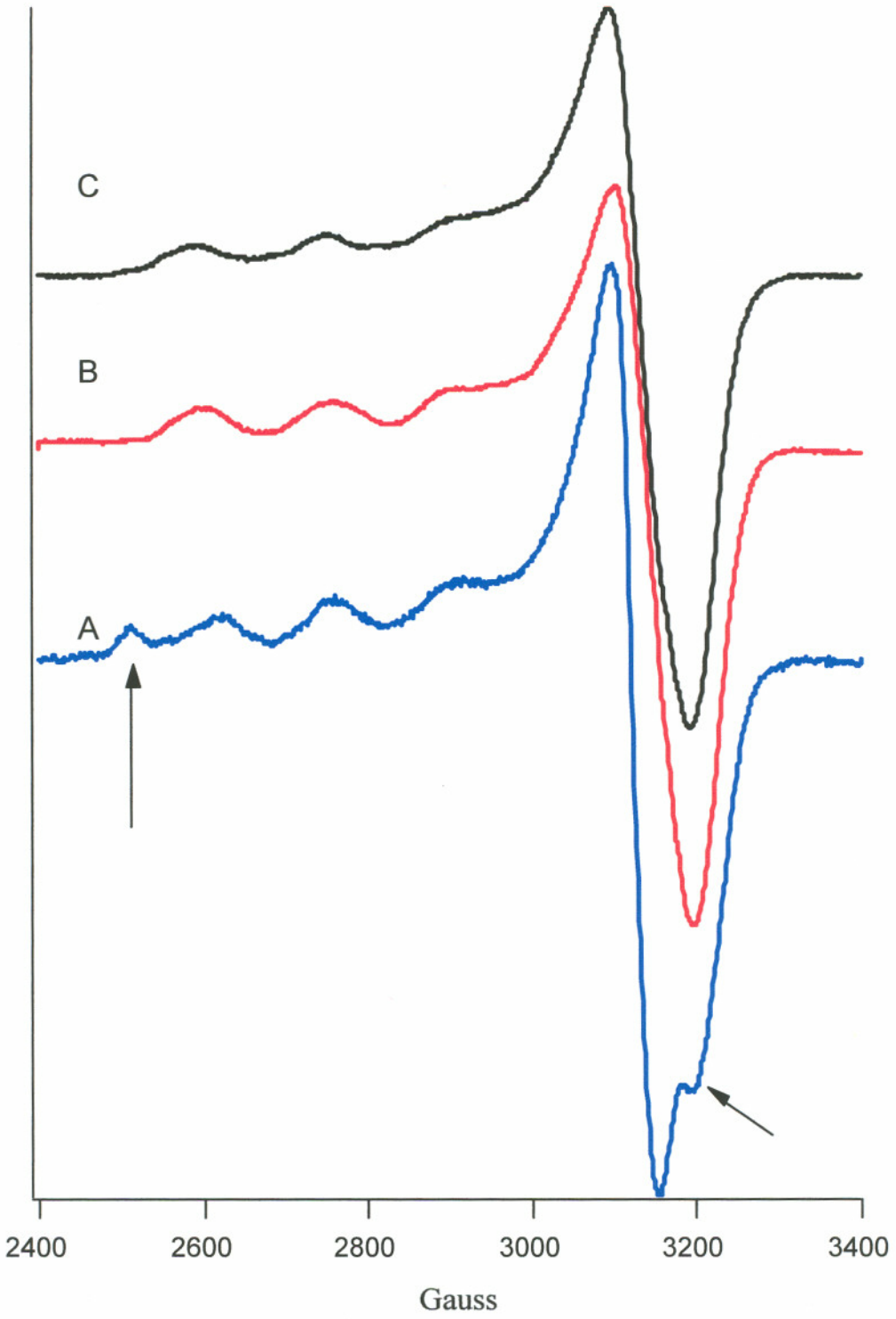


**Figure 2.11** Comparison of the EPR signals generated by three different reconstitution methods. (A) Via gel chromatography; (B) via dialysis; (C) via $^{63}Cu^{2+}$ titration.

bifunctional enzyme [Boswell et al., 1996]. Interestingly, the spectra also show that there may exist two separate copper signals that comprise the final fully metallated EPR signal for PHMcc, where a second signal is seen to grow in as the copper reconstitution increased.

### 2.4.3 EPR Titrations of Copper Binding

In order to examine the two different signals seen in the reconstitution study, the reconstitution behavior of the apo wild-type protein was investigated by EPR titration. Figure 2.12 shows the EPR spectra of a 200 $\mu$L sample of 335 $\mu$M PHMcc in 50 mM potassium phosphate, pH 7.5, titrated with 3.5 $\mu$L aliquots of a stock 10 mM solution of $^{63}$Cu cupric nitrate solution. The spectra show that the EPR signal of the fully metallated protein may be comprised of two distinct signals. It appears that as the copper concentration increased, the EPR spectrum appears to contain a $g_{\parallel}$ and $g_{\perp}$ region that was shifted to lower g-value when compared to the EPR signal of the lowest Cu/PHMcc spectrum. Also, a new spectral feature was seen to grow in ($\sim$2900 G) as the copper concentration increased.

The observed titratable EPR signal could arise from two different scenarios. The first possibility is that there are two different binding constants for each copper site, where one copper site is filled first, followed by copper incorporation into the second site. Therefore, each signal observed could be from the individual copper centers and each center has a distinct geometry contributing to the two different EPR signals. The second possibility is that each copper site is filled non-specifically. This would suggest that as the protein becomes more metallated, the geometry surrounding the Cu centers changes equally, resulting in a slight shifting of the EPR signal. However, this would suggest that the spectrum observed for the fully metallated protein be derived from two copper centers generating an equal EPR signal. Repeated attempts to simulate the spectrum using a single copper signal have not generated a sufficiently accurate fit.

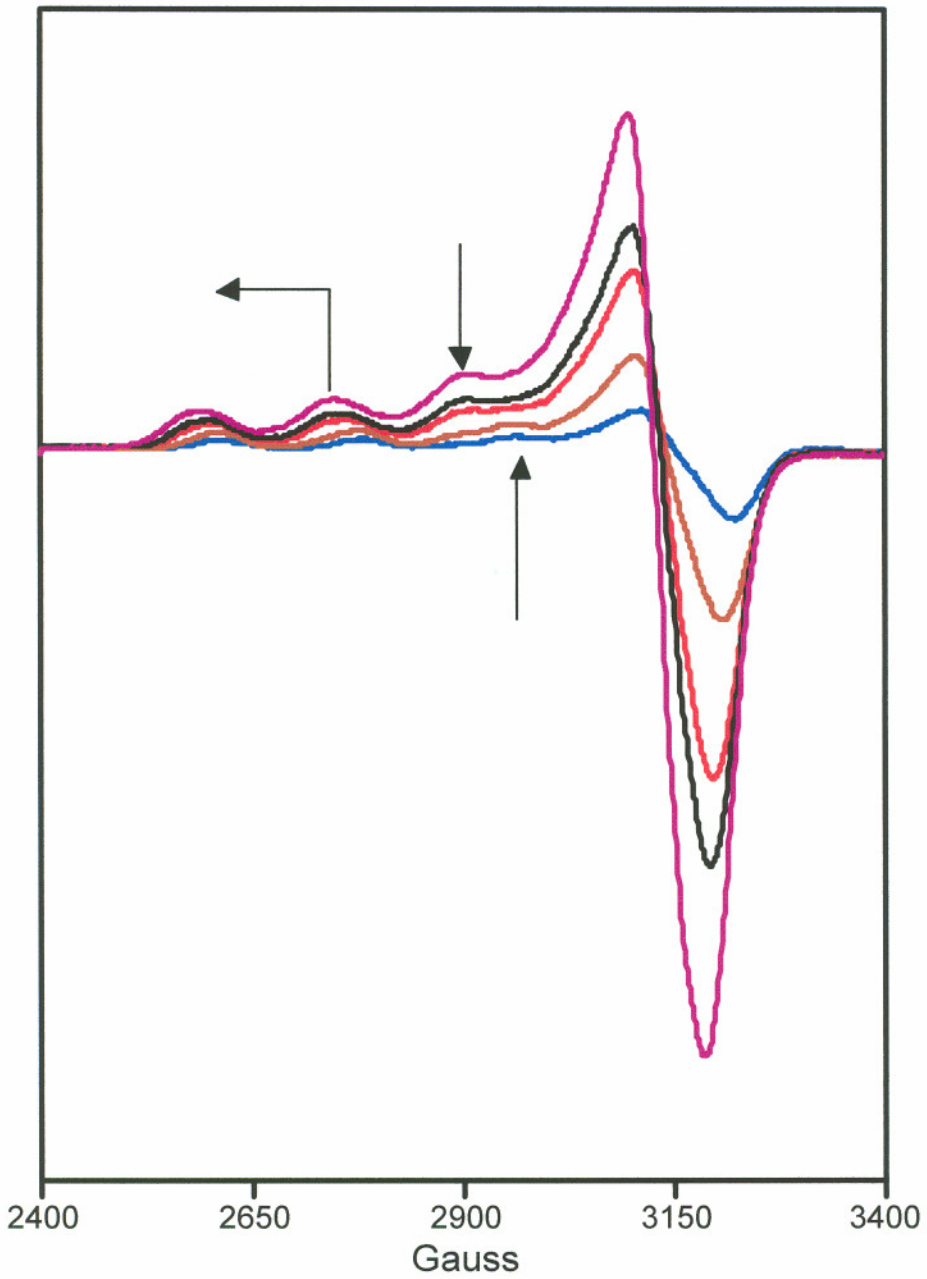


**Figure 2.12** EPR spectrum of PHMcc titrated with $^{63}Cu^{2+}$. Blue = 0.3 Cu/PHMcc; brown = 0.5 Cu/PHMcc; red = 1.0 Cu/PHMcc; black = 1.25 Cu/PHMcc; purple = 1.75 Cu/PHMcc. Labeled from lowest to highest intensity.

## 2.5 CONCLUSIONS

It was determined that the best method for reconstitution of the PHMcc enzyme was by dialyzing the protein against 25 $\mu$M $Cu^{2+}$ added to 50 mM potassium phosphate buffer (pH 7.4). The reasoning for selecting this protocol over the other methods tried are outlined below. Firstly, protein recovery before and after dialysis was virtually identical, with the only loss of protein arising from the transfer of the sample from the dialysis bag, whereas the chromatographic method required a greater amount of physical handling of the protein. Since the column could only be injected with a maximum of 200 $\mu$L of protein at a time, this required either multiple injections of the sample onto the column or starting with a highly concentrated sample. This also increased the time it took to reconstitute the protein greatly. Secondly, reconstitution via gel chromatography appeared to introduce a non-native copper species into the PHMcc protein that was not seen when the reconstitution was performed under the dialysis conditions.

# CHAPTER 3
# ISOCYANIDE BINDING TO WILD-TYPE PHMcc

## 3.1 INTRODUCTION

The crystal structure of the oxidized form of PHMcc has recently been solved (Figures 1.8–1.10) [Prigge et al., 1997]. The structure shows that the two Cu(II) ions are located on different sub-domains and are approximately 11 Å apart. The copper centers in PHMcc are inequivalent. The crystal structure and XAS of PHMcc has shown that the ligands surrounding each center are not the same for both atoms [Boswell et al., 1996; Prigge et al., 1997]. Whereas $Cu_A$ is ligated by three histidine (His107, 108, and 172) residues in both the reduced and oxidized forms, the $Cu_B$ center has two histidines (His 242 and 244) ligated to it in both oxidation states, and an additional methionine (Met 314) in the reduced form of the enzyme. Furthermore, there is growing evidence that the reactivity of the two centers appears to be quite different, where only one of the coppers ($Cu_B$) is believed to participate in the oxygen chemistry catalyzed by this enzyme and the $Cu_A$ center being responsible for electron donation. However, what the structure does not indicate is how electrons pass from one copper site to the other. Nor does it explain why the $Cu_B$ is involved in $O_2$ binding, since a 2 His/1 Met site seems more suited as an electron transfer center whereas the 3 His $Cu_A$ center is more analogous to $O_2$ binding sites in other copper enzymes and model compounds.

In this chapter, we describe the reactivity of the two copper sites in PHMcc. This has been accomplished by using isocyanide ligands as probes of the reduced Cu(I) centers. Although isocyanides have not been extensively used as probes to Cu(I) centers in proteins, there are a large number of inorganic Cu(I)–isocyanide complexes that have been structurally characterized [Pasquali et al., 1983; Fiaschi et

al., 1984; Toth et al., 1985, 1987, 1988; Ardizzoia et al., 1990, 1992]. Furthermore, previous work from this laboratory has demonstrated the effectiveness of Cu(I)–isocyanide ligation to the Cu(I) centers in D$\beta$M and hemocyanin [Reedy et al., 1995].

From the results described here, it appears that isocyanide binding occurs preferentially at the $Cu_B$ center. XAS analysis of isocyanide bound to PHMcc shows the ligand bound to the $Cu_B$ center only. Theses results further demonstrate the differences in the reactivity of these two Cu centers.

## 3.2 EXPERIMENTAL METHODS

### 3.2.1 Cell Growth/Enzyme Isolation/Activity Measurement/Copper Reconstitution

Details for these methods can be found in Chapter 2.

### 3.2.2 Isocyanide Titration

A typical titration consisted of the following: A 200 $\mu$L sample of oxidized PHMcc (1 mM in copper) was made anaerobic by repeated vacuum flushing with argon. It was then reduced with a five-fold molar excess of anaerobic sodium ascorbate (in potassium phosphate 50 mM, pH 7.4). In an anaerobic glove box, 50 $\mu$L aliquots of the reduced PHMcc were placed in separate 1.5 mL microcentrifuge tubes. To this sample, an aliquot (between 2 and 6 $\mu$L) of an anaerobic stock solution of 2,6-dimethylphenyl isocyanide (DIMPI) or isopropyl isocyanide (IPI) (10 mM in methanol) (Figure 3.1) was added to achieve the isocyanide to copper ratio that was desired. The isocyanide and the ascorbate were both prepared fresh daily. The sample was found to be fully reduced, as evidenced by the lack of any copper EPR signal.

### 3.2.3 Fourier Transform Infrared (FTIR) Measurements

FTIR spectra were recorded on a Perkin Elmer 2000 FTIR spectrophotometer. Solution IR protein spectra were collected at 10°C using a liquid nitrogen-cooled

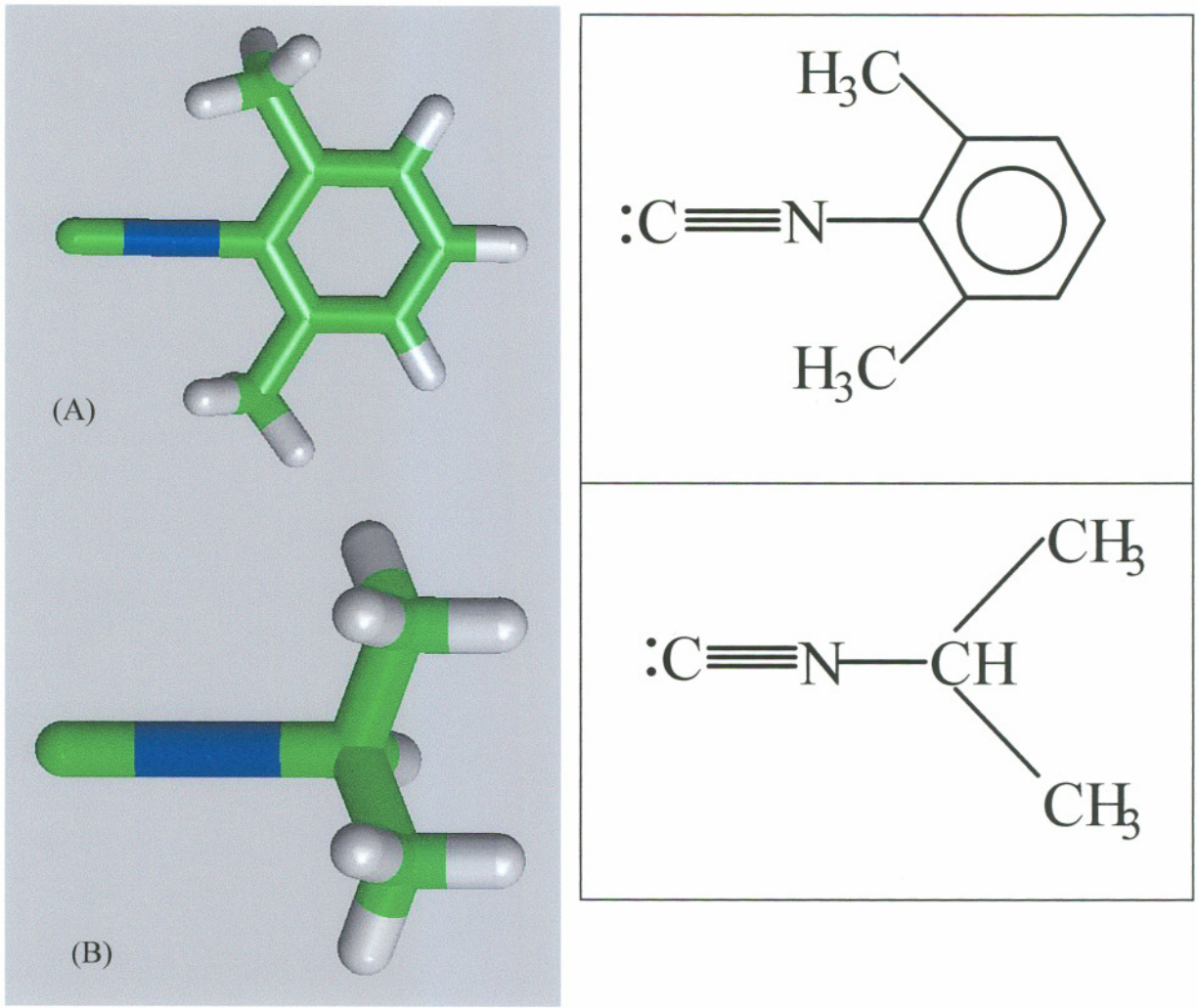


**Figure 3.1** The structures of (A) 2,6-dimethylphenyl isocyanide (DIMPI), and (B) isopropyl isocyanide (IPI).

MCT detector in 50 $\mu$m path-length calcium fluoride cells. Two hundred scans were collected for each protein and background sample under identical conditions. Instrument resolution was set to 2 $cm^{-1}$. Background spectrum was obtained by using molar equivalent (to copper) of isocyanide diluted in potassium phosphate buffer (50 mM pH 7.5). Each individual PHMcc-isocyanide spectrum was subsequently subtracted from the background spectrum of the potassium phosphate-isocyanide that correlated to the correct ratio of isocyanide to PHMcc. All reported spectra are differences of bound isocyanide and free isocyanide in buffer. Analysis and spectral deconvolution curve-fitting were performed using the program IGOR PRO (WaveMetrics). In all cases, bands containing more than one component were simulated by the sum of pure Gaussian components.

### 3.2.4 X-ray Absorption (XAS) Sample Preparation

To a reduced PHMcc sample (2.0 mM in copper) containing 20% v/v of ethylene glycol, 0.5 mol equivalent of DIMPI was added. To ensure a predominate single isocyanide species, the IR of the sample was taken. This sample was then frozen in liquid $N_2$ anaerobically and stored in liquid $N_2$.

### 3.2.5 XAS Data Collection and Analysis

XAS data for the DIMPI complex of PHM were collected at the Stanford Synchrotron Radiation Laboratory (SSRL) on beam line 7.3, operating at 3.0 GeV with beam currents between 100 and 50 mA. An Si220 monochromator with 1.2 mm slits was used to provide monochromatic radiation in the 8.8 to 10 KeV energy range. The monochromator was detuned 50% to reject harmonics. The protein sample was measured as a frozen glass in 20% ethylene glycol at 11-16 K in fluorescence mode using a 13-element Ge detector. To avoid detector saturation, the count rate of each detector channel was kept below 110 kHz by adjusting the hutch entrance slits or by moving the detector in or out from the cryostat windows. No dead-time correction was necessary under these conditions. The summed data for each detector were then inspected, and only those channels that gave high quality backgrounds free from

glitches, drop outs, or scatter peaks were included in the final average. Seventeen 35-min scans were collected for the PHMcc–DIMPI complex.

Raw data were averaged, background subtracted, and normalized to the smoothly varying background atomic absorption using the EXAFS data reduction package EXAFSPAK [George, 1990]. Energy calibration was achieved by reference to the first inflection point of a copper foil (8980.3 eV) placed between the second and third ion chambers. In any series of scans, the measured energy of the first inflection of the copper foil spectrum varied by less than 1 eV. Averaged EXAFS data were referenced to the copper calibration of the first scan of a series, since the energy drift in any series of scans was too small to perturb the EXAFS oscillations.

Data analysis was carried out by the least squares curve-fitting program EXCURV98 which utilizes full curved-wave calculations as described by Gurman and coworkers [Gurman et al., 1984, 1986; Binsted et al., 1988; Gurman, 1989]. The application to metalloprotein systems, and particularly the treatment of imidazole rings from histidine residues, and of linearly coordinated carbonyl groups by multiple scattering analysis has been described in detail in previous papers from this laboratory [Strange et al., 1987; Blackburn et al., 1991; Pettingill et al., 1991; Sanyal et al., 1993]. The parameters refined in the fit were as follows: $E_0$, the photoelectron energy threshold; $R_i$ the distance from Cu to atom $i$, and $2\sigma^2_i$, the Debye-Waller (DW) term for atom $i$. In general, coordination numbers were fixed at values consistent with the crystallographic description of PHMcc, and the DIMPI binding stoichiometry inferred from IR titration data, but were allowed to float in some fits to test the consistency between spectroscopic, biochemical, and crystallographic results. In the latter case, the coordination numbers were constrained so as to produce DW factors within reasonable limits (first shell: $0<2\sigma^2<0.015$; second shell $\geq$ first shell). The goodness of fit was judged by reference to a goodness of fit parameter F, defined as

$$F^2 = \frac{1}{N}\sum_{i=1}^{n} k^6 \left( Data_i - Model_i \right)^2$$

## 3.3 RESULTS

### 3.3.1 DIMPI Binding to Wild-type Enzyme

Depending on the ratio of DIMPI to copper, either one or two spectral features were seen in the IR study (Figure 3.2). At 0.25 DIMPI-Cu(I) ratio, only a single peak at 2138 $cm^{-1}$ was observed. As the ratio of DIMPI-Cu(I) ratio was increased to 0.5, this band increased in intensity. However, when the ratio reached 1.0 DIMPI per copper, a second band is seen at 2160 $cm^{-1}$.

Gaussian curve fitting was performed on each of these spectra (Figure 3.3) and the frequencies of the peaks, along with their width at half height is reported in Table 3.1. In the spectrum A, when 0.25 equivalent of the isocyanide was added to the PHMcc, a single DIMPI-Cu(I) species was present. Curve fitting of this peak revealed a single peak centered at 2138 $cm^{-1}$. When the 0.5 to 1 spectrum was compared to the lower DIMPI ratio, again, a single stretching frequency predominated that was fitted to a single peak at 2138 $cm^{-1}$. However, there was a second species that was fitted to a Gaussian peak at 2158 $cm^{-1}$. Upon increasing the ratio of isocyanide to copper to 1 to 1, a high frequency shoulder appeared on the main 2138 $cm^{-1}$ band. These were fitted to bands at 2138 and 2160 $cm^{-1}$. Repeated attempts to increase the DIMPI to copper ratio above 1 to 1 resulted in precipitation of the protein. Thus, no IR spectra could be collected.

### 3.3.2 Isopropyl Isocyanide Binding to Copper

The titration of PHMcc with IPI from 0.5 isocyanide per copper up to 2.0 per copper was also studied (Figure 3.4). At low levels of IPI, only one IR frequency was seen at 2172–2174 $cm^{-1}$. As the ratio was increased, a second band was seen at 2192–2193 $cm^{-1}$. Curve fitting analysis has been performed on each of these spectra (Figure 3.5). The analysis showed that the predominate peak in the lower ratio spectra centered at 2174 $cm^{-1}$. A second Gaussian fitted peak was centered at 2193 $cm^{-1}$ and this peak was only present in the higher IPI to copper ratio spectra. In contrast to the DIMPI results, spectra at ratios of IPI to copper higher than 1 to 1 could be obtained with IPI since precipitation did not occur.

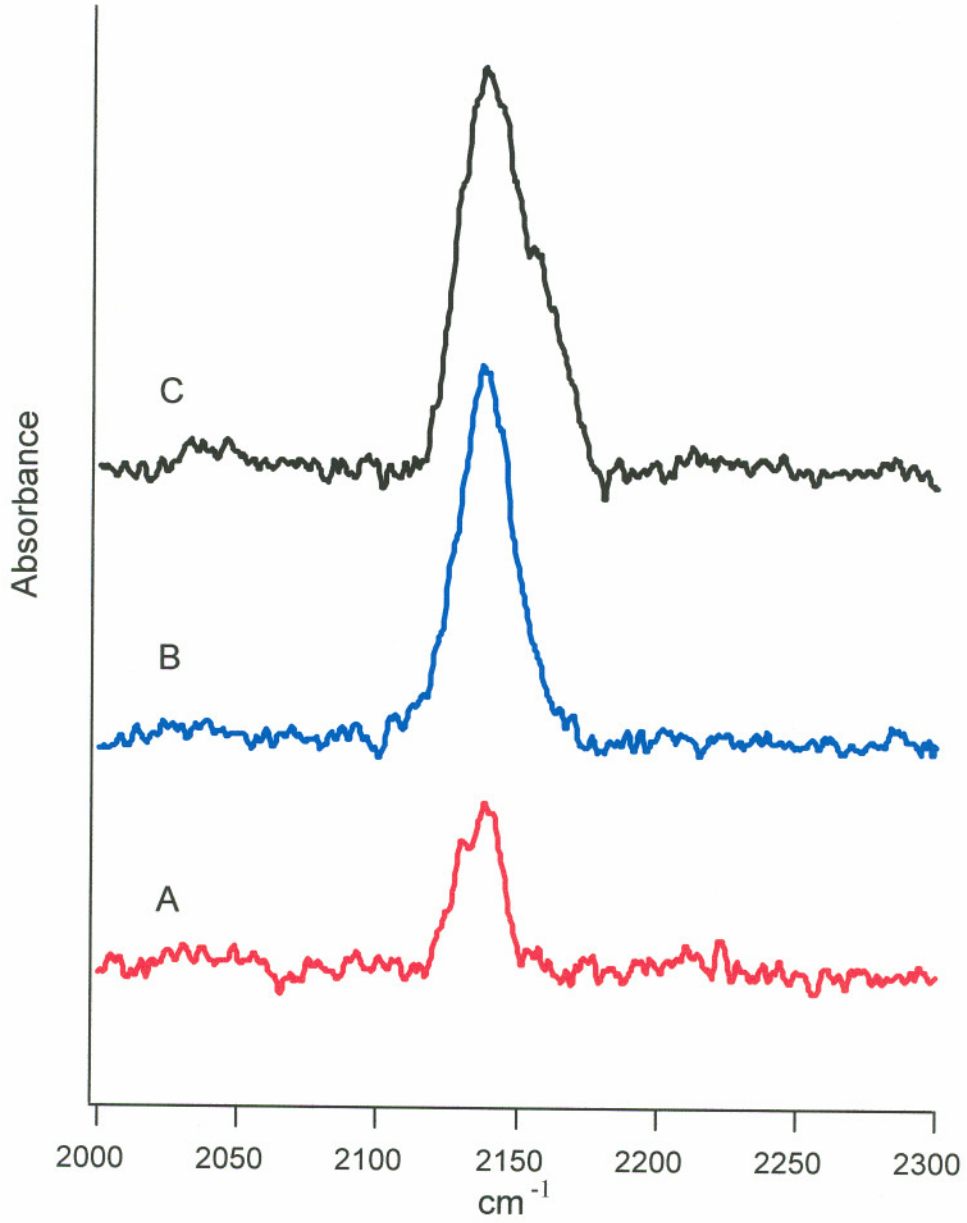


**Figure 3.2** IR spectra of the titration of DIMPI with PHMcc. (A) 0.25 to 1; (B) 0.5 to 1; (C) 1 to 1 ratio of DIMPI to Cu(I).

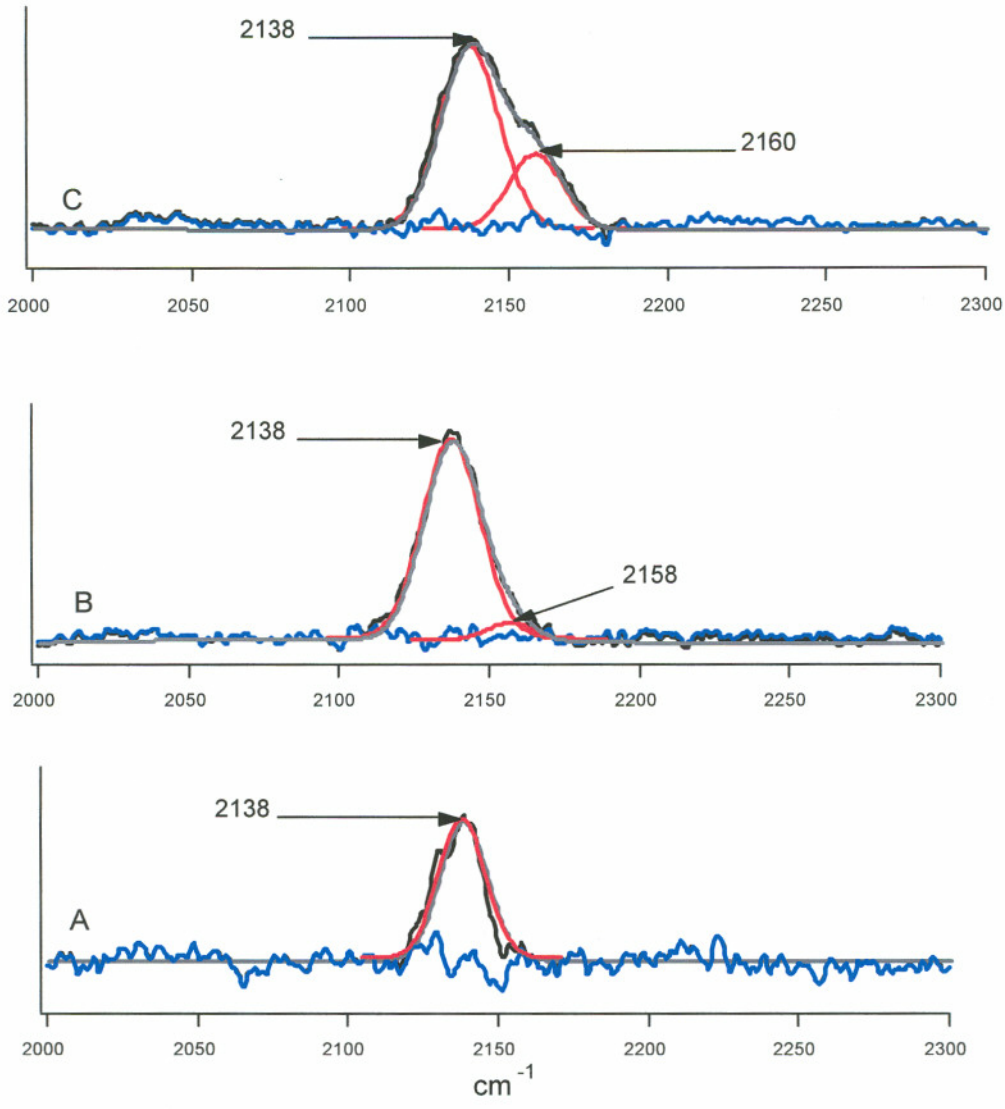


**Figure 3.3** Spectral fitting of the titration of DIMPI to Cu(I). (A) 0.25 to 1; (B) 0.5 to 1; (C) 1 to 1 ratio of DIMPI to Cu(I). Black = actual spectrum; gray dashed = simulated spectrum; red = fitted peak; blue= residuals.

**Table 3.1**

Peak Frequencies and Widths for DIMPI and IPI Bound to PHMcc

| **Ratio of DIMPI to Cu(I)** | $\nu(cm^{-1})$ | FWHH ($cm^{-1}$) |
|---|---|---|
| 0.25 to 1 | 2138 | 18.6 |
| 0.50 to 1 | 2138, 2160 | 22.1, 22.1 |
| 1 to 1 | 2138, 2160 | 22.1, 19.8 |
| **Ratio of IPI to Cu(I)** | | |
| 0.5 to 1 | 2172 | 16.3 |
| 1.0 to 1 | 2174, 2193 | 16.7, 16.7 |
| 1.5 to 1 | 2174, 2193 | 16.9, 16.4 |
| 2.0 to 1 | 2174, 2193 | 16.5, 15.4 |

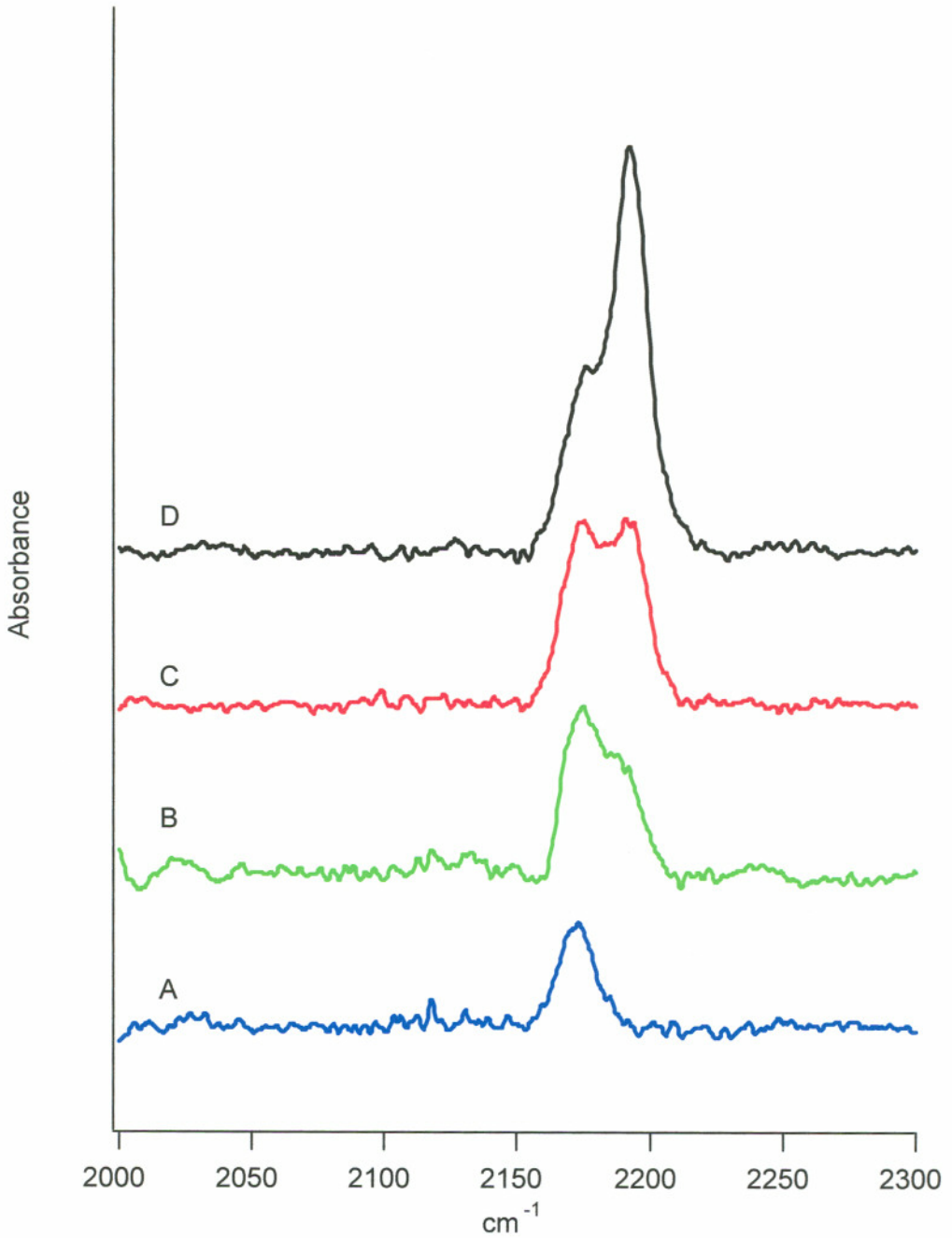


**Figure 3.4** IR spectra of the titration of IPI with PHMcc. (A) 0.5 to 1; (B) 1 to 1; (C) 1.5 to 1; (D) 2.0 to 1 ratio of DIMPI to Cu(I).

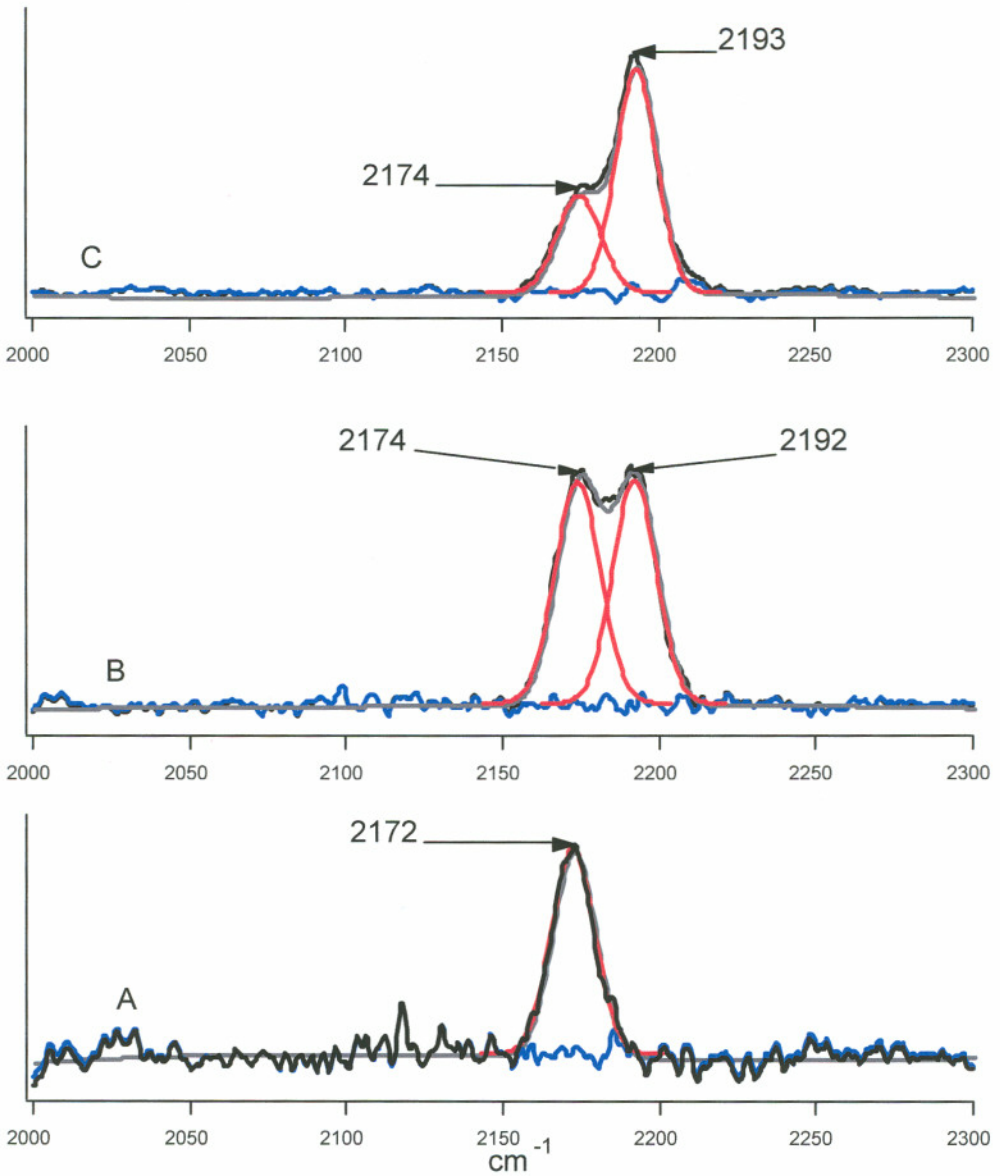


**Figure 3.5** Spectral simulation of the IR spectra of the titration of IPI with PHMcc. (A) 0.5 to 1; (B) 1.5 to 1; (C) 2.0 to 1 ratio of IPI to Cu(I). Black = actual spectrum; gray dashed = simulated spectrum; red = fitted peak; blue = residuals.

### 3.3.3 XAS Analysis of DIMPI Bound to PHMcc

EXAFS data for a sample of the PHM–DIMPI complex (0.50 DIMPI/Cu) are shown in (Figure 3.6). The data are remarkably similar to those recently reported for CO binding to reduced PHM [Jaron and Blackburn, 2000]. The Fourier transform shows a well-resolved splitting of the first shell due to the presence of short (~1.8–2.0 Å) Cu-C(CO) and Cu-N(imid) interactions and the longer (2.3 Å) Cu-S(Met314) interaction. Since both the crystal structure and the CO binding studies have confirmed the inequivalence of the two copper centers, meaningful simulation of the EXAFS data can only be achieved by using a two-site model which treats each copper center separately. Our simulation method thus allowed the imidazole shells (single and multiple scattering) associated with each copper to refine independently, together with the contributions from 0.5 DIMPI and 0.5 S(Met314) ligands. The best fit obtained is shown in Figure 3.6, with metrical parameters listed in Table 3.2. The EXAFS simulations give Cu-C(CNR) and Cu-S(Met) distances of $1.87 \pm 0.03$ and $2.32 \pm 0.01$ Å, respectively, and show the presence of two distinct populations of Cu-imidazole interactions at $1.90 \pm 0.01$ and $2.02 \pm 0.01$ Å, respectively. Although this splitting is at the limit of the resolution of the data ($\Delta R = \pi/2\Delta k = 0.11$ Å), it is consistent with one 2- or 3-coordinate center ($Cu_A$) with histidine-only coordination (Cu-N(imid) 1.90 Å) and one 4-coordinate copper center ($Cu_B$) with two histidines (2.02 Å), methionine-S (2.32 Å) and CNR(DIMPI) (1.87 Å). The Cu-S(Met) distance is $0.07 \pm 0.02$ Å longer than found in uncarbonylated reduced enzyme [Boswell et al., 1996], which is consistent with replacement of a weakly bound coordinated solvent with the stronger-field isocyanide ligand, and provides strong evidence that the isocyanide is bound at the methionine site. The Cu-C(CNR) distance of 1.87 Å is in the range expected for a Cu(I)-isocyanides [Pasquali et al., 1983; Fiaschi et al., 1984; Toth et al., 1985, 1987, 1988; Ardizzoia et al., 1990, 1992]. Interestingly, the absence of strong multiple scattering from the supposedly linear Cu-C-N-C(phenyl) unit suggests that the isocyanide may be coordinated in a tilted fashion. The simulations lead to an estimate of the Cu-C-N tilt angle of about 150°.

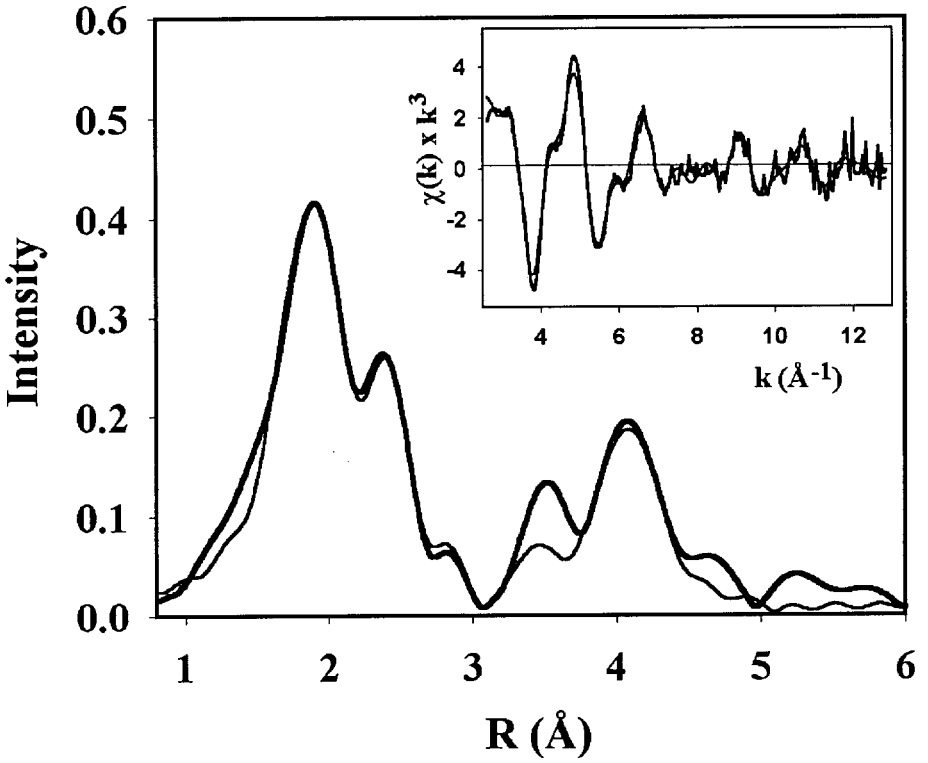


**Figure 3.6** Fourier transform and EXAFS (inset) of DIMPI bound to PHMcc. Solid thick lines represent the experimental data, solid thin lines represent the simulated data. Parameters used to generate the fit to the EXAFS data are listed in Table 3.2.

**Table 3.2**

Parameters Used to Simulate the EXAFS and Fourier Transform of Reduced PHMcc Reacted with 0.5 mol Equivalents of DIMPI per Copper

Estimated errors in distances are ±0.01 Å for the first shell and ±0.03 Å for outer shells. Estimated errors in coordination numbers are ± 25%. Estimated errors in angles are ± 5°. ∠Cu-X-Y ° represents the angle between the first shell scatterer *(X)* and the outer shell scatterer *(Y)*.

| *First Shell* | | | *Outer Shells* | | | |
|---|---|---|---|---|---|---|
| *Shell (X)* | *R (Å)* | $2\sigma^2$ *(Å $^2$)* | *Shell (Y)* | *R (Å)* | *∠Cu-X-Y °* | $2\sigma^2$ *(Å $^2$)* |
| | | | *F = 0.441, $E_0$ = -1.72 eV* | | | |
| 0.5 C (C≡NR) | 1.87 | 0.0080 | 0.5 N(C≡NR) | 3.02 | 153 | 0.0400 |
| | | | 0.5 C(C≡NR) | 4.42 | | 0.0400 |
| 1 $N_\alpha$ (imid) | 2.02 | 0.0040 | 1 $C_\beta$ (imid) | 2.99 | 236 | 0.0100 |
| | | | 1 $C_\beta$ (imid) | 3.06 | 128 | 0.0100 |
| | | | 1 $C_\gamma$/$N_\gamma$(imid) | 4.14 | 202 | 0.0100 |
| | | | 1 $C_\gamma$/$N_\gamma$(imid) | 4.32 | 164 | 0.0100 |
| 1 $N_\alpha$ (imid) | 1.90 | 0.0080 | 1 $C_\beta$ (imid) | 2.83 | 128 | 0.0090 |
| | | | 1 $C_\beta$ (imid) | 2.90 | 234 | 0.0090 |
| | | | 1 $C_\gamma$/$N_\gamma$(imid) | 4.12 | 162 | 0.0090 |
| | | | 1 $C_\gamma$/$N_\gamma$(imid) | 4.18 | 197 | 0.0090 |
| 0.5 S(met) | 2.32 | 0.013 | | | | |

The EXAFS data thus provide strong evidence for coordination of the DIMPI ligand to PHM. The perturbation of the Cu-S(Met314) bond provides additional evidence that DIMPI binds at the $Cu_B$ center. On the other hand, the short 1.90-Å distance obtained for one of the populations of imidazole ligands is identical to the distance obtained in two-site simulations of the unliganded reduced enzyme (Jaron et al., in press), and suggests that the $Cu_A$ center does not interact with DIMPI.

## 3.4 DISCUSSION

Since isocyanides have not been extensively used as ligand probes to reduce copper centers in proteins, it is difficult to draw conclusions on IR frequencies seen here and compare them to other literature values. However, we can compare the stretching frequencies reported here with the frequencies reported for D$\beta$M complexes (Figure 1.17) [Reedy et al., 1995]. When ascorbate-reduced D$\beta$M is allowed to react (by dialysis in phosphate buffer) with low concentrations of DIMPI, three different time dependent bands were observed. When this experiment was performed using substoichiometric amounts of DIMPI to copper, the FTIR spectrum was composed mainly of the two bands at 2148 and 2129 $cm^{-1}$. Spectral deconvolution of these spectra revealed that the two bands were of equal contribution and there was a small contribution from the peak at 2160 $cm^{-1}$. Therefore, it was determined that the two bands at the lower frequency were from mono isocyanide species bound to each copper. As the reaction progressed via the addition of increasing amounts of DIMPI, the 2160 $cm^{-1}$ band increased in intensity and the two lower bands disappeared. Results from further studies using IR and Raman on a number of structurally characterized inorganic Cu(I) DIMPI complexes confirmed that the band corresponding to the frequency at 2160 $cm^{-1}$ may be from a Cu(I) bound to three DIMPI ligand complexes, suggesting that the copper was extracted from its ligand environment in the protein.

In order to determine which of the two lower frequency bands corresponds to which copper site, the reaction of the copper centers with DIMPI was repeated molluscan hemocyanin. Since the dicopper site of Hc had three histidines on each

copper one would expect only one IR band when DIMPI was bound at stoichiometric concentrations. Deoxyhemocyanin with two mol per Cu of DIMPI showed a single IR band at 2148 $cm^{-1}$. As the concentration of DIMPI increased, the band at 2148 $cm^{-1}$ converted to 2160 $cm^{-1}$. Comparing the results from the hemocyanin experiments with the results from D$\beta$M suggested that the 2148 $cm^{-1}$ band was due to an isocyanide bound to the $Cu_A$ site of D$\beta$M, and the 2129 $cm^{-1}$ band was from the ligand at $Cu_B$. Thus, we can use these assignments to help understand what is occurring when isocyanides are bound to PHMcc.

When DIMPI is titrated against PHMcc, only two bands are seen: 2138 $cm^{-1}$ and 2160 $cm^{-1}$ (Scheme 3.1). By comparison to the results obtained in the D$\beta$M study, the 2160 $cm^{-1}$ band can be assigned to a tris-ligated DIMPI-Cu(I) species. Although the 2138 $cm^{-1}$ is 10 $cm^{-1}$ higher that the corresponding $Cu_B$-DIMPI signal in D$\beta$M, it is still believed to originate from the DIMPI-$Cu_B$ center in PHMcc. This is supported by two additional factors. First, EXAFS on the DIMPI-Cu(I) PHMcc species showed that the Cu-S(Met) distance increases, from 2.27 to 2.33 Å, indicating perturbation of the Cu-methionine bond. Second, recent IR studies of DIMPI reactions with mutant forms of PHMcc where the $Cu_B$ center is absent show no 2138 $cm^{-1}$ band (Chapter 4). Similarly, we can assign the 2173 $cm^{-1}$ and 2192 $cm^{-1}$ frequencies in the IPI-PHMcc spectra as arising from the isopropyl isocyanide bound to the $Cu_B$ and $Cu_A$ centers, respectively.

Although D$\beta$M and PHMcc are thought to be very similar with respect to copper coordination and reactivity, it is interesting to note that the spectroscopy regarding DIMPI binding to $Cu_B$ is not similar in the two enzymes. As stated earlier, the Cu(I)–DIMPI frequency of 2138 $cm^{-1}$ in PHMcc is $\sim$10 $cm^{-1}$ higher than that observed in D$\beta$M. This shifting of the frequency may be due in part to the presence of Arg 240. This arginine residue has been shown to coordinate the carboxylic acid group of the terminal glycine on the peptide substrate [Prigge et al., 1997]. In D$\beta$M, this residue is a glutamine and is believed to aid in coordination of the amine group of the substrate dopamine. The change from a neutral amino acid to a positively charged amino acid may well shift the frequency to higher energy in PHMcc.

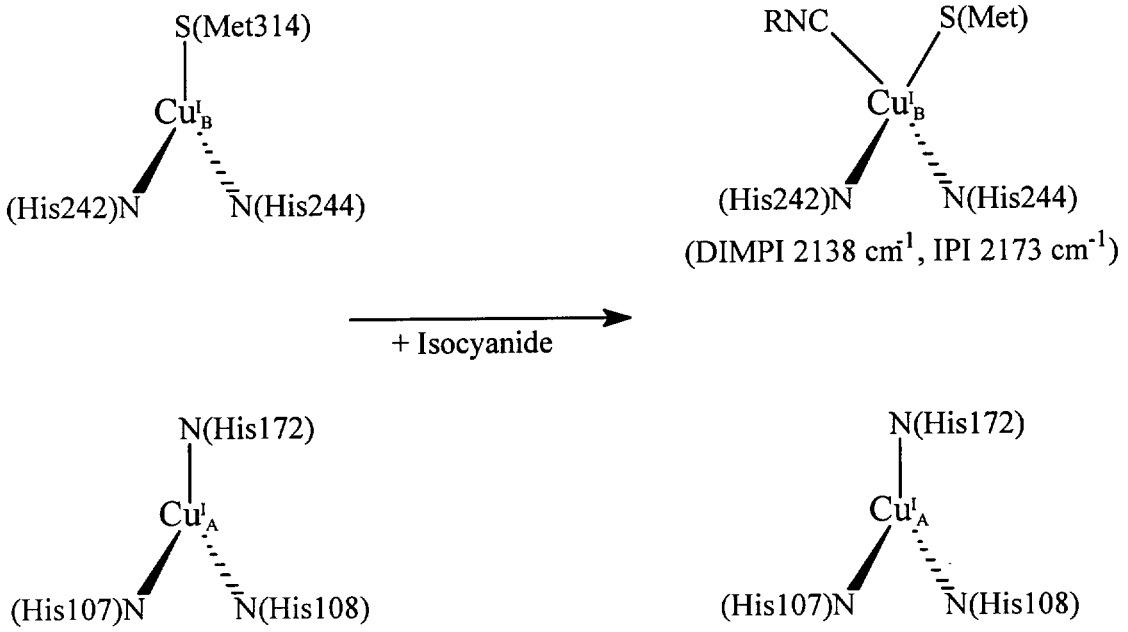


**Scheme 3.1** Proposed ligation of isocyanide to PHMcc.

Modeling of the DIMPI molecule onto the open coordination position in PHMcc may provide further reasoning for the shift in frequency between the two enzymes (Figure 3.7). What we observe is that the phenyl ring of the DIMPI molecule lies very close (5–6 Å) to the phenyl ring of amino acid Tyr79. Thus, ð-stacking interactions could occur between the two rings. This interaction may actually weaken the bond between the Cu and the isocyanide carbon, causing the 10 $cm^{-1}$ shift in the observed stretching frequency. It would be interesting to be able to compare the IPI stretching frequencies with those of D$\beta$M, and see if the ring interaction of DIMPI and Tyr79 are the cause of the shift, because one would predict that since IPI does not have a phenyl ring, there would be no shifting of the frequencies between the two enzymes. However, since there is no data available for D$\beta$M–IPI complexes, this cannot be done. Furthermore, with PHMcc, we have yet to observe an IR frequency of Cu(I)-DIMPI (or Cu(I)-IPI) associated with the $Cu_A$ center in native PHMcc. The lack of $Cu_A$-isocyanide signal could simply be attributed to steric interference between ligands preventing an isocyanide from binding at each copper simultaneously. By inspecting the modeled DIMPI bound to $Cu_B$, one can see that the complex extends far into the active site pocket. Furthermore, the calculated distance from the cyano carbon to the C-4 hydrogen on the ring is approximately 7 Å. Since the active site pocket is only 11 Å between the two copper centers, it is conceivable that an isocyanide on the $Cu_B$ center would directly interfere with the ability for an isocyanide to coordinate to the $Cu_A$ site. One would not expect the isocyanide to be able to bend in the pocket due to the triple bond between the C and the N of the cyanide. This would limit the flexibility of the ligand. However, it is possible that some ring motion about the phenyl group could occur. Therefore, in the case of DIMPI, it appears that binding of one isocyanide ligand precludes a second isocyanide from binding at the other copper center due to steric hindrance of the size of the isocyanide ligand. One could infer from this that binding of isocyanide to $Cu_B$ is more favorable than binding of an isocyanide to $Cu_A$.

The belief that steric bulk was governing isocyanide binding to the $Cu_A$ center in PHMcc led to the exploration of using the IPI ligand binding to probe the two centers. One can picture the size of the IPI ligand as the top half of the DIMPI

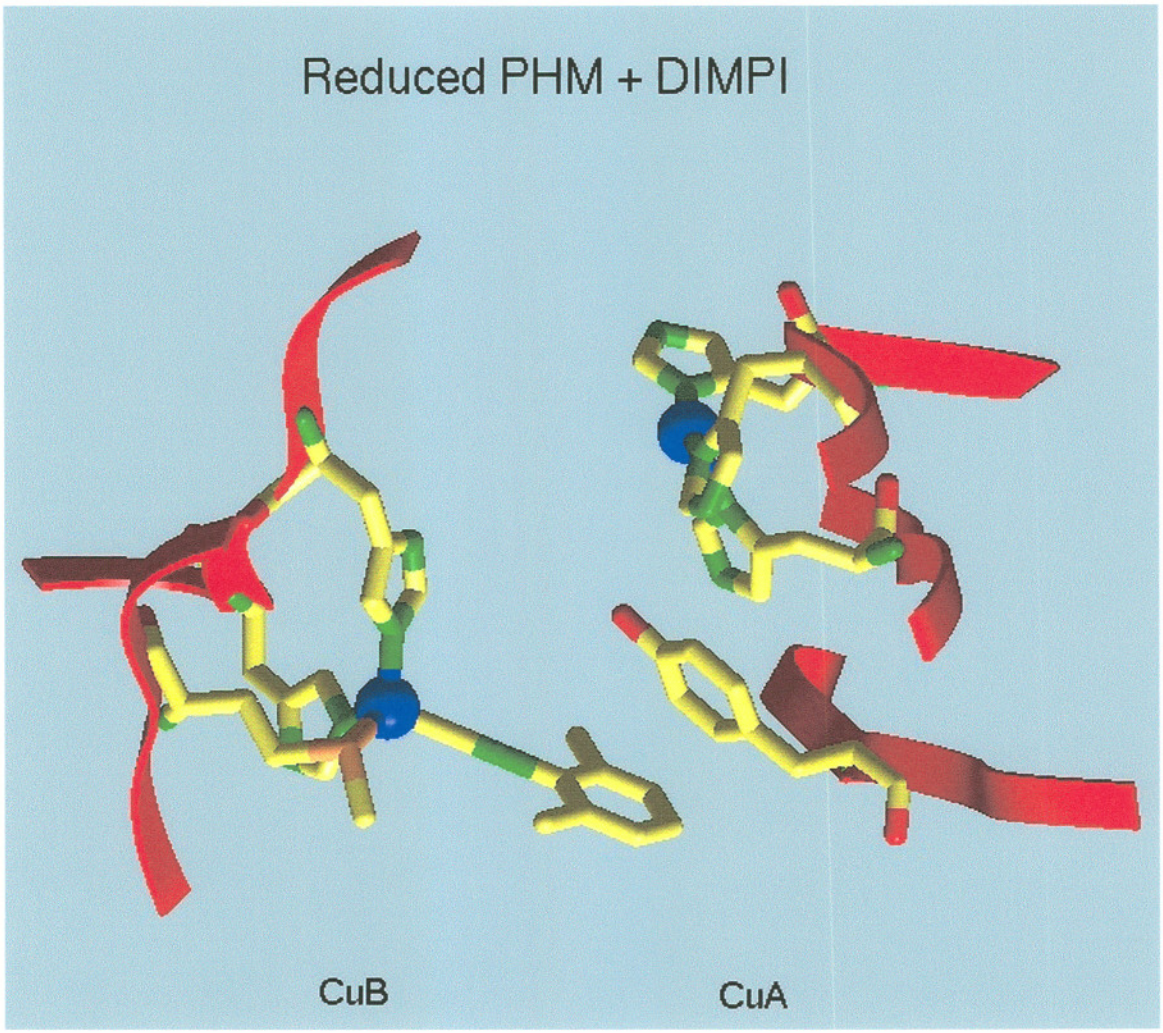


**Figure 3.7** Modeling of DIMPI bound to the active site of PHMcc.

molecule minus the 2,6-dimethyl groups. Therefore, being much smaller in size, it was felt that we would be able to see simultaneous binding of IPI to both copper centers. However, this was not observed and only the IR signal attributed to $Cu_B$-IPI was seen. Again, steric hindrance may be the predominate factor in limiting the isocyanide from binding to the $Cu_A$ center. However, modeling of IPI bound to the active site in PHMcc depicts that there should be ample room for binding of one ligand at each copper site (Figure 3.8). This modeling may rule out interference between two IPI ligands, but it does not eliminate steric hindrance from nearby amino acids affecting IPI binding to $Cu_A$.

A second attempt at ligating isocyanides to the $Cu_A$ center was tried. This involved equilibrating the enzyme with 2.5 molar excess of peptide (N-Ac-YVG). The reasoning behind the addition of substrate was to investigate if any structural changes occurred at the $Cu_A$ site that would enable an isocyanide to bind with peptide present. The presence of substrate did not affect ligand binding to $Cu_A$. However, in some instances a decrease in the IR intensity of the $Cu_B$-isocyanide frequency was observed (data not shown). This change could be due to competition between the isocyanide and the substrate for space in the active site pocket. What could be occurring is that the isocyanide ligand is displacing bound peptide slowly. In cases where there was no change in the IR frequency, it could either be that the ligand has totally displaced the substrate, or that peptide binding has no affect on either copper sites.

Another difference between DIMPI binding to PHMcc and D$\beta$M is the precipitation of PHMcc upon addition of more than 1 DIMPI per copper. In D$\beta$M, no precipitation of the enzyme was observed upon addition of excess DIMPI [Reedy et al., 1995]. The precipitation of PHMcc upon the addition of excess DIMPI may simply be due to an increase of large hydrophobic ligands to the active site. Since the active site of PHMcc is relativity close to the surface of the enzyme [Prigge et al., 1997], the additional phenyl rings from DIMPI are possibly destabilizing the PHMcc structure and causing the enzyme to fall out of solution. Furthermore, in D$\beta$M, the additional disulfide linkages across monomers may help to stabilize and prevent

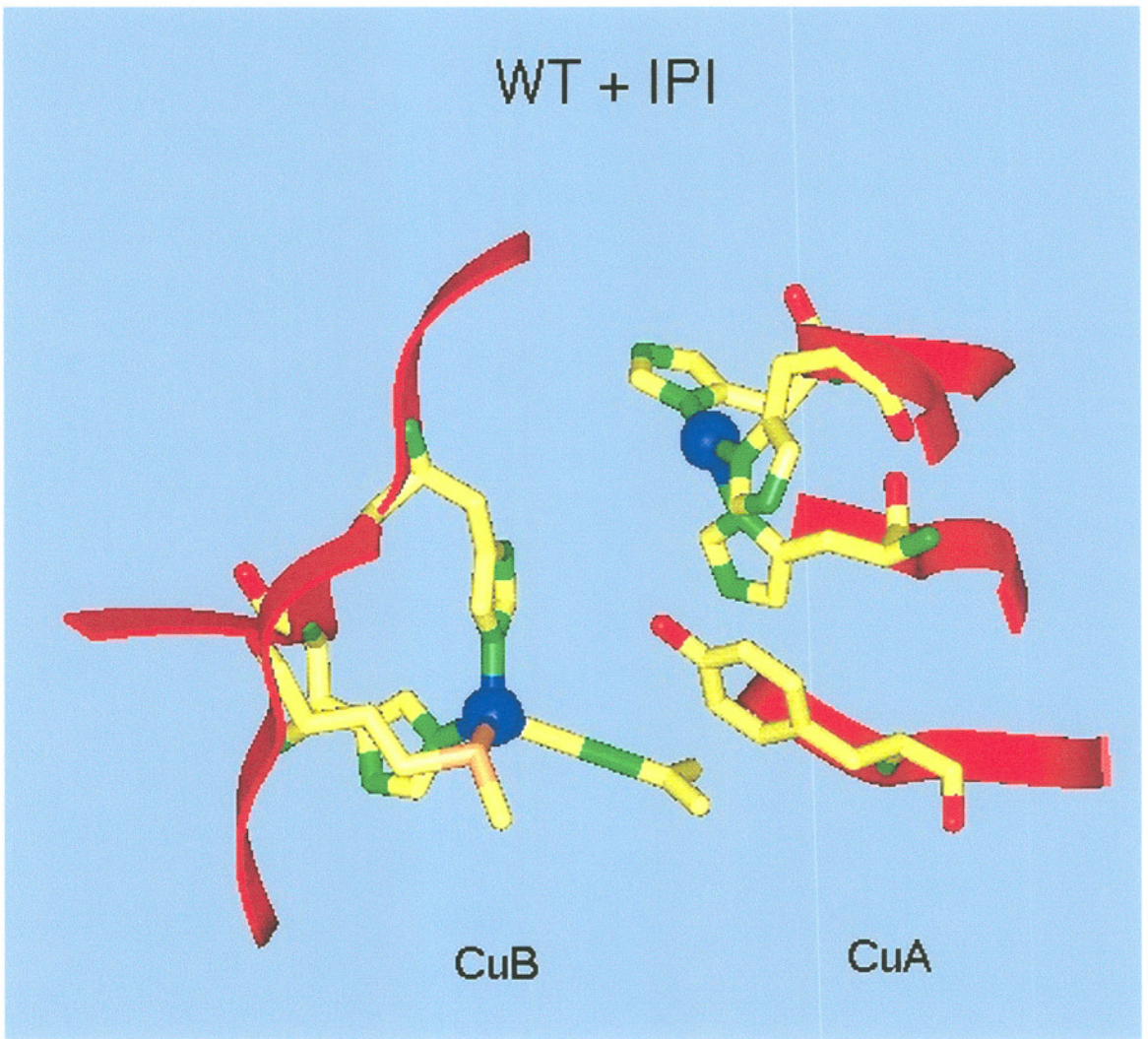


**Figure 3.8** Modeling of IPI bound to the active site of PHMcc.

unfolding of the enzyme when large hydrophobic ligands are present in its active site [Robertson et al., 1994].

## 3.5 CONCLUSIONS

Using isocyanides as ligand directed probes to the copper centers in PHMcc has established further evidence for the inequivalency between the two copper sites. By comparing the findings from D$\beta$M with DIMPI bound to its active site with the results presented here, we are starting to observe differences between the reactivity of the copper centers in each enzyme. Even though it appears that these two enzymes are members of a new class of copper monooxygenases, it is relevant to note that the environment governing the chemistry occurring at each site appears to be different.

# CHAPTER 4

# ISOCYANIDE LIGATION TO MUTANT FORMS OF PHMcc

## 4.1 INTRODUCTION

Whereas the crystal structure gives a very good representation of the oxidized state of the enzyme, it can reveal little about changes at the copper centers in the reduced enzyme. Since the reduced system is the $O_2$ binding state, it does not predict the reactivity of the individual copper centers. It also fails to explain how an electron is transferred from the $Cu_A$ center to the oxygen bound at the $Cu_B$ center. In this chapter we explore the reactivity of the individual Cu(I) sites in PHMcc by utilizing a series of active site mutants of PHMcc in which specific amino acid ligands have been altered.

Four different mutants that target individual copper centers were studied. These four mutants can be divided into two groups depending upon which copper center they affect (Figures 1.9 and 1.10). Met314Ile and His242Ala are mutants that have an integral $Cu_B$ ligand changed to a non-ligating amino acid. Therefore, the expressed protein is predicted to be lacking the $Cu_B$ center. Interestingly, the Met314Ile mutant should only affect the binding of copper in the reduced form of the enzyme since in the oxidized form, the Met is not seen as a ligand to the $Cu_B$ center. The second set is composed of His172Ala and His107/108Ala mutants. These are mutants of PHMcc in which ligands to the $Cu_A$ center have been altered, thus eliminating the $Cu_A$ center.

By studying each mutant with respect to isocyanide binding, we can selectively analyze the behavior of an individual copper center without the second site present. Spectroscopic investigation of reduced copper is limited by the $d^{10}$ electronic state of the metal. However, much information can be gained by using metal directed ligand

probes and following their formation via FTIR. Isocyanides are one such probe that can be used to study Cu(I). Its binding to the metal center and the location of the IR stretching frequency are sufficiently strong to be followed spectroscopically. Although isocyanides have not been extensively used as probes to Cu(I) centers in proteins, there are a large number of inorganic Cu(I)–isocyanide complexes that have been structurally characterized [Pasquali et al., 1983; Fiaschi et al., 1984; Toth et al., 1985, 1987, 1988; Ardizzoia et al., 1990, 1992]. The effectiveness of isocyanide binding to copper centers in proteins has previously been demonstrated in studies utilizing D$\beta$M and PHMcc [Reedy et al., 1995; Chapter 3]. Earlier isocyanide ligation to the copper centers in wild-type PHMcc showed preferential binding of the ligand to the $Cu_B$ center. The results of the present study show that isocyanide binding can occur at both copper centers in PHMcc. However, it appears that ligation of an isocyanide at the $Cu_A$ center is dependent on the absence of the second copper center ($Cu_B$). Different reactivity of the $Cu_B$ center was also observed when compared to results obtained from the wild-type PHMcc isocyanide study, thus demonstrating that mutations at one copper center appear to affect the reactivity of the remaining copper center that is 11 Å distant [Chapter 3].

## 4.2 EXPERIMENTAL METHODS

### 4.2.1 Cell Growth/Enzyme Isolation

Mutant forms of PHMcc were expressed in Chinese hamster ovary cells (cell line DG44) as described previously in Chapter 2.

### 4.2.2 Isocyanide Titration

A typical titration consisted of the following: A 200 $\mu$L sample of oxidized mutant ($\sim$2 to 1 mM in copper) was made anaerobic by repeated vacuum flushing with argon. It was then reduced with a five-fold molar excess of anaerobic sodium ascorbate (in potassium phosphate 50 mM, pH 7.4) and the copper concentration was remeasured via AAS. The sample was found to be fully reduced, as evidenced by the lack of any Cu(II) EPR signal. In an anaerobic glove box, 50 $\mu$L aliquots of the

reduced mutant were placed in separate 1.5 mL microcentrifuge tubes. To this sample, an aliquot (between 2 and 6 $\mu$L) of an anaerobic stock solution of 2,6-dimethylphenyl isocyanide (DIMPI) or isopropyl isocyanide (IPI) (Figure 3.1) (10 mM in methanol) was added to achieve the isocyanide to Cu ratio that was desired. The isocyanide and the ascorbate were both freshly prepared before use.

### 4.2.3 Fourier Transform Infrared (FTIR) Measurements

FTIR spectra were recorded on a Perkin Elmer 2000 FTIR spectrophotometer. Solution IR protein spectra were collected using a liquid nitrogen-cooled MCT detector, in 50 $\mu$m path-length calcium fluoride cells housed in a copper thermostatic block connected to a recirculating water bath set to 10°C. Two hundred scans were collected for each protein and background sample under identical conditions. Instrument resolution was set to 2 $cm^{-1}$. The background spectrum was obtained by using molar equivalent (to copper) of isocyanide diluted in potassium phosphate buffer (50 mM pH 7.5). Each individual mutant-isocyanide spectrum was subsequently subtracted from the background spectrum of the potassium phosphate-isocyanide that correlated to the correct ratio of isocyanide to PHMcc. All reported spectra are differences of bound isocyanide and free isocyanide in buffer. Analysis and spectral deconvolution curve-fitting were performed using the program IGOR PRO (WaveMetrics). In all cases, bands containing more than one component were simulated by the sum of pure Gaussian components.

## 4.3 RESULTS

### 4.3.1 Copper Reconstitution

After dialysis against free copper (as outlined in Chapter 2), the copper to protein ratio was recalculated. In the Cu(II) state, the ratio of Cu/protein for the mutants was found to vary from 1 Cu/protein to 1.8 Cu/protein (Table 4.1). The highest Cu/protein ratio observed in the oxidized form was that for Met314Ile (1.5 Cu/protein). His172Ala and His107/108Ala had ratios slightly lower than that found

**Table 4.1**

Copper-to-Protein Ratios for Each Mutant

| Mutant | Average Cu/protein (oxidized) | Average Cu/protein (reduced) |
|---|---|---|
| **Met314Ile** | 1.5 | 0.99 |
| **His242Ala** | 1.1 | 0.99 |
| **His172Ala** | 1.40 | 1.48 |
| **His107/108Ala** | 1.32 | 1.09 |

for Met314Ile (1.40 and 1.32, respectively). His242Ala was determined to have the lowest Cu/protein ratio of the mutants at 1.1 Cu/protein.

After reduction with ascorbate, two of the four mutants had dramatically different Cu/protein ratios (Table 4.1). Met314Ile and His107/108Ala ratios decreased from nearly 1.5 Cu/protein to a value close to 1 to 1. However, His172ala Cu ratio essentially remained unchanged upon reduction with an average of 1.5 Cu/protein. It appears that for this mutant, Cu can bind at both centers in both the reduced and oxidized states.

### 4.3.2 EPR Spectra of Each Mutant

The EPR spectrum from each individual mutant was compared to the spectrum obtained from the fully metallated wild-type PHMcc (Figure 4.1). The spectra of the mutants exhibited typical type 2 copper EPR signal ($g_{\parallel} > g_{\perp} \cdot 2.00$, $A_{\parallel} > 140 \times 10^{-4}$ $cm^{-1}$). The wild-type PHMcc EPR signal was shown to be comprised of 2 titratable Cu signals [Chapter 3]. The mutants that bound more than 1 copper per monomer exhibited signals resembling those of the native enzyme. However, comparisons of the His107/108Ala signal with that of the native signal revealed a difference between these two proteins (Figure 4.2). Upon closer inspection of the His107/108Ala against the wild-type spectrum, it appears that the mutant contains a signal that is concurrent to that observed for wild-type PHMcc at low Cu/protein ratios.

### 4.3.3 FTIR of $Cu_A$ Active Site Mutants

*4.3.3.1 His172Ala.* Mutations aimed at eliminating the $Cu_A$ (His172Ala, His107/108Ala) binding site were studied through binding DIMPI to the remaining Cu center. Titration of DIMPI against His172Ala revealed a mixture of isocyanide bands (Figure 4.3). At substoichiometric isocyanide to Cu ratios, a single broad peak was observed. As the concentration of DIMPI was increased to a ratio of 1 to 1, the main spectral band gained in intensity. Further increase in DIMPI concentration resulted in a peak that was clearly comprised of 2 or more components.

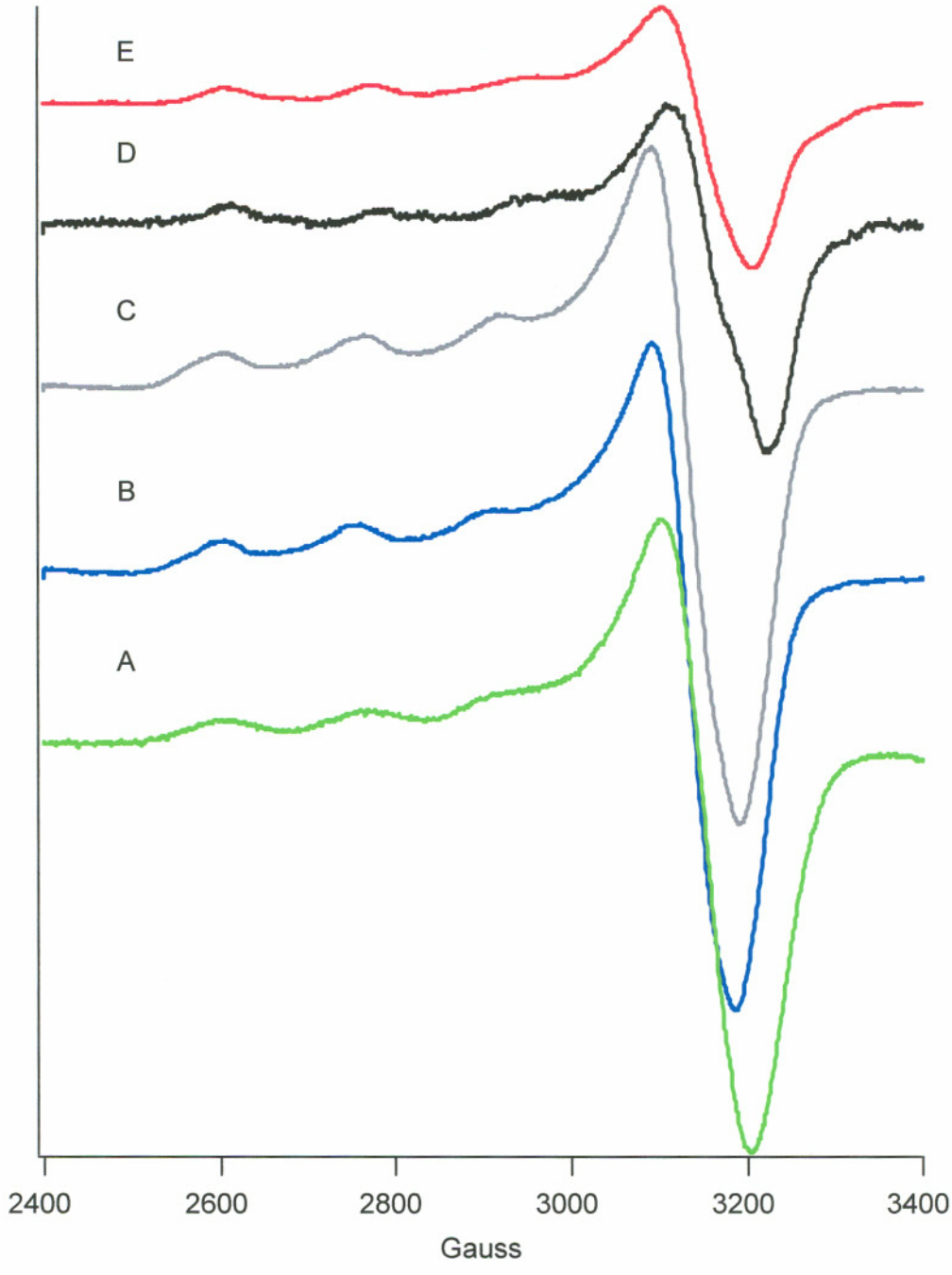


**Figure 4.1** EPR of mutants and wild-type PHMcc after reconstitution by dialysis. Cu/protein ratios are given in Table 4.1. (A)Wild-type PHMcc; (B)His242Ala; (C)His172Ala; (D)His107/108Ala; (E)Met314Ile.

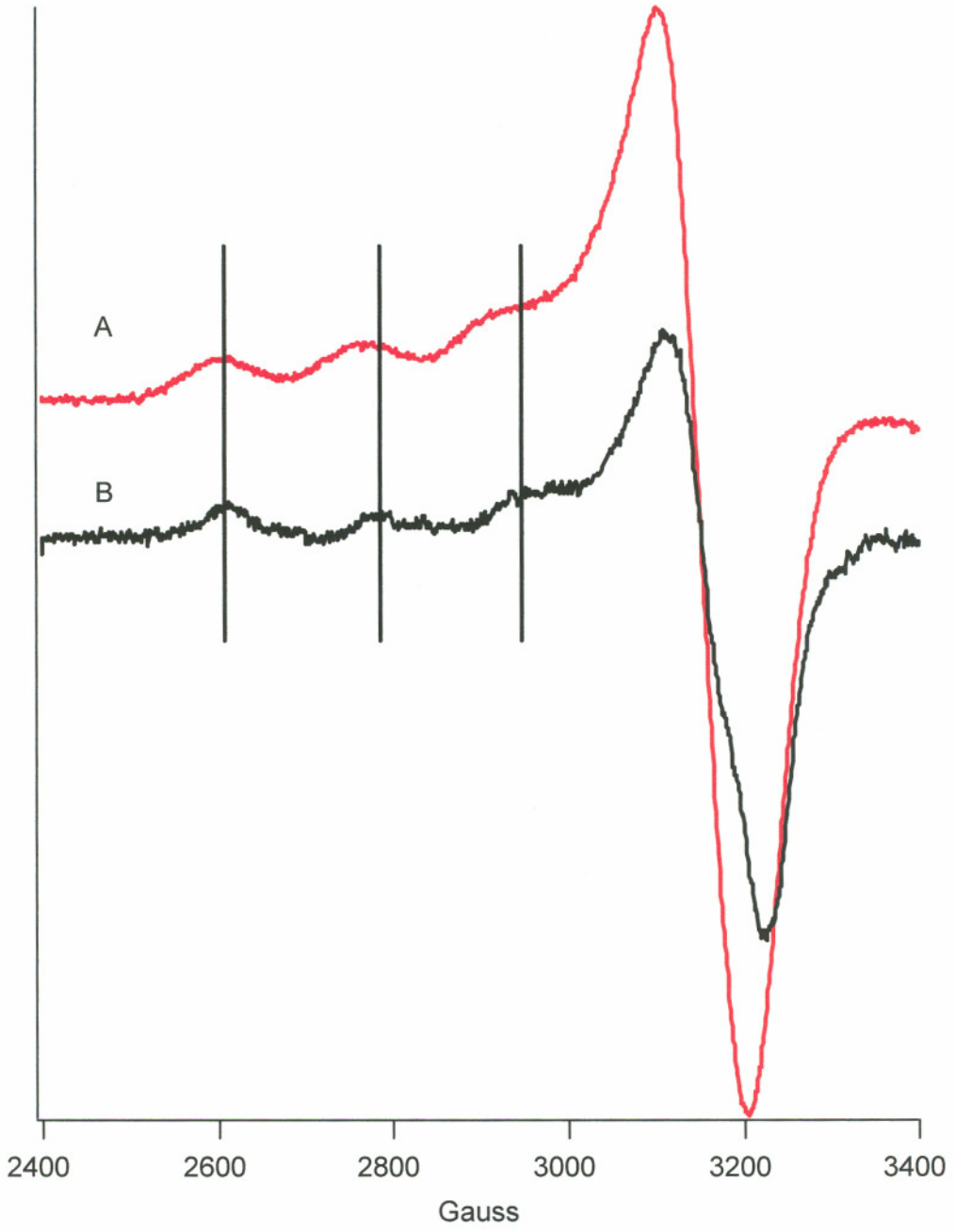


**Figure 4.2** Comparison of the EPR signal from His107/108Ala and wild-type PHMcc. The vertical bars highlight the differences between the two signals. (A) Wild-type PHMcc; (B) His107/108Ala.

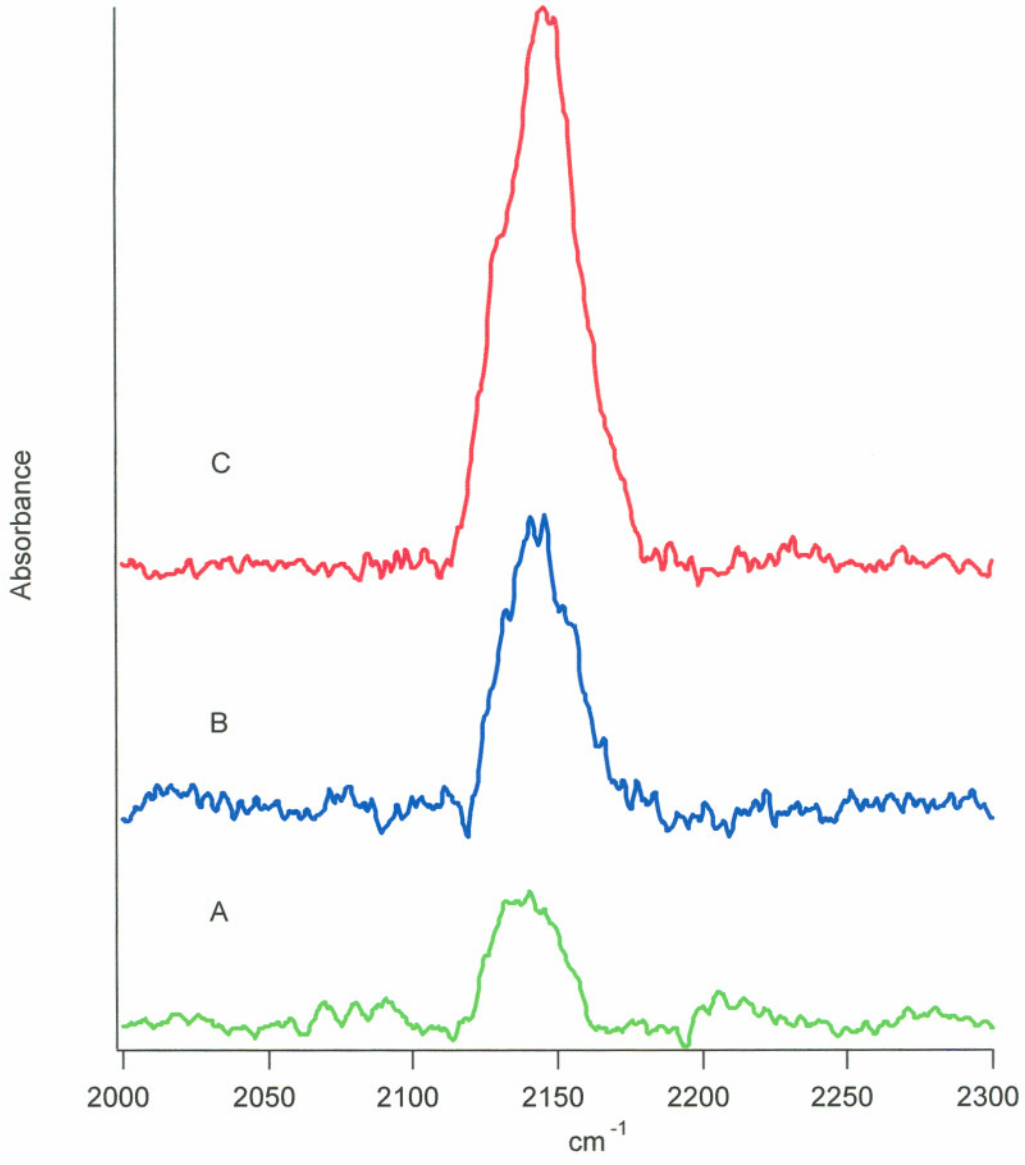


**Figure 4.3** IR spectrum of the titration of DIMPI with His172Ala. (A) 0.5 to 1; (B) 1.0 to 1; (C) 2.0 to 1 ratios of DIMPI/Cu(I).

Spectral simulation of these peaks employing pure Gaussian stretching modes was carried out using the parameters for the full width at half height (FWHH) derived from the mono-DIMPI copper stretch observed from previous work with wild-type PHMcc [Chapter 3]. By constraining the FWHH to ranges between 15 and 18 $cm^{-1}$, the spectrum for the 0.5–1 DIMPI-to-copper ratio was determined to be comprised of 2 components with one peak centered at 2133 $cm^{-1}$ and the second centered at 2148 $cm^{-1}$ (Figure 4.4). Fitting of the 1:1 spectrum revealed the presence of 3 peaks (2135, 2148, and 2158 $cm^{-1}$), with an increase in intensity for the two low energy bands. For the 2:1 spectrum, the result of the simulation was again three peaks at the above noted frequencies (Tables 4.2 and 4.3), with the predominate band now being the 2148 $cm^{-1}$ frequency and the high frequency band shifting slightly to 2164 $cm^{-1}$.

Isopropyl-isocyanide binding to His172Ala was also investigated. However, due to the low concentration of the sample being analyzed, the data are not very conclusive. With respect to this, the spectra were still analyzed and fitted (Figure 4.5). It also appears that at low isocyanide to copper ratio, 2 bands are seen that can be fitted to stretches at 2170 and 2185 $cm^{-1}$.

***4.3.3.2 His107/108Ala.*** When the double mutant His107/108Ala was titrated with DIMPI at substoichiometric isocyanide to Cu ratios, a single peak was observed (Figure 4.6A). As the isocyanide concentration was increased to a ratio of 1 to 1, the main band appeared to broaden (Figure 4.6B). Increasing the DIMPI to copper ratio to 2 to 1 produced a spectrum where the main peak now contained evidence of a definitive shoulder at lower energy (Figure 4.6C). Further increase of DIMPI resulted in the disappearance of the low frequency shoulder and the appearance of a new shoulder at higher energy (Figure 4.6D).

Spectral deconvolution of the lowest DIMPI/Cu spectrum resulted in the best simulation being represented by two different species responsible for the observed band. The two bands were determined to be at 2137 $cm^{-1}$ and 2150 $cm^{-1}$, with the lower frequency being the more intense of the two (Figure 4.7A). Fitting of the 1 to 1 spectrum also determined that the broad band was comprised of two bands at slightly down shifted frequencies (2141 $cm^{-1}$ and 2152 $cm^{-1}$, respectively), when compared to the previous spectrum. The fitting to the 2 to 1 spectral results showed

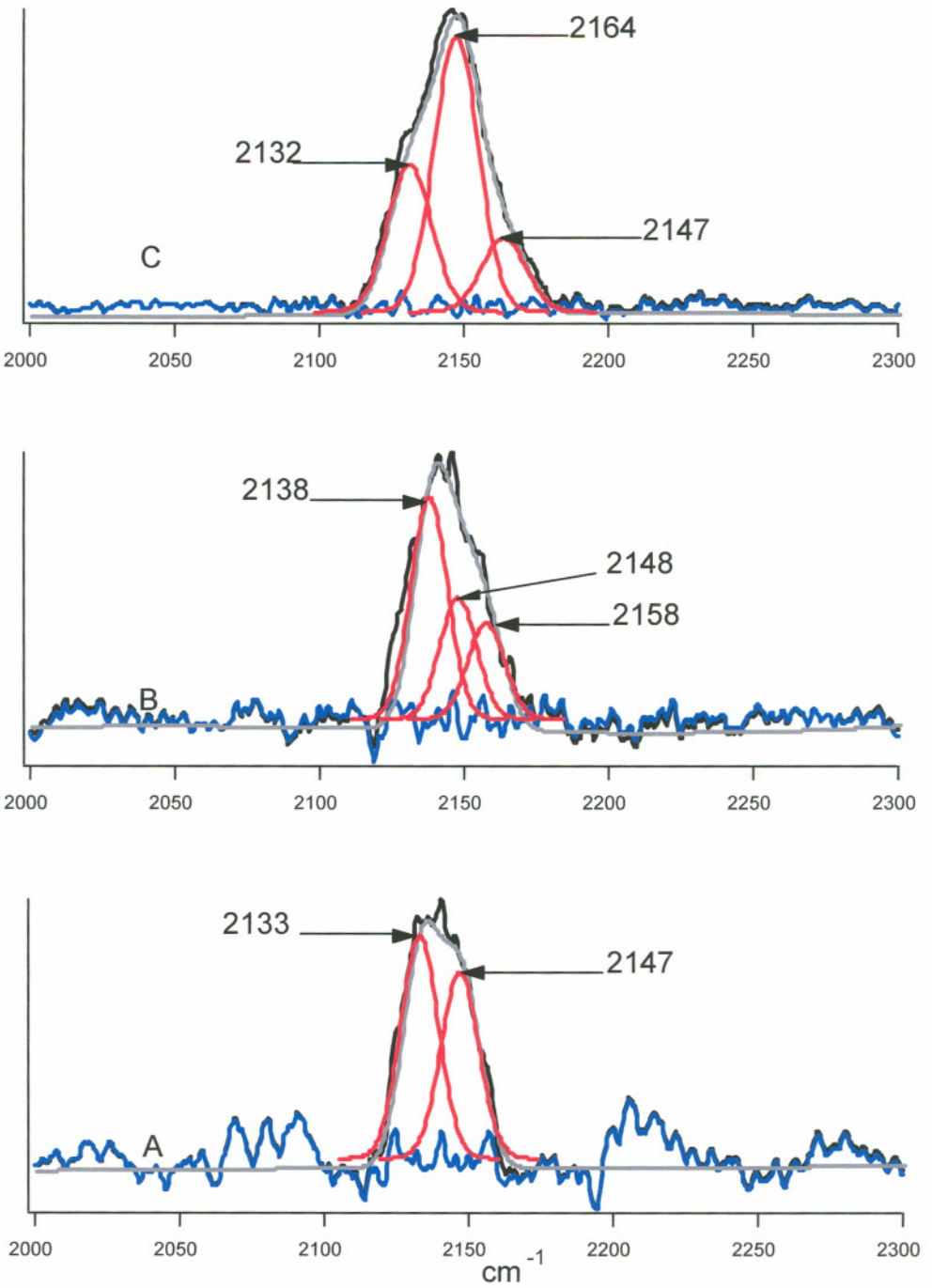


**Figure 4.4** Spectral simulation of the IR spectrum from the titration of DIMPI with His172Ala. (A) 0.5 to 1; (B) 1.0 to 1; (C) 2.0 to 1 ratios of DIMPI/Cu(I). Black = original; gray dashed = simulated spectrum; red = individual fitted peaks; blue = residuals.

**Table 4.2**

DIMPI-Cu(I) Frequencies for Each Mutant

| Ratio of DIMPI to Cu in His242Ala | $\nu$ ($cm^{-1}$) | FWHH ($cm^{-1}$) |
|---|---|---|
| 0.5 to 1 | 2145 | 18 |
| 1.0 to 1 | 2148 | 16.4 |

| Ratio of DIMPI to Cu in Met314Ile | $\nu$ ($cm^{-1}$) | FWHH ($cm^{-1}$) |
|---|---|---|
| 0.5 to 1 | 2149 | 20 |
| 1.0 to 1 | 2148 | 18 |

| Ratio of DIMPI to Cu in His172Ala | $\nu$ ($cm^{-1}$) | FWHH ($cm^{-1}$) |
|---|---|---|
| 0.5 to 1 | 2133<br>2147 | 15.5 |
| 1.0 to 1 | 2138<br>2148<br>2158 | 15 |
| 2.0 to 1 | 2132<br>2147<br>2164 | 18 |

| Ratio of DIMPI to Cu in His107/108Ala | $\nu$ ($cm^{-1}$) | FWHH ($cm^{-1}$) |
|---|---|---|
| 0.5 to 1 | 2137<br>2150 | 16.8 |
| 1.0 to 1 | 2141<br>2152 | 14.3 |
| 2.0 to 1 | 2132<br>2147 | 17 |
| 3.0 to 1 | 2147<br>2161 | 16.3 |

**Table 4.3**

IPI-Cu(I) Frequencies for Each Mutant

| Ratio of IPI to Cu in His242Ala | $\nu$ ($cm^{-1}$) | FWHH ($cm^{-1}$) |
|---|---|---|
| 0.5 to 1 | 2182 | 15 |
| 1.0 to 1 | 2181 | 14 |
| 2.0 to 1 | 2178<br>2190 | 14 |
| 3.0 to 1 | 2177<br>2191 | 14 |

| Ratio of IPI to Cu in Met314Ile | $\nu$ ($cm^{-1}$) | FWHH ($cm^{-1}$) |
|---|---|---|
| 1.0 to 1 | 2182 | 19.4 |
| 2.0 to 1 | 2181<br>2192 | 17 |
| 3.0 to 1 | 2192 | 12 |

| Ratio of IPI to Cu in His172Ala | $\nu$ ($cm^{-1}$) | FWHH ($cm^{-1}$) |
|---|---|---|
| 0.5 to 1 | 2170<br>2185 | 13.8 |

| Ratio of DIMPI to Cu in His107/108Ala | $\nu$ ($cm^{-1}$) | FWHH ($cm^{-1}$) |
|---|---|---|
| 0.5 to 1 | 2182 | 16 |
| 1.0 to 1 | 2184 | 18.5 |
| 2.0 to 1 | 2181<br>2194<br>2212 | 16.8 |

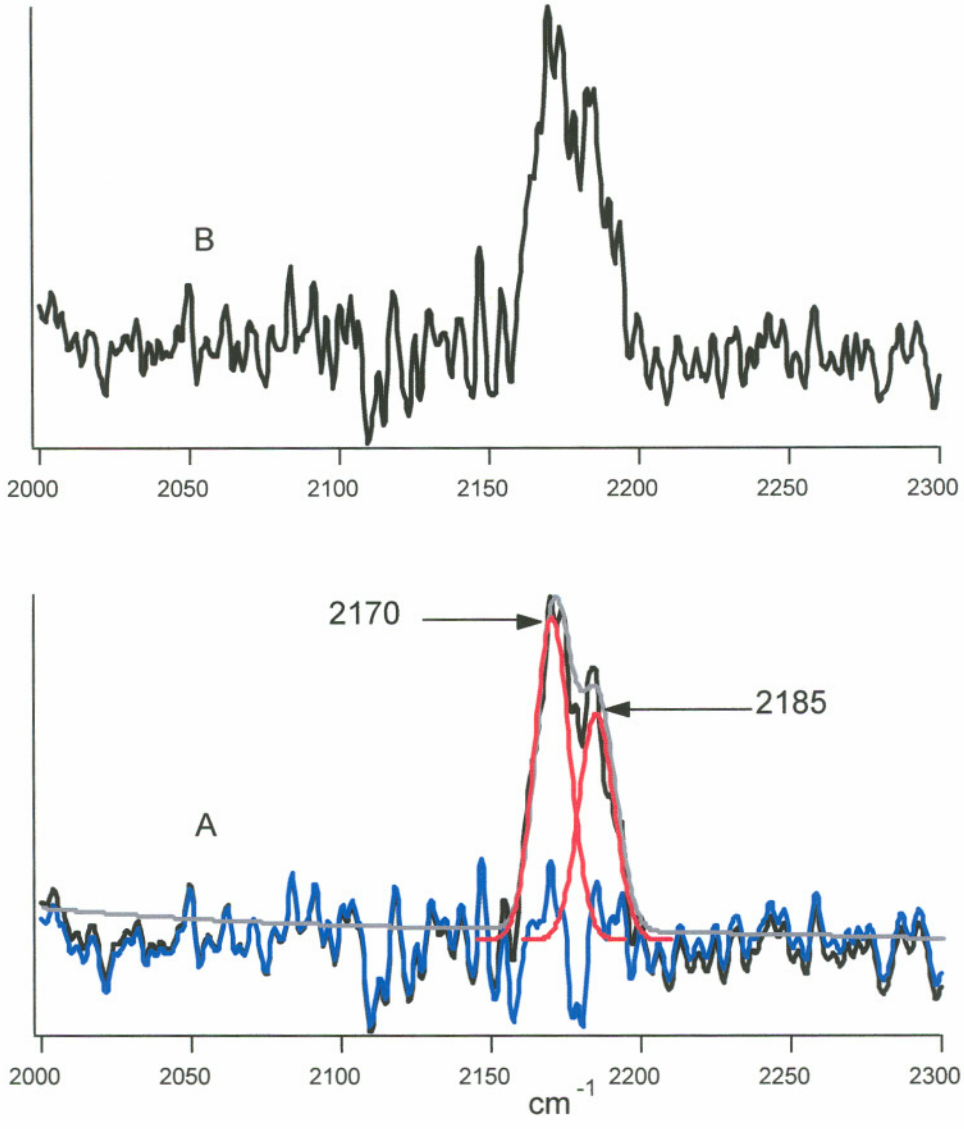


**Figure 4.5** IR spectrum of the titration of IPI with His172Ala. (A) Actual; (B) fitted spectrum. Black = original; gray dashed = simulated spectrum; red = individual fitted peaks; blue = residuals.

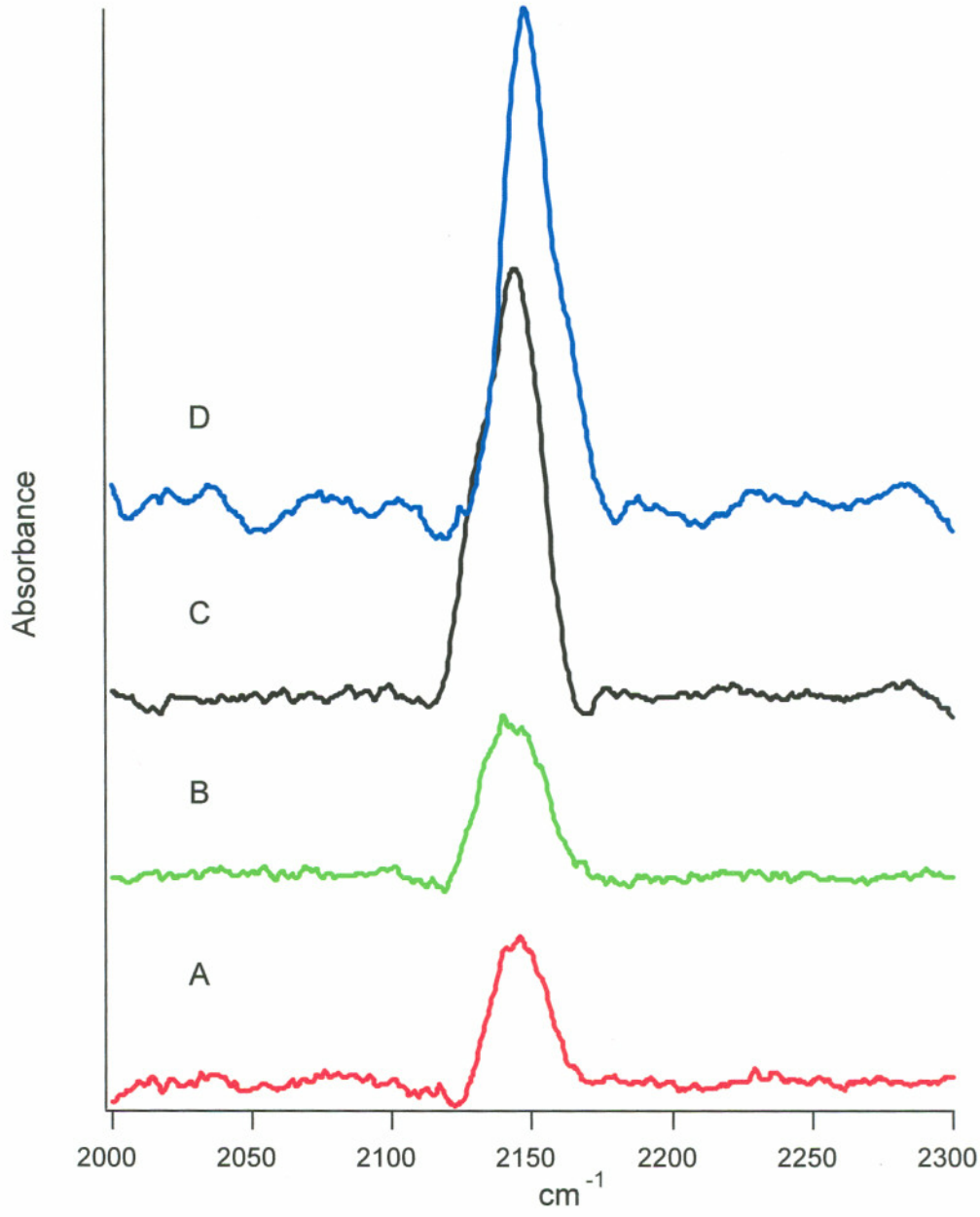


**Figure 4.6** IR spectra of the titration of DIMPI against His107/108Ala. (A) 0.5 to 1; (B) 1.0 to 1; (C) 2.0 to 1; (D) 3.0 to 1 ratios of DIMPI/Cu(I).

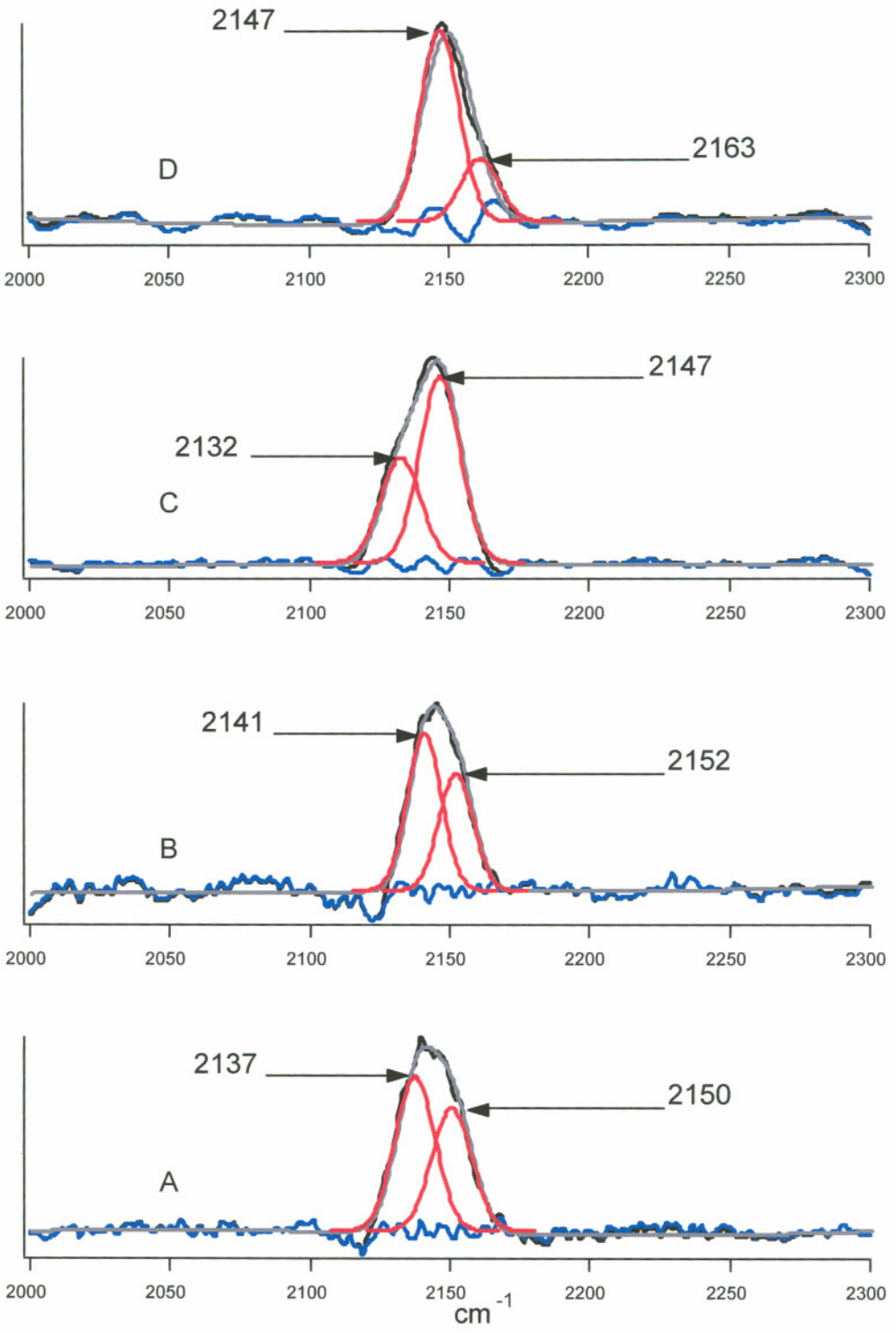


**Figure 4.7** Spectral simulation of the IR spectrum from the titration of DIMPI with His107/108Ala. (A) 0.5 to 1; (B) 1.0 to 1; (C) 2.0 to 1; (D) 3.0 to 1 ratios of DIMPI/Cu(I). Black = original; gray dashed = simulated spectrum; red = individual fitted peaks; blue = residuals.

a decrease in the intensity of the 2132 $cm^{-1}$ band and the 2147 $cm^{-1}$ stretch had gained in intensity to a point at which it was now the dominate feature (Figure 4.7C). Finally, fitting of the final DIMPI/Cu ratio studied (3 to 1) (Figure 4.7D) revealed that the low energy stretch previously observed at ~2137 $cm^{-1}$ had disappeared. This spectrum could be fitted to two peaks at 2147 $cm^{-1}$ and 2163 $cm^{-1}$.

Titration of IPI into His107/108Ala resulted in less variation of the peak position of the IPI-Cu complexes than were determined with DIMPI. At 0.5 and 1.0 IPI/Cu, one band was observed (Figure 4.8A,B). Upon increasing the IPI concentration, the observed stretch did gain intensity. As the IPI/Cu ratio was increased to 2 to 1 (Figure 4.8C), a definite high energy shoulder appeared.

Fitting of the 0.5 and 1.0 to 1 IPI/Cu spectra, using FWHH derived from mono IPI-Cu complex formed with wild-type PHMcc, resulted in a fit that was comprised of a single species centered at 2182 $cm^{-1}$ (Figure 4.9). The fitting of the higher ratio spectra revealed a 3 component spectrum. In that fit, the main peak was centered at 2181 $cm^{-1}$, and the shoulder was comprised of two peaks, one centered at 2192 $cm^{-1}$ and the second at 2212 $cm^{-1}$.

### 4.3.4 FTIR of $Cu_B$ Active Site Mutants

FTIR investigation of $Cu_B$ mutants (His242Ala and Met314Ile) were also investigated. IR analysis of samples containing substoichiometric ratios of DIMPI bound to His242Ala resulted in a spectrum that contained a single narrow stretch (Figure 4.10A). Increasing the concentration of DIMPI added to the sample did not result in the appearance of more stretching frequencies, just a gain in intensity (Figure 4.10B). Fitting of these spectrum, using the mono-DIMPI-Cu FWHH, resulted in a simulation that determined the peak to be centered at 2148 $cm^{-1}$ for both ratios (Figure 4.11A,B).

Analogous results were seen when DIMPI was titrated against Met314Ile. At both low and high concentrations of DIMPI, a single stretch was observed that gained intensity as the concentration of isocyanide was increased (Figure 4.12A,B). Spectral simulation of Met314Ile was best fit with a single band at 2145 $cm^{-1}$ and a FWHH of

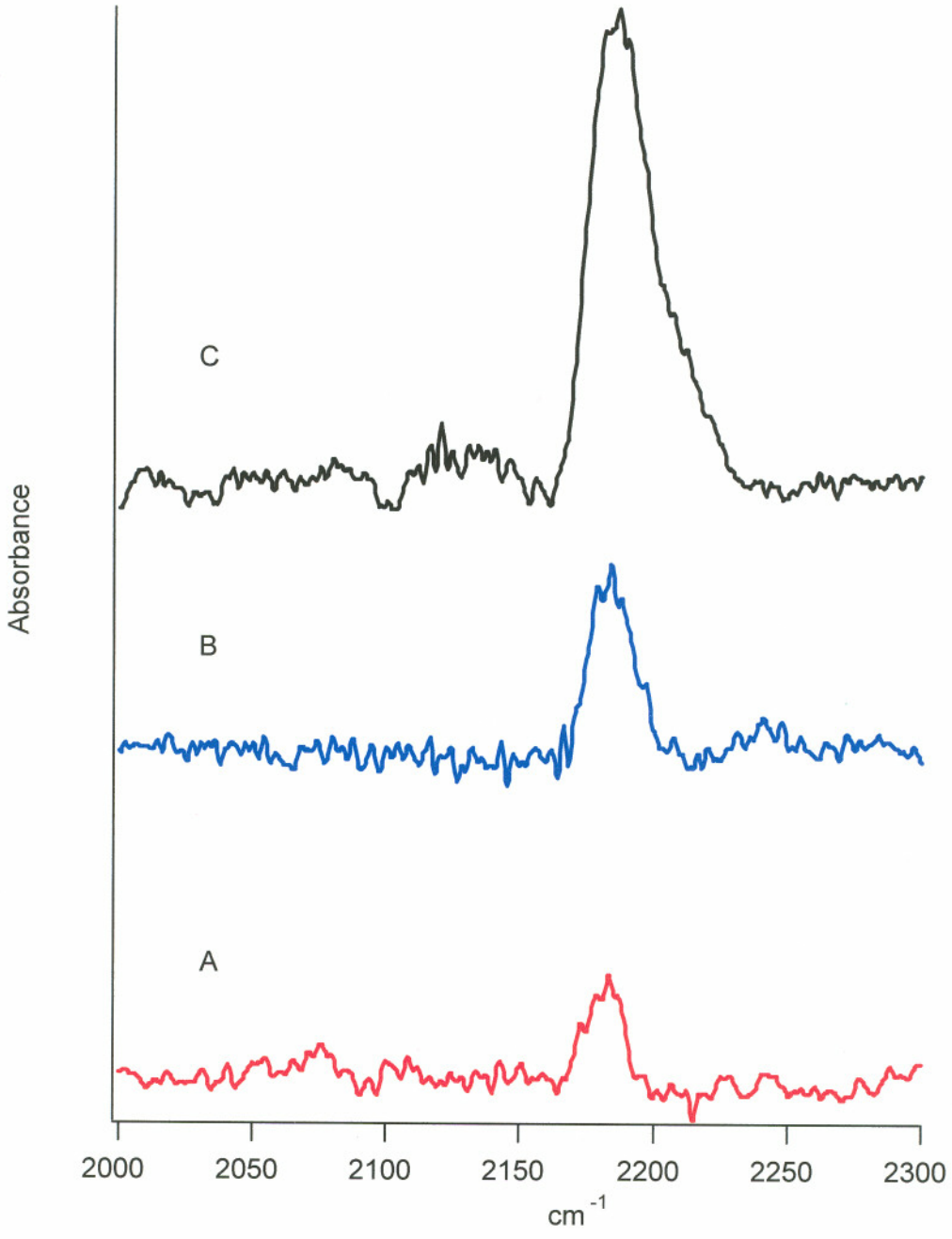


**Figure 4.8** IR spectra of the titration of IPI against His107/108Ala. (A) 0.5 to 1; (B) 1.0 to 1; (C) 2.0 to 1 ratios of IPI/Cu(I).

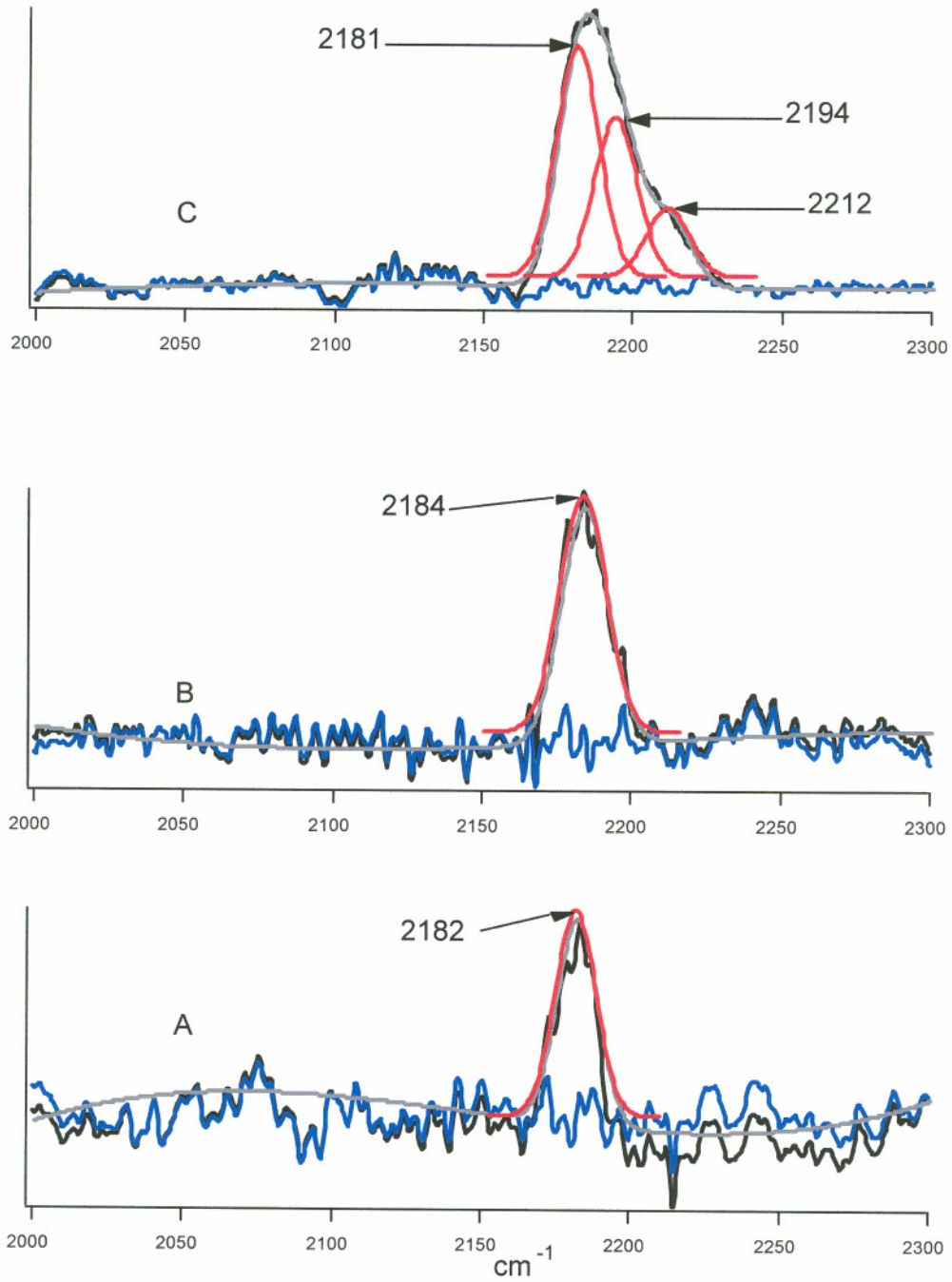


**Figure 4.9** Spectral simulation of the IR spectrum from the titration of IPI with His107/108Ala. (A) 0.5 to 1; (B) 1.0 to 1; (C) 2.0 to 1 IPI/Cu(I). Black = original; gray dashed = simulated spectrum; red = individual fitted peaks; blue = residuals.

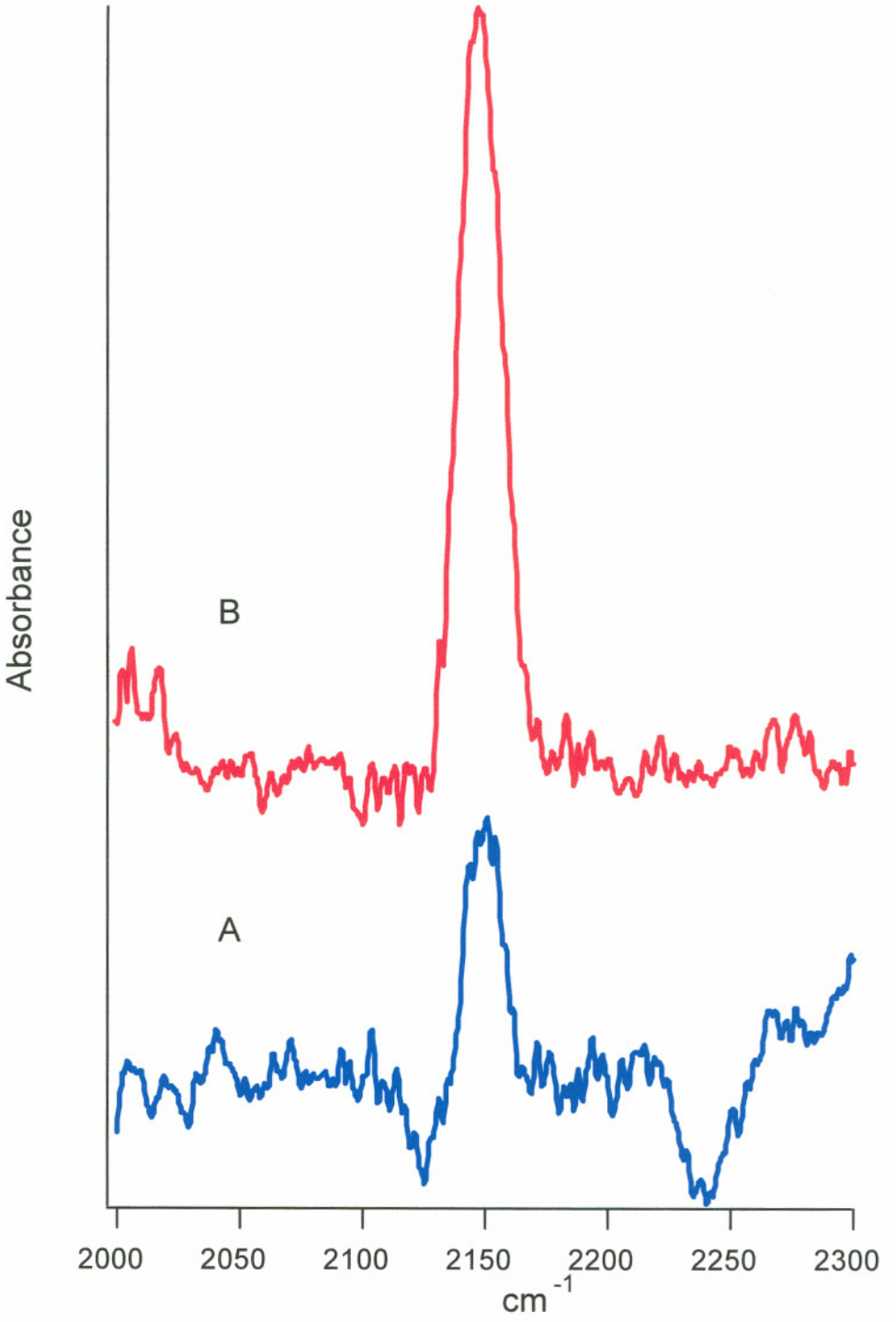


**Figure 4.10** IR spectra of the titration of DIMPI against His242Ala. (A) 0.5 to 1; (B) 1.0 to 1 ratios of DIMPI /Cu(I).

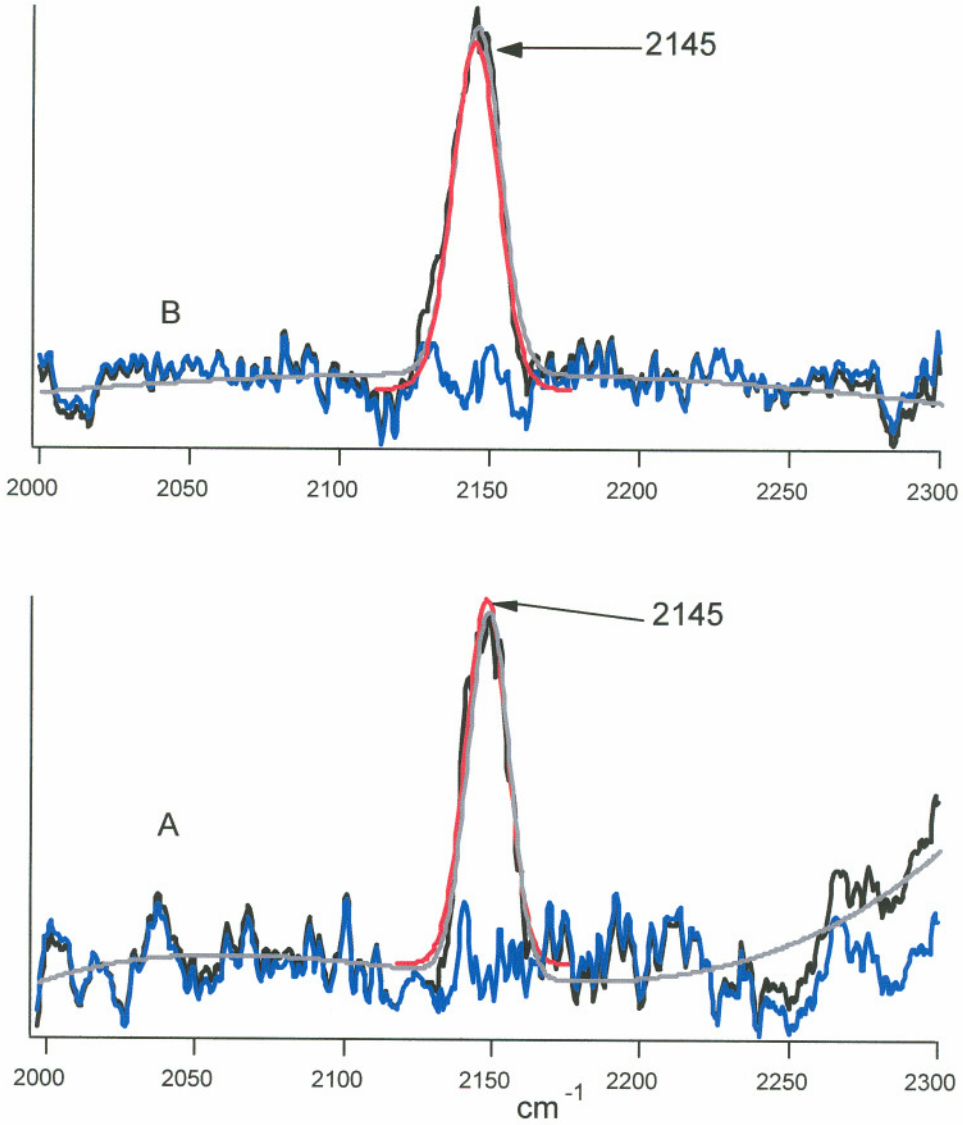


**Figure 4.11** Spectral simulation of the IR spectrum from the titration of DIMPI with His242Ala. (A) 0.5 to 1; (B) 1.0 to 1 ratio of DIMPI/Cu(I). Black = original; gray dashed = simulated spectrum; red = individual fitted peaks; blue = residuals.

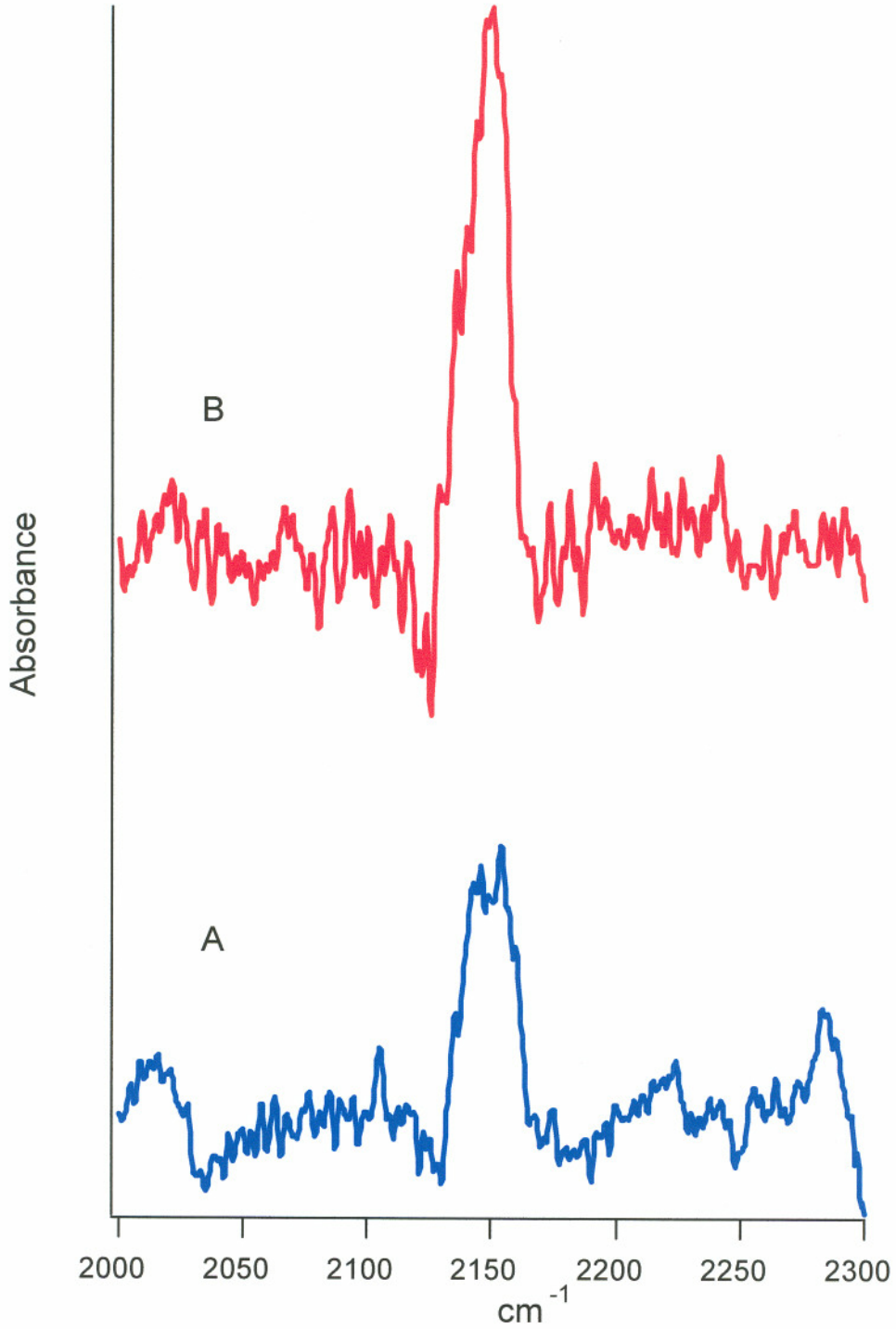


**Figure 4.12** IR spectra of the titration of DIMPI against Met314Ile. (A) 0.5 to 1; (B) 1.0 to 1 ratio of DIMPI/Cu(I).

18 $cm^{-1}$ for the 0.5 to 1 ratio, and at 2148 $cm^{-1}$ with a FWHH of 16.4 $cm^{-1}$ for the 1 to 1 spectrum (Figure 4.13A,B).

Titration of Met314Ile with IPI resulted in spectra with similar results compared to the DIMPI titrations, but with frequencies shifted in accordance with the expected frequencies for an IPI-Cu stretch (Figure 4.14). At an IPI/Cu ratio of 1 to 1, a single stretch was observed that could be fitted to a single Gaussian peak centered at 2183 $cm^{-1}$ (FWHH 19.4 $cm^{-1}$) (Figure 4.15A). As the ratio of isocyanide to Cu increased above the 1 to 1 ratio, a second band appeared. The two component spectra could be simulated with two peaks, one centered at 2183 $cm^{-1}$ and a second at 2193 $cm^{-1}$ both with FWHH of 14 $cm^{-1}$ (Figure 4.15B). As the ratio of DIMPI/Cu was increased to 3 to 1 (Figure 4.15C), the fitting showed that the 2182 $cm^{-1}$ stretch was no longer present, and the observed peak was totally comprised of the 2192 $cm^{-1}$ species.

Results obtained from titration of His242Ala with IPI were similar to what was seen in Met314Ile (Figure 4.16). At 0.5 and 1.0 IPI/Cu, a single band was observed. As the concentration of isocyanide was increased, a two component spectrum was also observed. Fitting of the low ratio complexes determined that the single species was centered at 2182 $cm^{-1}$ with FWHH of $\sim$15 $cm^{-1}$ (Figure 4.17A,B). Fitting of the two component spectrum resulted in one peak being centered at 2178 $cm^{-1}$ and the second at 2192 $cm^{-1}$ (Figure 4.17C,D). At the highest IPI/Cu ratio of 3 to 1, the intensity of the 2192 $cm^{-1}$ stretch is now the predominate spectral component.

## 4.4 DISCUSSION

### 4.4.1 Copper Binding to the Mutants in the Oxidized and Reduced State

The results showing that the Cu/protein ratio (in the oxidized state) after reconstitution was greater than 1 to 1 in three out of the four mutants studied was somewhat surprising since it was believed that the mutated copper binding site would not be able to ligate a copper atom. Met314Ile was shown to bind an average of 1.4 Cu/protein in the oxidized state meaning that the altered $Cu_B$ site may still be capable of loosely binding one copper atom. This is a plausible argument since EXAFS

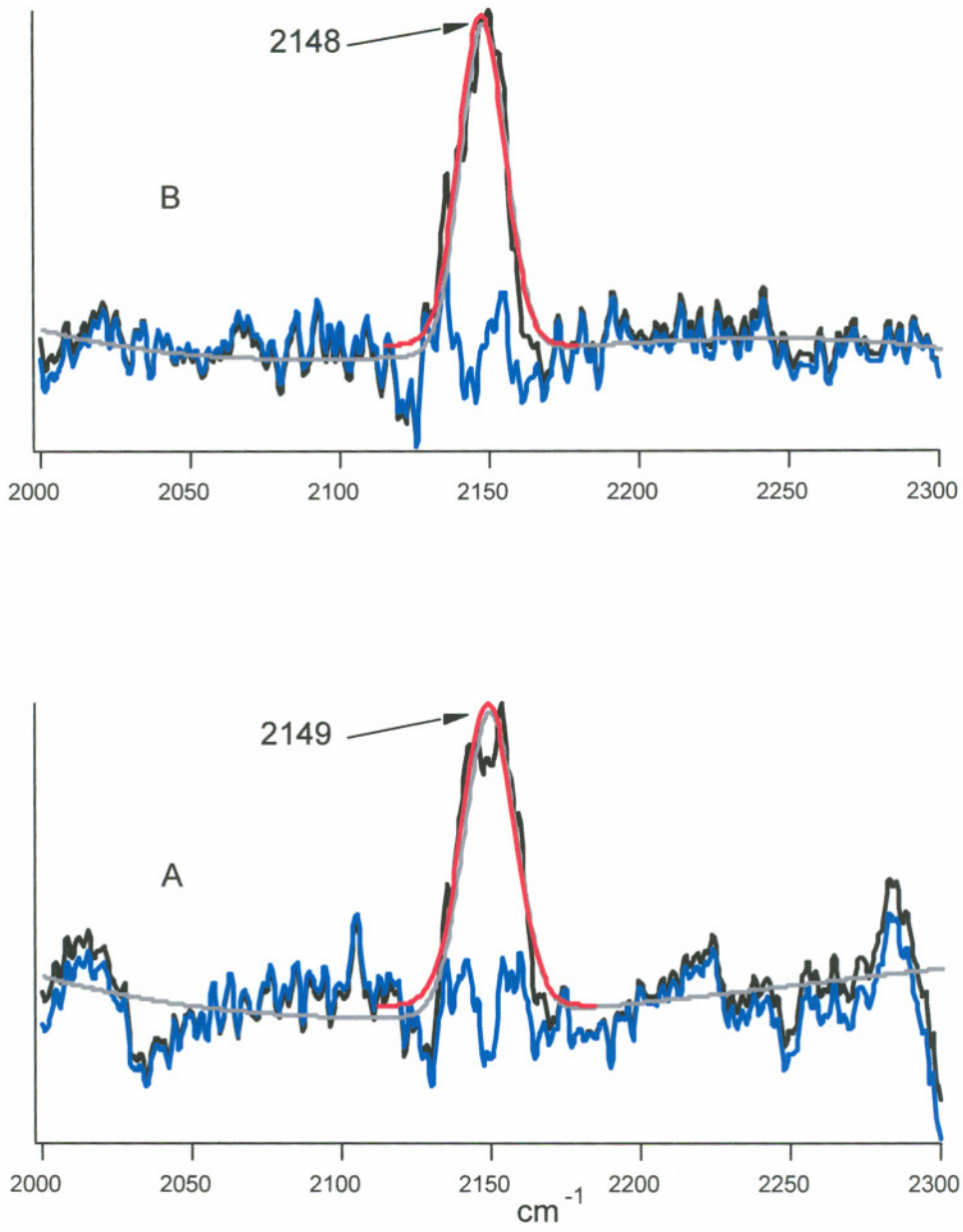


**Figure 4.13** Spectral simulation of the IR spectrum from the titration of DIMPI with Met314Ile. (A) 0.5 to 1; (B) 1.0 to 1 ratio of DIMPI/Cu(I). Black = original; gray dashed = simulated spectrum; red = individual fitted peaks; blue = residuals.

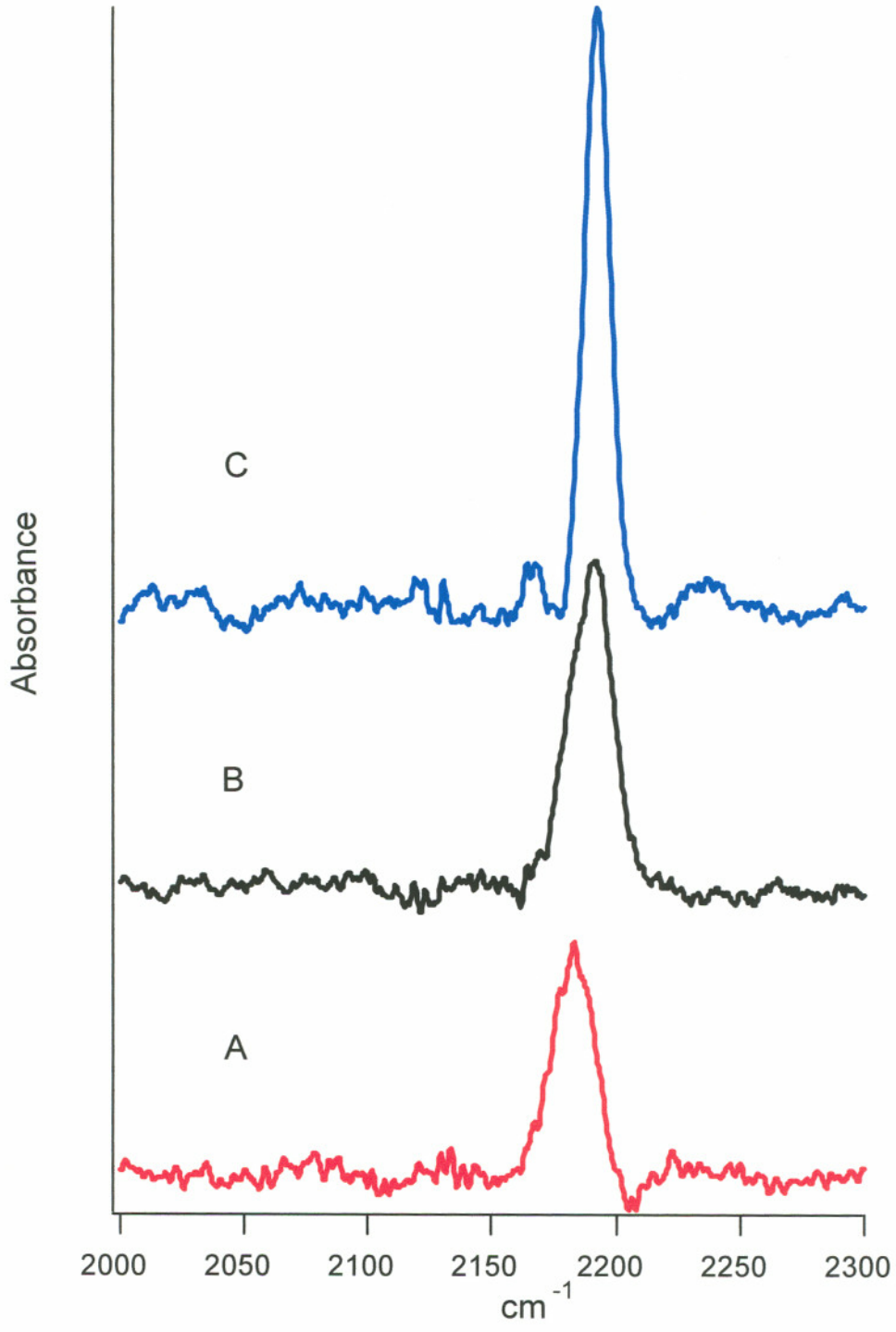


**Figure 4.14** IR spectra of the titration of IPI against Met314Ile. (A) 0.5 to 1; (B) 2.0 to 1; (C) 3.0 to 1 ratios of IPI/Cu(I).

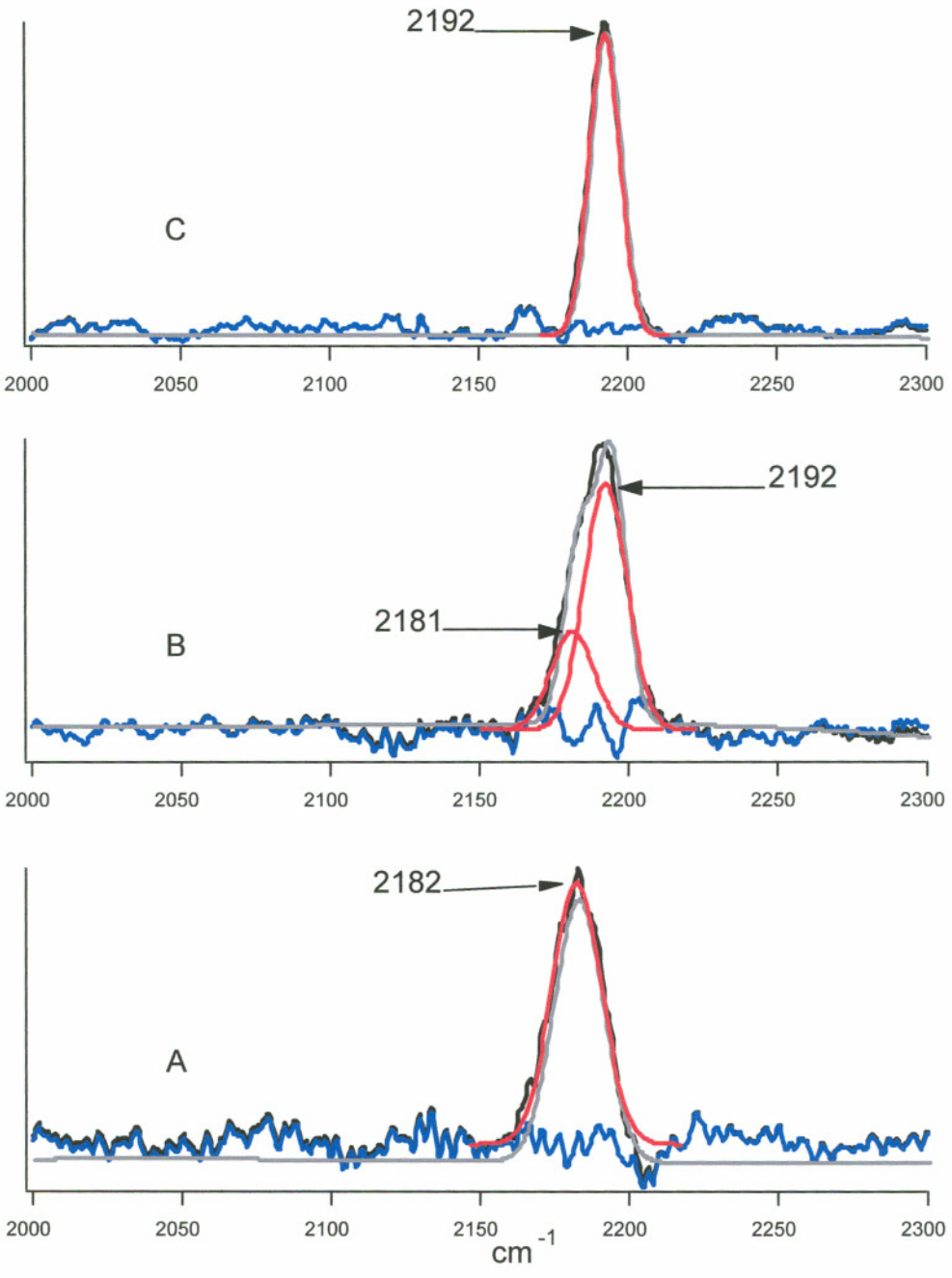


**Figure 4.15** Spectral simulation of the IR spectrum from the titration of IPI with Met314Ile. (A) 0.5 to 1; (B) 2.0 to 1; (C) 3.0 to 1 ratio of IPI/Cu(I). Black = original; gray dashed = simulated spectrum; red = individual fitted peaks; blue = residuals.

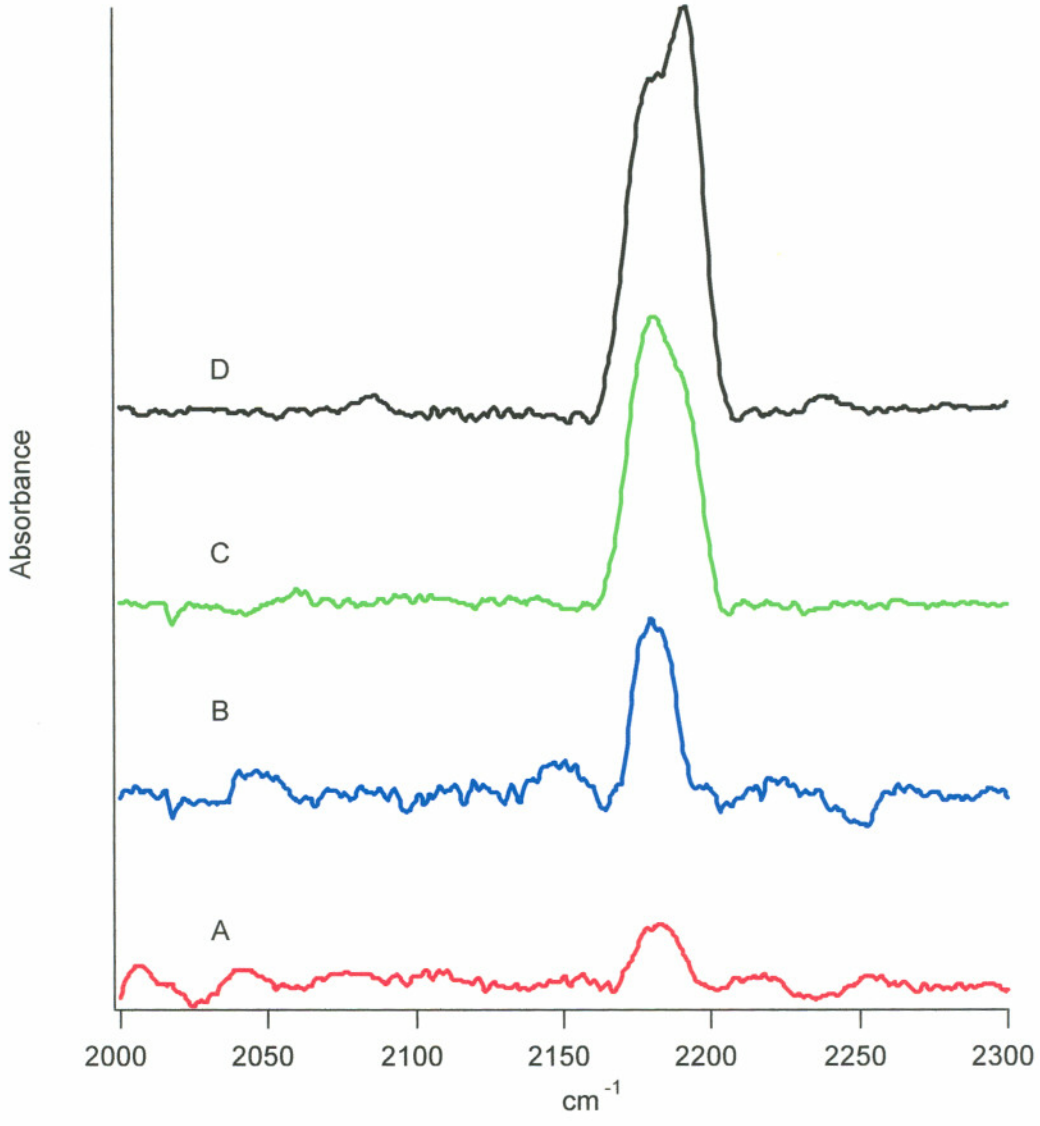


**Figure 4.16** IR spectra of the titration of IPI against His242Ala. (A) 0.5 to 1; (B) 1.0 to 1; (C) 2.0 to 1; (D) 3.0 to 1 ratio of IPI/Cu(I).

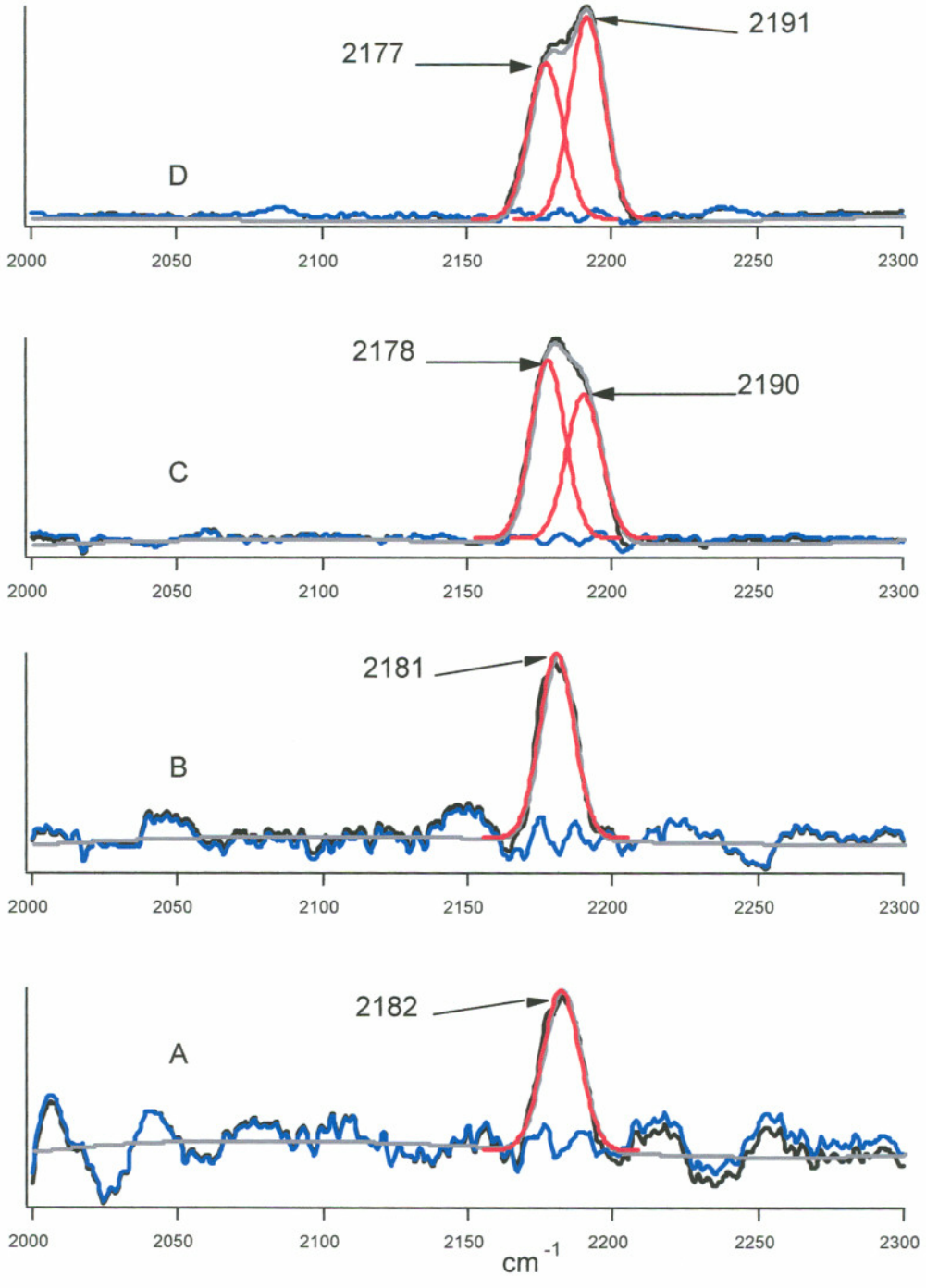


**Figure 4.17** Spectral simulation of the IR spectrum from the titration of IPI with His242Ala. (A) 0.5 to 1; (B) 1.0 to 1; (C) 2.0 to 1; (D) 3.0 to 1 ratio of IPI/Cu(I). Black = original; gray dashed = simulated spectrum; red = individual fitted peaks; blue = residuals.

analysis of wild-type PHMcc has demonstrated that the methionine ligand is only associated in ligation of the Cu in the reduced form of the enzyme and is not seen as a ligand to the copper in the oxidized state of the enzyme. Thus, mutating the Met314 ligand to an isoleucine appears to affect only Cu(I) ligation and not Cu(II), since in the oxidized state the Cu(II) binds to H242 and H244 and these are unchanged in this mutant. This is further evidence that the methionine ligand to the $Cu_B$ center in PHMcc is only associated with binding of the Cu(I) species and not the Cu(II).

Upon reduction of this mutant with ascorbate, the Cu/protein ratio fell to 1 to 1. This suggests that in the reduced state, the $Cu_B$ binding site cannot ligate a copper atom with just two histidine residues. Therefore, it appears that the methionine residue is important in stabilizing the Cu(I) atom in the active site and is an integral Cu(I) ligand. This conclusion is further supported by previous studies that had already shown that this Met314Ile mutant was an inactive enzyme [Boswell et al., 1996]. These copper reconstitution studies suggest that the inactivation of the mutant may be caused by its inability to bind copper to the $Cu_B$ site upon reduction.

Further evidence of the importance of the two histidine (His242 and His244) ligands in binding oxidized copper in the $Cu_B$ site was seen from the reconstitution of His242Ala with copper. After the dialysis against copper, the ratio of copper bound to protein was consistently near 1.1 Cu/protein. This suggested that upon substitution of this histidine residue with an alanine, the protein loses its ability to bind Cu(II) at the $Cu_B$ center. This is what was expected since evidence from both EXAFS and the crystal structure has shown that the $Cu_B$ site is ligated mainly by two histidine residues and two water molecules in the oxidized state. Upon reduction, no further loss or increase of copper was observed, which in turn implies that His244 and Met314 are not sufficient ligands to stabilize the binding of copper to that center in the reduced state.

His172Ala was studied in the belief that it would produce protein which lacked a $Cu_A$ center, since His172Ala has been shown to be one of the copper ligands [Prigge et al., 1997]. Reconstitution of His172Ala with copper resulted in the uptake of an average of 1.4 Cu/protein. Reduction of this mutant resulted in no decrease of

the Cu/protein ratio. This suggests that the $Cu_A$ center can ligate the copper with only two histidine ligands (His107 and His108) to the copper in both the oxidized and reduced states. Furthermore, recent EXAFS analysis of reduced wild-type PHMcc has shown that, upon reduction, the His172Ala ligand is not detectable suggesting that this histidine may be somewhat labile in its ligation of the copper atom and not critical for copper binding at the $Cu_A$ center. However, the mutation of this ligand does produce an inactive enzyme [Yonekura et al., 1996; Kolhekar et al., 1997]. Therefore, although His172 may not be important for copper ligation, it is important for enzymatic activity.

The ratio of copper to protein for the His107/108Ala was also measured to be greater than 1 to 1 in the oxidized state. This was not expected and cannot be rationalized as a copper bound to both sites in the protein since the only remaining copper ligand in the $Cu_A$ site is a lone histidine (His172). Therefore, it is believed that the excess copper is most likely associated with adventitious copper bound to the protein. A second explanation is a copper atom that is weakly bound to the $Cu_A$ site by the remaining His172, nearby Tyr79, and 2 water molecules. This extra Cu does dissociate upon reduction of the mutant, as the ratio of Cu/protein falls to 1 to 1.

### 4.4.2 Analysis of His107/108Ala Isocyanide Complexes

Through the reconstitution study in the reduced protein, it was determined that the His107/108Ala mutant could bind only 1 copper per protein. EXAFS analysis and structural inference has determined that the lone Cu atom resides at the $Cu_B$ center (unpublished data). Therefore, in theory the binding of DIMPI to $Cu_B$ should give analogous results with respect to what was observed for wild-type PHMcc with DIMPI bound, namely a single stretch at 2138 $cm^{-1}$ associated with a single DIMPI bound to the $Cu_B$ center and the expected tris-DIMPI-Cu(I) complex (2160 $cm^{-1}$) at high isocyanide concentrations [Chapter 3]. The results do show a band at $\sim$2135 $cm^{-1}$ indicative of a monoisocyanide bound to the $Cu_B$ site in the His107/108Ala mutant and a tris isocyanide stretch at high DIMPI concentration was also observed (Scheme 4.1). However, what was also seen was a second titratable band at $\sim$2147 $cm^{-1}$. Comparison of this frequency with frequencies previously reported for DIMPI

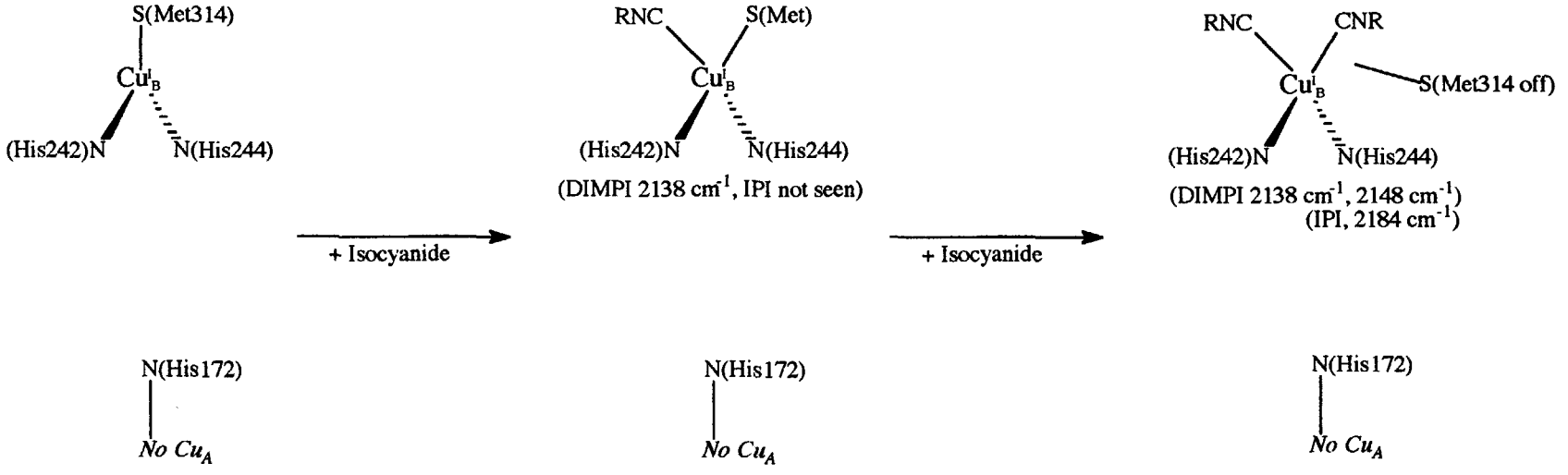


**Scheme 4.1** Predicted isocyanide ligation to His107/108Ala.

bound to the copper centers in DβM and hemocyanin would suggest that this stretch arises from a Cu-DIMPI complex with three histidine ligands (i.e., $Cu_A$-DIMPI) [Reedy et al., 1995]. However, since this mutant is devoid of the tris-histidine-$Cu_A$ center, it is more probable that the 2148 $cm^{-1}$ signal is derived from a copper atom that has two isocyanides bound and only two histidine ligands, possibly from the displacement of the methionine to $Cu_B$ ligand by the second DIMPI molecule. Thus it appears that for both DβM and Hc the correct assignment for the 2148 $cm^{-1}$ band observed in that study arose from this type of complex (i.e., a bis-His, bis-DIMPI rather than a mono DIMPI- tris-histidine-Cu(I) complex).

Wild-type PHMcc was shown to bind the IPI ligand as both a monomer (2178 $cm^{-1}$) and a tris (2192 $cm^{-1}$) Cu(I) isocyanide complex [Chapter 3]. Therefore, addition of IPI to His107/108Ala mutant should give rise to three stretching frequencies associated with the mono, bis, and tris IPI-Cu complex, analogous to the DIMPI experiments. Analysis of the results of the titration of IPI with His107/108Ala showed two main spectral features (Scheme 4.1). The isocyanide stretch seen at 2194 $cm^{-1}$ is analogous to what was observed for a tris-IPI-Cu(I) complex in wild-type and can be assigned to the same complex in this mutant. However, the 2182 $cm^{-1}$ band is a novel frequency and cannot arise from a mono-IPI-Cu(I) stretch since that frequency lies at 2172 $cm^{-1}$. Therefore, it is believed that the 2182 $cm^{-1}$ band is from a bis-histidine, bis-IPI-Cu(I) complex. Furthermore, as will be discussed shortly, comparison of the observed frequency with the frequency seen in the IPI titration against the $Cu_B$ mutants suggests that the isocyanide copper complex responsible for this frequency has to arise from a bis-isocyanide-Cu(I) structure. It should be noted that the bis-IPI complex appears to be shifted nearly the same amount (10 $cm^{-1}$) as was the case for the shift between mono and bis-DIMPI-Cu(I) frequencies.

### 4.4.3 Analysis of the $Cu_B$ Depleted Mutants with Isocyanide Present

It was reasoned that binding of an isocyanide to the $Cu_B$ center prevented ligation of a second isocyanide at the $Cu_A$ center through steric hindrance [Chapter 3]. Thus, in order to probe the binding properties of the $Cu_A$ center, removal of the

copper at the $Cu_B$ site seemed critical. Both Met314Ile and His242Ala were shown to bind only one equivalent of copper in the reduced state. Furthermore, this copper was believed to be at the intact $Cu_A$ center. Therefore, by investigating these mutants, it became possible to probe the $Cu_A$ center without interfering effects from the $Cu_B$ center where it appeared that binding of isocyanide to that site prohibits simultaneous binding of an isocyanide at the $Cu_A$ site.

Investigation of these two $Cu_B$ depleted mutants with DIMPI resulted in the observation of a single stretching frequency of 2148 $cm^{-1}$ (Schemes 4.2 and 4.3). This correlates directly to the same frequency that was attributed to the bis-DIMPI complex seen in the His107/108Ala mutant. Therefore, by comparison of the results obtained from the DIMPI-Cu spectra of the Met314Ile and His242Ala mutants with the previous results from the His107/108Ala mutant study, we can conclude that the 2148 $cm^{-1}$ stretching frequency observed in the $Cu_B$ depleted mutants must be derived from two DIMPI molecules bound to the $Cu_A$ center which has had one of its histidine ligands replaced by an isocyanide. Concurrent with the results obtained with DIMPI, the IPI experiments produced a bis complex also. Thus it appears that isocyanide binding to the $Cu_A$ center displaces one of the protein derived Cu(I) ligands. Preliminary EXAFS analysis of the reduced forms of these mutants shows a lengthening of the His172–Cu(I) bond distance upon reduction (unpublished data). This lengthening most likely results in a weakening of the H172–Cu bond, therefore making that histidine the best candidate for displacement.

The isocyanide stretch at 2148 (DIMPI) and 2182 $cm^{-1}$ (IPI) can definitively be assigned to a bis-isocyanide bis-histidine–Cu(I) complex and not a mono-isocyanide tris-histidine–Cu(I) complex as previously believed by comparing the results obtained from the three mutants studied (His107/108Ala, His242Ala, and Met314Ile). Since the double mutant lacks a copper center that is coordinated by three histidine residues, it cannot have a tris-histidine isocyanide copper complex. It can have either the described bis-isocyanide complex, where the copper is also ligated by two protein derived histidine ligands, or a mono-isocyanide–Cu(I) complex that has one methionine and two histidine ligands. The latter complex is definitively ruled out as being responsible for the 2148/2182 $cm^{-1}$ frequency by analyzing the observed IR

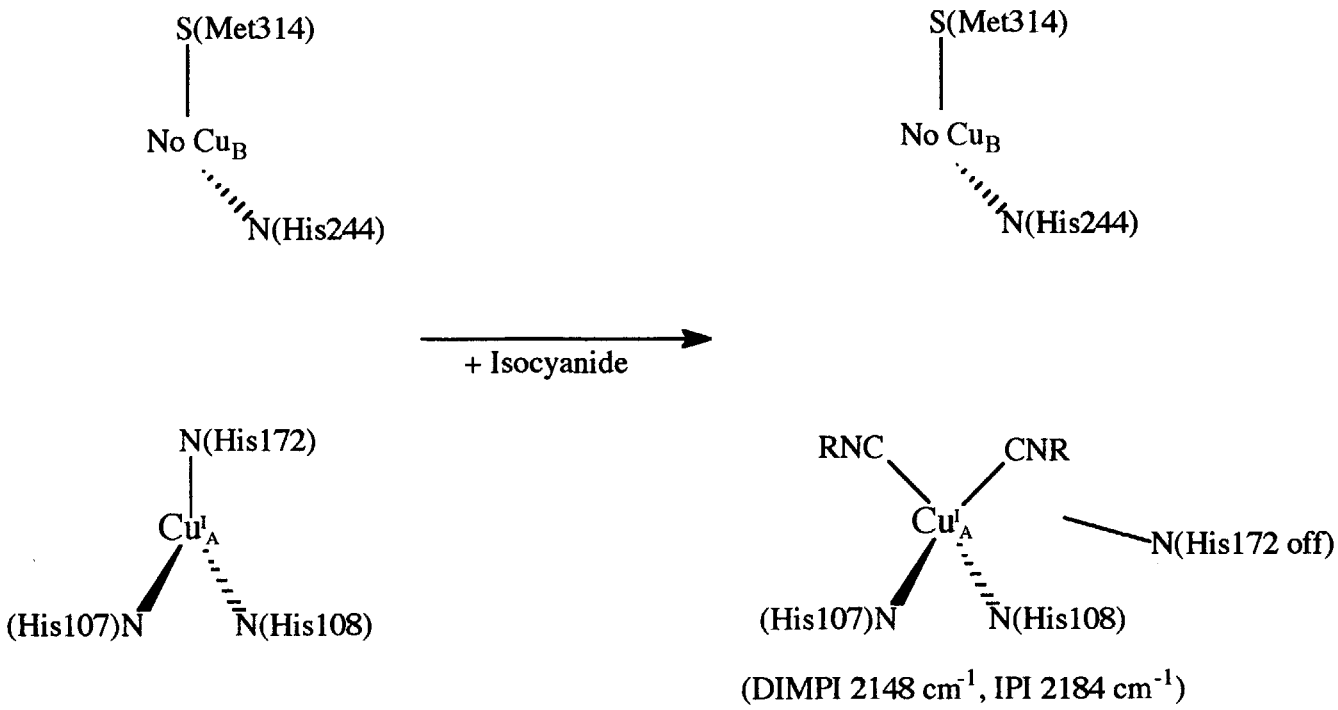


**Scheme 4.2** Predicted isocyanide ligation to His242Ala.

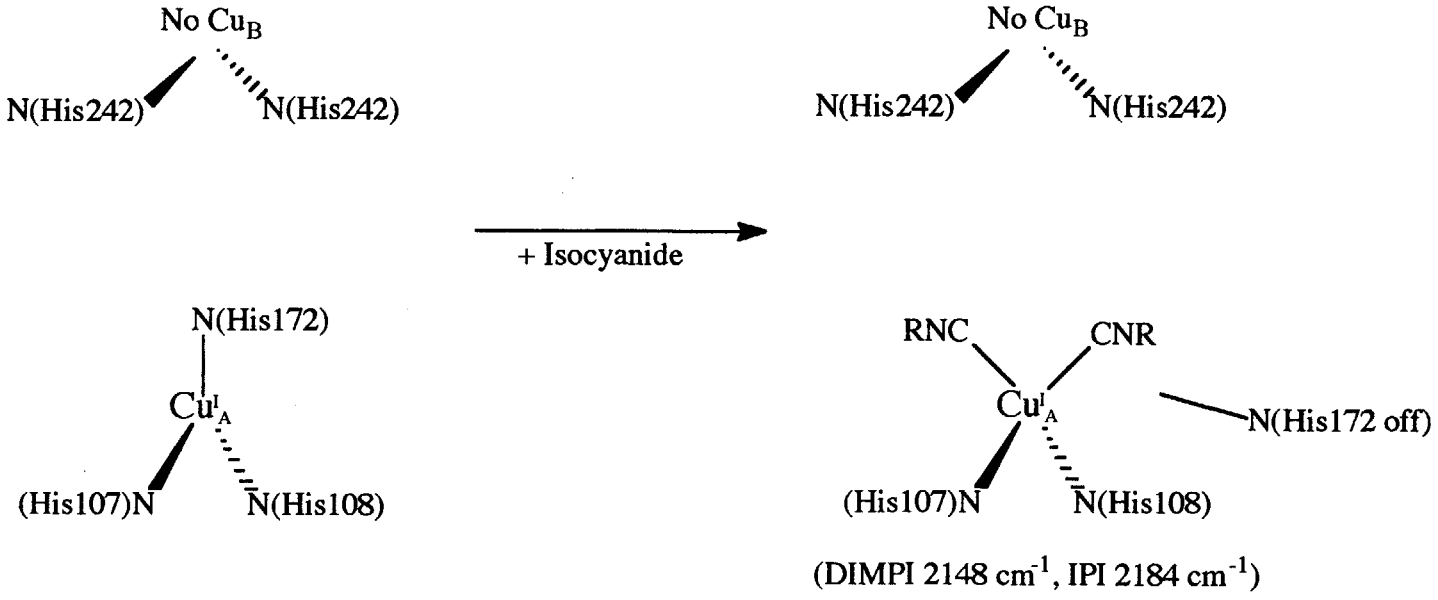


**Scheme 4.3** Predicted isocyanide ligation to Met314Ile.

frequencies of the Cu(I)–isocyanide bound to the $Cu_B$ depleted mutants. Here, the possible origins for this frequency are either a tris-histidine isocyanide copper complex, or the bis-isocyanide, bis-histidine complex. The only possible configuration shared by these two sets of mutants is the bis complex, since the copper center in the His107/108Ala mutant is not ligated by three histidine ligands. Therefore, the 2148 and 2182 $cm^{-1}$ stretch most likely arise from a copper center that is ligated by two histidine residues and two isocyanide molecules.

### 4.4.4 FTIR Analysis of Bound Isocyanide to His172Ala

Initially it was believed that by replacing the His172 ligand to the $Cu_A$ center with an alanine residue, the protein would lose its ability to bind copper at that site, thus allowing characterization of PHMcc that was lacking the $Cu_A$ center. However, as previously stated, from the copper reconstitution studies, it appears that this mutant has retained its ability to bind copper at both centers. The FTIR analysis of DIMPI bound to His172Ala displayed a stretching frequency that was indicative of an isocyanide bound to the $Cu_B$ center (Scheme 4.4). The 2135 $\pm$ 3 $cm^{-1}$ stretch coincides with the observed frequency that was seen in wild-type PHMcc and was determined to be from mono-DIMPI–$Cu_B$ species. What was also seen at all isocyanide/Cu ratios was a second stretching frequency at 2148 $cm^{-1}$. Comparison of this stretch with data obtained from the $Cu_B$ depleted mutants and the His107/108Ala have determined that this frequency is derived from a bis-isocyanide–Cu(I) center that is ligated by only two histidine ligands and no methionine. This could either describe isocyanide incorporation at both copper centers where the 2138 $cm^{-1}$ stretch is a mono-DIMPI–Cu complex, and the 2148 $cm^{-1}$ is a bis-DIMPI–Cu(I) complex at the $Cu_A$ center. It could also be indicative of what was seen with the His107/108Ala mutant where the two frequencies arose from formation of mono and bis complexes at the same copper center. Thus, it appears that the His172Ala mutant not only binds two copper atoms in the reduced state, but both copper centers now have the ability to bind an isocyanide ligand simultaneously. Preliminary IR results using the IPI as a ligand probe with this mutant also exhibited two stretching frequencies that corresponded to both copper centers.

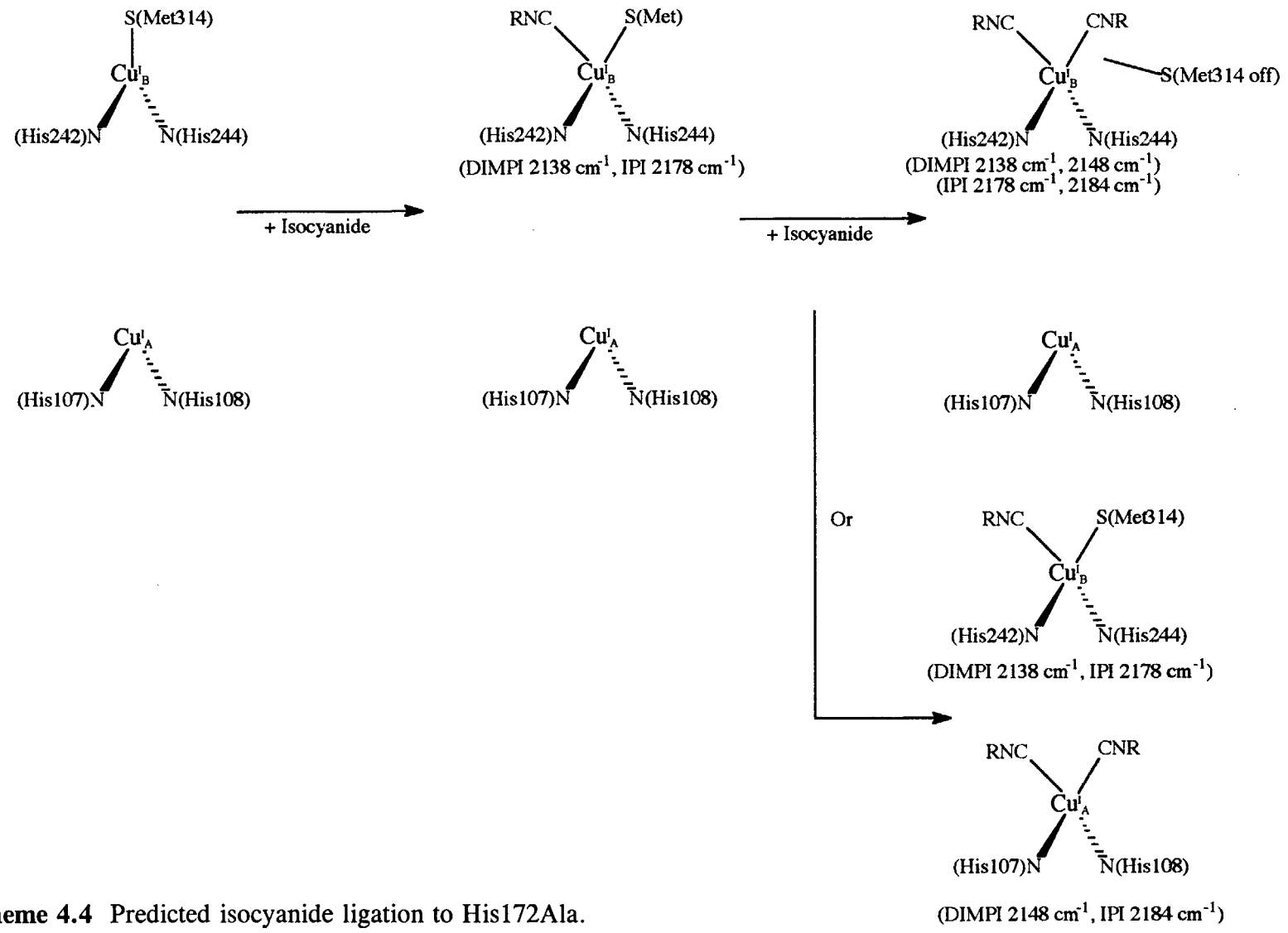


**Scheme 4.4** Predicted isocyanide ligation to His172Ala.

Analysis of the crystal structure of wild-type PHMcc may explain why this mutant can now bind an isocyanide at both copper centers. Modeling of a DIMPI bound to the $Cu_B$ site in wild-type PHMcc appeared to create a strong p-stacking interaction with tyrosine 79 [Chapter 3]. This residue is closely associated with the His172 residue. It is possible that upon ligation of an isocyanide at the $Cu_B$ site, the isocyanide may force the Tyr79 residue closer to the His172 copper ligand, thus protecting the site from ligation of an isocyanide at $Cu_A$. However, upon mutagenesis of the His172 residue, the Tyr-His interaction is no longer present, allowing for increased access to the $Cu_A$ site and simultaneous ligation of an isocyanide at both centers.

## 4.5 CONCLUSIONS

It now appears that the $Cu_A$ center is indeed reactive to exogenous ligand binding, contrary to what was observed with the wild-type enzyme [Chapter 3], possibly in both the presence and absence of the $Cu_B$ center. This may suggest a different role for the $Cu_A$ site. Since this center is able to bind small molecules, it may actually be the copper center that binds $O_2$ first, donating an electron to the oxygen to form superoxide which then migrates to the other $Cu_B$ center. Furthermore, a definite cooperation between the two metal centers has been observed. It is apparent that mutations affecting one copper center, which either deletes that site or modifies the copper binding geometry has a definite affect on the reactivity of the second copper center.

# CHAPTER 5
# CARBON MONOXIDE BINDING TO HEMOCYANIN

## 5.1 INTRODUCTION

Hemocyanin (Hc) is a coupled binuclear copper containing protein that functions as the major oxygen carrier protein in molluscs and arthropods [Eickman et al., 1979]. Crystal structures exist for three varieties of Hc: deoxy and oxy form of *Limulus polyphemus* [Hazes et al., 1993; Magnus et al., 1994] the deoxy form of *Panulirus interruptus* [Volbeda and Hol, 1989], and one molluscan from *Octopus dofleini* [Cuff et al., 1998]. The structures confirmed that each copper is ligated by three histidines. Hc reversibly binds $O_2$ as peroxide in a $\mu$-$\eta^2$:$\eta^2$ configuration [Freedman et al., 1976; Kitajima et al., 1992a,b; Magnus et al., 1993]. The ground state of oxyHc is EPR silent due to a strong antiferromagnetic coupling of the two Cu(II) ions by the exogenous peroxo ligand that bridges the two metal centers [Solomon et al., 1976; Dooley et al., 1978].

Carbon monoxide reversibly binds to deoxy Hc (Cu(I) Cu(I)) in a stoichiometry of 1 CO/2 Cu [Zolla and Brunori, 1983]. Formation of CO-Hc is associated with the appearance of a weak absorption band near 320 nm and an emission in the visible region when excited in the near UV [Fager and Alben, 1972; Van der Deen and Hoving, 1979; Kuiper et al., 1980]. This emission is dependant upon the presence of both coppers, since neither half-met nor half-apo CO-Hc exhibit this spectral feature [Finazzi-Agrò et al., 1982; Zolla et al., 1984]. Infrared investigation of CO bound to Hc has determined the $\nu_{CO}$ for molluscan (2063 $cm^{-1}$), arthropodal (2043 $cm^{-1}$) and *Limulus* (2053 $cm^{-1}$) Hc [Fager and Alben, 1972]. Comparison of $\nu_{CO}$ for Hc with pyridine CO-Cu complexes in solution indicated that the bound CO in Hc was most likely ligated to a single copper and not bridging both

coppers. At that time, no bridging CO–Cu complexes existed. Therefore, direct comparison of CO–Hc to a bridged CO model complex could not be made. However, bridging CO to both Fe and Co display IR frequencies in the 1800–1900 $cm^{-1}$ region and this was used to suggest that a CO–Hc bridging geometry would have a much lower $\nu_{CO}$ than what was observed for Hc [Fager and Alben, 1972].

Since both coppers are required for correct spectroscopic properties of CO–Hc, removal of one of the copper atoms to form a half-apo species may produce an interesting avenue for studying the binuclear nature of the copper active site. Experiments utilizing FTIR to analyze a series of fully metallated and half-apo CO–Hc derivatives were performed to determine what role the second copper plays with respect to the binding of CO. Hc that was dialyzed against cyanide was determined to contain various levels of copper in its active site, most likely as a mixture of half-apo and fully metallated protein. Ligation of CO to the half-apo Hc resulted in the appearance of a new stretching frequency in the IR region. This peak was shown to shift concurrently upon the binding of $^{13}CO$. Thus, it appears that both copper centers may be responsible for CO ligation in fully metallated Hc.

## 5.2 EXPERIMENTAL METHODS

### 5.2.1 Isolation of Hemocyanin

Molluscan whelks, *Busycotypus canaliculatum*, were obtained from the Marine Biological Laboratory at Woods Hole, MA. The hemolymph was collected through foot puncture and passed through cheesecloth into a flask that was kept on ice. The raw hemocyanin was extensively dialyzed against 50 mM TRIS at pH 8.7 for two days with a buffer change every 12 h.

After the second day, the hemocyanin was centrifuged for 70 min at 7500 rpm to remove any precipitate that had formed. The hemocyanin was dialyzed for an additional two days against 50 mM sodium bicarbonate at pH 9.7. After dialysis, the hemocyanin was concentrated, using a 350 mL Amicon stirred cell with a YM 30 membrane, to a final copper concentration of 5 mM. The hemocyanin was filtered

through a 0.8 $\mu$m and a 0.2 $\mu$m sterile filter into an autoclaved serum bottle that was sealed with a septum and stored at 4°C.

### 5.2.2 Determination of Copper and Protein Concentrations

All protein and copper concentrations were measured using the following procedure. A 5 $\mu$L sample of Hc was diluted to 1 mL in a UV/Vis cell. The UV/Vis spectrum was recorded on a Shimadzu UV-265. The protein concentration was calculated from the $\epsilon_{280}$ (71.64 $mM^{-1}cm^{-1}$). The copper concentration was calculated from the $\epsilon_{340}$ (10 $mM^{-1}$ $cm^{-1}$).

Carbonlyated and deoxy Hc samples do not exhibit an absorption at 340 nm. Thus, the copper concentration of these samples was measured by flame atomic absorption using a Varian Techtron Spectrophotometer. The amount of cyano-copper present in the wash buffer was also determined by atomic absorption

### 5.2.3 Preparation of Half-Apo Hemocyanin

OxyHc was deoxygenated by bubbling argon through a stoppered flask overnight at 5°C, which contained the Hc in a dialysis bag dissolved in 50 mM TRIS buffer at pH 8. Half-apo hemocyanin was prepared by dialyzing a 1.0 mL sample of deoxyHc against 30 mM NaCN buffered in 50 mM TRIS at pH 8.2 for 1 h in an anaerobic glove box. The removal of copper by the cyanide was stopped by a rapid dilution technique which involved placing the 1.0 mL sample into a 350 mL Amicon stirred cell fitted with a YM 30 membrane and filled with 50 mM TRIS at pH 8. Under 2.4 atm of $N_2$, the TRIS wash diluted the $CN^-$ present in the sample, essentially stopping further copper removal. The excess $CN^-$ and any copper cyanide species passed through the membrane. This wash was performed until the copper concentration present in the wash could no longer be measured by atomic absorption. The half-apo hemocyanin mixture was concentrated to the original protein concentration using a 3 mL Amicon concentrator in the glove box.

### 5.2.4 Preparation of Carbonlyated Species

The fully metallated CO–Hc complex was prepared from deoxyhemocyanin that had been exposed to CO for 10 min at 1.2 atm. Demetallated CO–Hc samples were prepared by equilibrating the half-apo Hc with CO in a septum-sealed vial for 5 min. $^{13}CO$ half-apo Hc samples were prepared by injection of $^{13}CO$ via a Hamilton gas tight syringe into an evacuated septum-sealed vial containing the half-apo Hc.

### 5.2.5 Data Collection and Analysis

Infrared spectra were recorded on a Perkin-Elmer 1800 series FTIR spectrophotometer. The instrument was interfaced to a Perkin-Elmer 7500 computer. The IR cell consisted of two rectangular $CaF_2$ windows separated by a 0.05 mm Teflon spacer (McArthy Scientific). The entire assembly was contained in a thermostated copper block maintained at a temperature of 10°C through the use of an external water bath. Each sample was scanned a total of 200 times. A deoxy half-apo Hc protein sample of the same concentration as either of the $^{13}CO$ half-apo Hc or $^{12}CO$ half-apo Hc served as the background from which the carbonylated Hc protein samples were subtracted. The subtracted spectra were transferred from the 7500 computer to a Macintosh computer where the deconvolution and spectral analysis were generated using the Igor Pro software (WaveMetrics).

## 5.3 RESULTS/DISCUSSION

### 5.3.1 Measurement of the Amount of Copper Removed via $CN^-$ Dialysis

The amount of time required for 50% reduction in total Cu concentration by $CN^-$ was followed by stopping the reaction at different time points and washing the sample by the previously outlined procedure. Time points between 10 and 60 min were measured in 10-min increments. Dialysis of Hc with $CN^-$ of less than 1 h resulted in samples that were reduced in total Cu by 20 to 40%. It was determined that dialyzing the sample against $CN^-$ for 1 h resulted in Hc samples that contained residual copper levels of between 40 and 50%. Thus, all subsequent experiments for which half-apo Hc was needed involved $CN^-$ dialysis of 1 h.

IR spectral analysis of the half-apo CO–Hc complex demonstrated that copper removal by $CN^-$ did not selectively remove copper from the Hc, confirming previously reported conclusions [Zolla et al., 1984]. Rather, treatment of Hc with $CN^-$ produced a mixture of proteins with either no copper (apo), one copper (half-apo), or two coppers (fully metallated), present in the active site of Hc. With time, the half-apo sites reconverted to the fully metallated form of the protein. The reconversion occurred either anaerobically or in the presence of oxygen. This rescrambling was followed by examining the CO–Cu IR stretch before $CN^-$ treatment, after removal of the Cu, and after sitting for 5 h. The CO–Cu stretch before $CN^-$ dialysis was observed to be a single peak at 2063 $cm^{-1}$. After $CN^-$ treatment, two spectral features were observed at 2063 $cm^{-1}$ and 2074 $cm^{-1}$, indicative of formation of the half-apo CO species. After 5 h, a single stretching frequency, of reduced intensity, was observed at 2063 $cm^{-1}$. This reduced intensity closely correlated to the reduction in the total copper present in the sample.

### 5.3.2 Fully Metallated CO-Hc

Figure 5.1 shows the FTIR spectrum of $^{12}CO$ bound to fully metallated Hc. As reported previously, the $^{12}CO$–Hc complex exhibits a single narrow band centered at 2062 $cm^{-1}$. The peak was subjected to Gaussian fitting analysis in which the frequency and full width at half height (FWHH,$\omega$) were allowed to vary. This analysis gave $\nu_{CO}$= 2062 $cm^{-1}$ with $\omega$= 11.5 $cm^{-1}$ (Table 5.1).

Figure 5.2 depicts the FTIR spectrum of $^{13}CO$ bound to fully metallated Hc. The $^{13}CO$–Hc complex shows a similar narrow band but shifted to lower frequency (2018 $cm^{-1}$) by 44 $cm^{-1}$, the expected isotope shift for the C–O diatomic linear harmonic oscillator. A Gaussian analysis gave a FWHH value of 10.5 $cm^{-1}$ for the $\nu$(CO)= 2018 $cm^{-1}$. The [$^{12}CO$–Hc]–[$^{13}CO$–Hc] difference spectrum is shown in Figure 5.3.

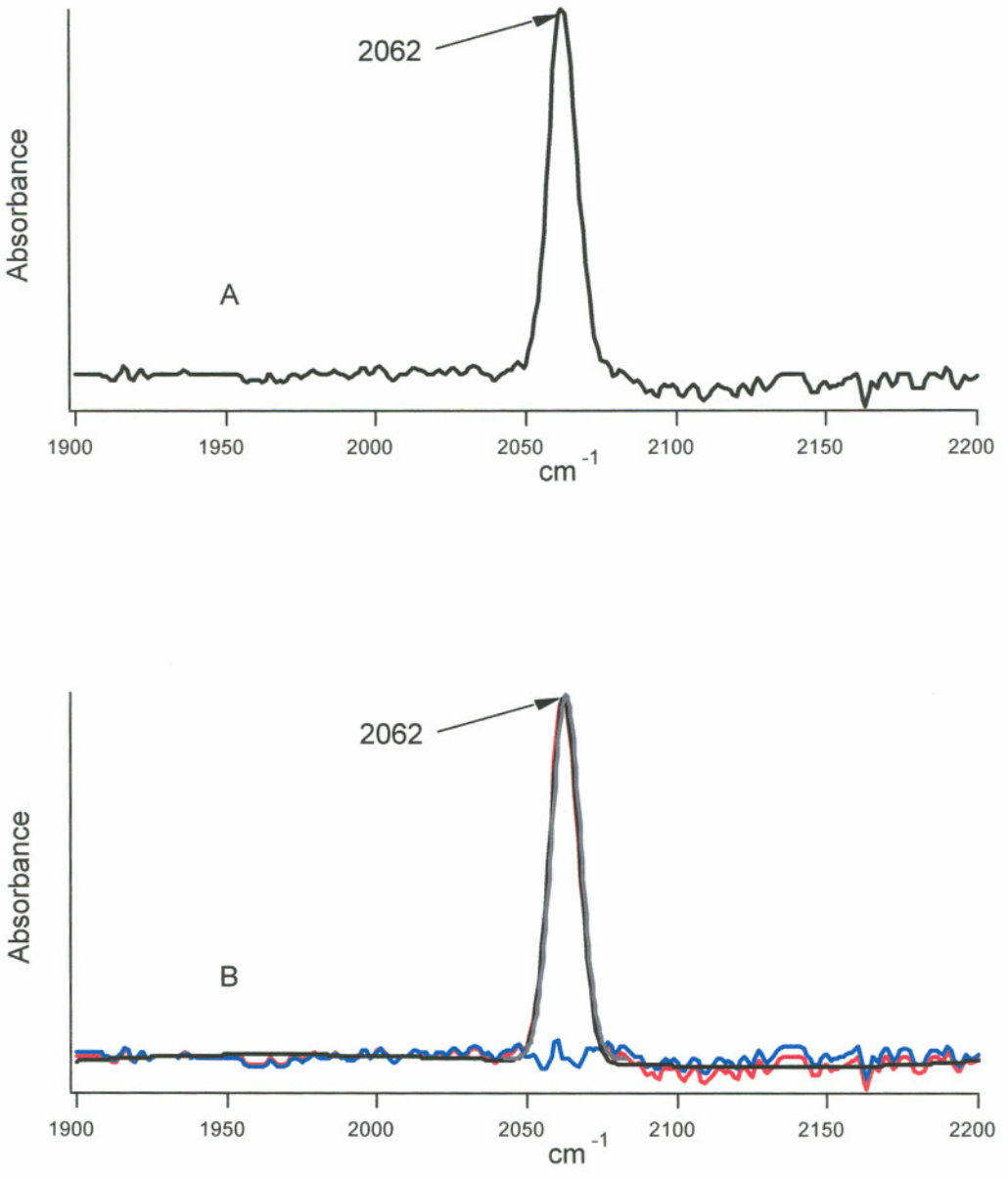


**Figure 5.1** IR spectra of $^{12}$CO-Hc complex (A). Spectral simulation of $^{12}$CO-Hc (B). Black = actual spectrum; gray-dashed = simulated spectrum; red = fitted peak; blue = residual.

**Table 5.1**

Carbon Monoxide Stretching Frequencies
and Peak Widths for the Hemocyanin Complexes

| | $\nu$(CO) $cm^{-1}$ | *FWHH* ($cm^{-1}$) |
|---|---|---|
| Fully metallated | | |
| $^{12}$CO-Hc | 2062 | 11.5 |
| $^{13}$CO-Hc | 2018 | 10.6 |
| Half-apo | | |
| $^{12}$CO-Hc | 2064, 2076 | 12.9, 19.5 |
| $^{13}$CO-Hc | 2018, 2029 | 10.8, 15.5 |

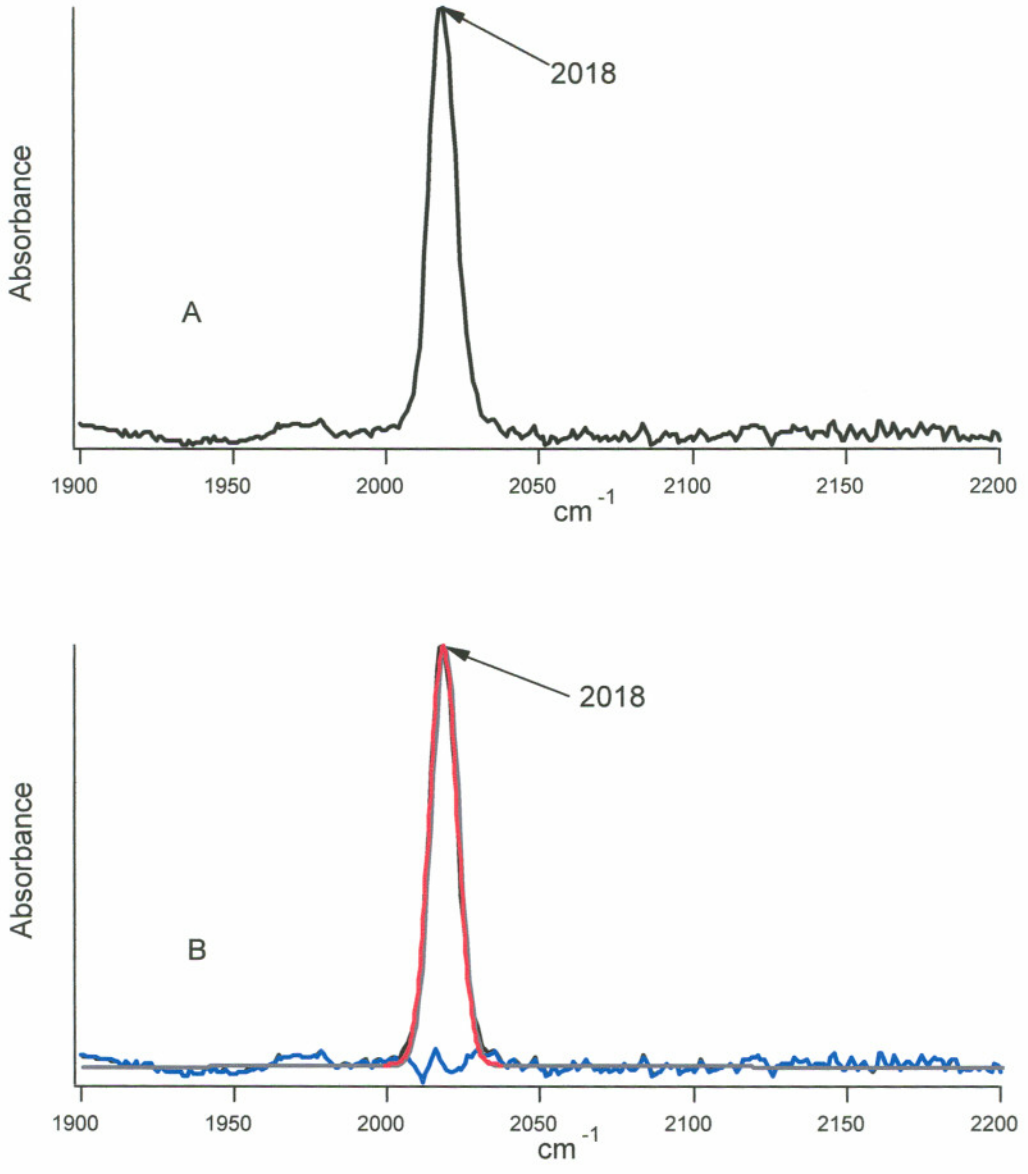


**Figure 5.2** IR spectra of $^{13}$CO-Hc complex (A). Spectral simulation of $^{13}$CO-Hc (B). Black = actual spectrum; gray-dashed = simulated spectrum; red = fitted peak; blue = residual.

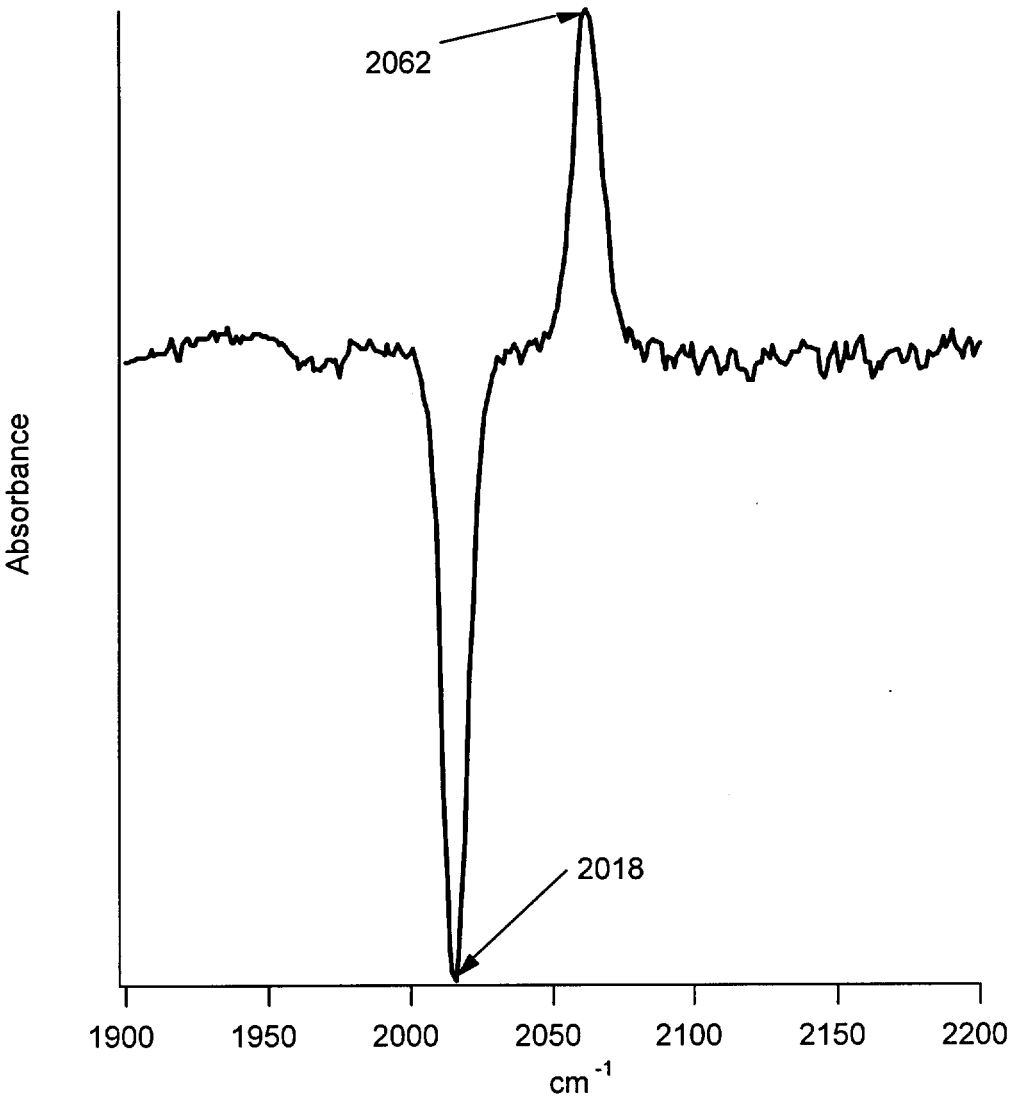


**Figure 5.3** Difference spectrum of $^{12}$CO-Hc subtracted from $^{13}$CO-Hc.

### 5.3.3 Characterization of Half-Apo $^{12}$CO–Hc

Exposure of half-apo Hc to CO resulted in a spectrum with two species present (Figure 5.4). The main spectral feature is no longer a single symmetrical peak as seen in the fully metallated CO–Hc spectrum, but is now a broad band that appears to contain a shoulder at higher energy. Spectral deconvolution of the half-apo CO–Hc spectrum using the previously determined frequency of the pure CO–Hc stretch and its FWHH, determined that the spectrum can be fitted to two species. This fitting showed that one band arises from a CO stretch at 2063 $cm^{-1}$ ($\omega$ = 12.5 $cm^{-1}$) and the shoulder to that band can be fitted at 2077 $cm^{-1}$ ($\omega$ = 19.5 $cm^{-1}$) (Figure 5.4C).

### 5.3.4 Half-Apo $^{13}$CO–Hc IR Spectrum

Figure 5.5 shows the IR spectrum of the half-apo $^{13}$CO–Hc mixture. This broad peak also appeared to contain a mixture of two CO stretching frequencies. The main peak was fitted at a maximum of 2018 $cm^{-1}$ ($\omega$ = 10.8 $cm^{-1}$), analogous to the fully metallated $^{13}$CO–Hc band. The shoulder could be fitted to a $^{13}$CO stretch at 2029 $cm^{-1}$ ($\omega$ = 15.5 $cm^{-1}$).

### 5.3.5 Peak Heights and Half-Widths

Table 5.1 contains the fitted peak heights and FWHH for all of the samples investigated. For both of the fully metallated Hc samples with either $^{13}$CO or $^{12}$CO bound, the single peak was very narrow with a width of 10–11 $cm^{-1}$. However, the half-apo mixtures could not be fitted so that the two peaks contained the same widths. When simulation of the mixtures was performed with parameters that constrained the two peaks to the same widths, the narrow band associated with the fully metallated CO–Hc single peak widened to 16 $cm^{-1}$. However if the two bands were fitted so that the width would vary, the CO–Hc widths returned to the value determined from the pure CO stretch and the half-apo stretch widened.

Although removal of copper from Hc was non-specific, comparison of the fully metallated CO spectrum to that of the half-apo CO spectrum revealed the appearance of a second stretching frequency at 2074 $cm^{-1}$ in the half-apo complex. Present in both spectra was the 2063 $cm^{-1}$ $\nu_{CO}$ that has been attributed to the fully

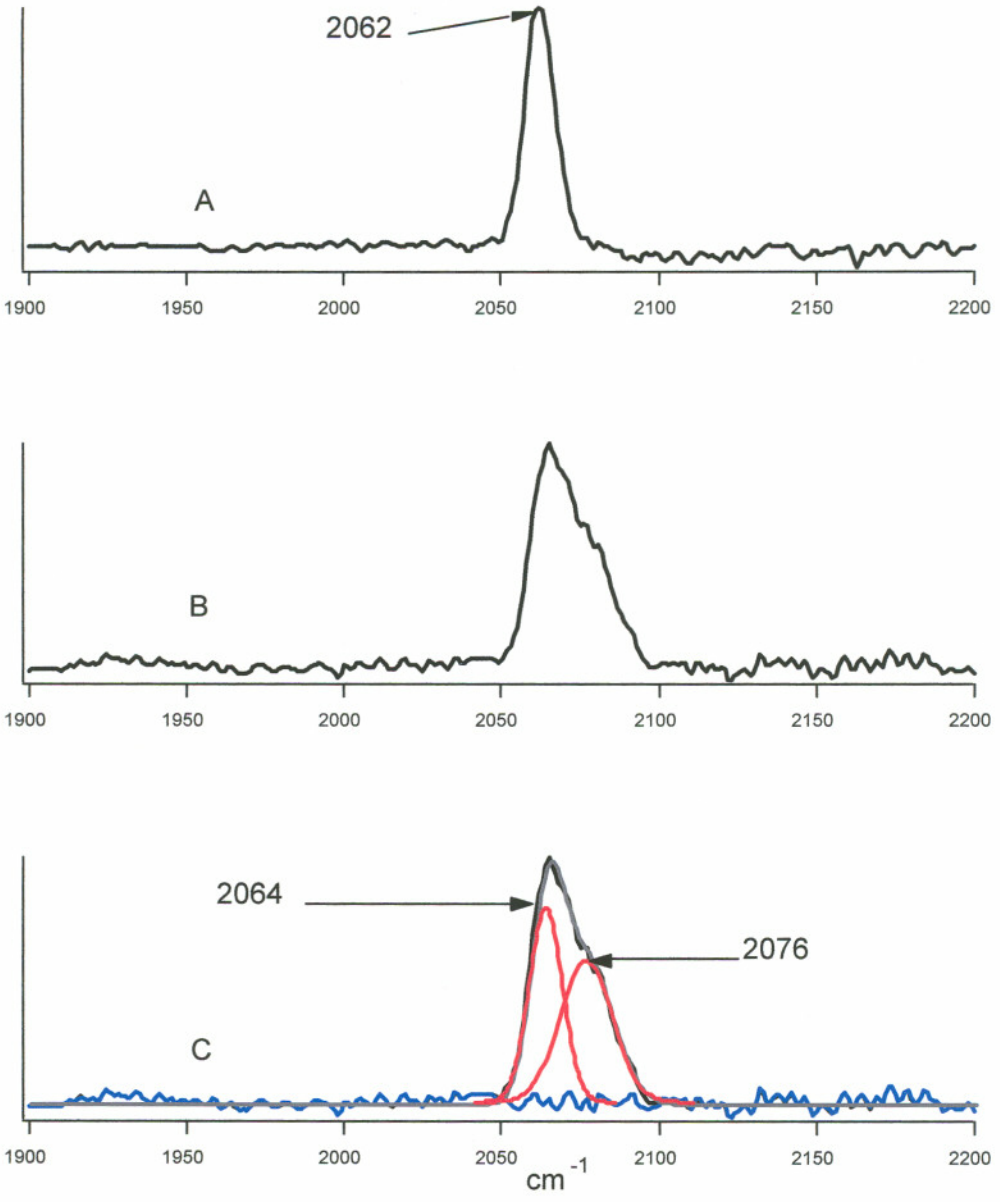


**Figure 5.4** IR spectra of $^{12}$CO-Hc complex (A). Spectrum of the half-apo $^{12}$CO-Hc complex (B). Spectral simulation of the half-apo $^{12}$CO-Hc complex (C). Black = actual spectrum; gray-dashed = simulated spectrum; red = fitted peak; blue = residual.

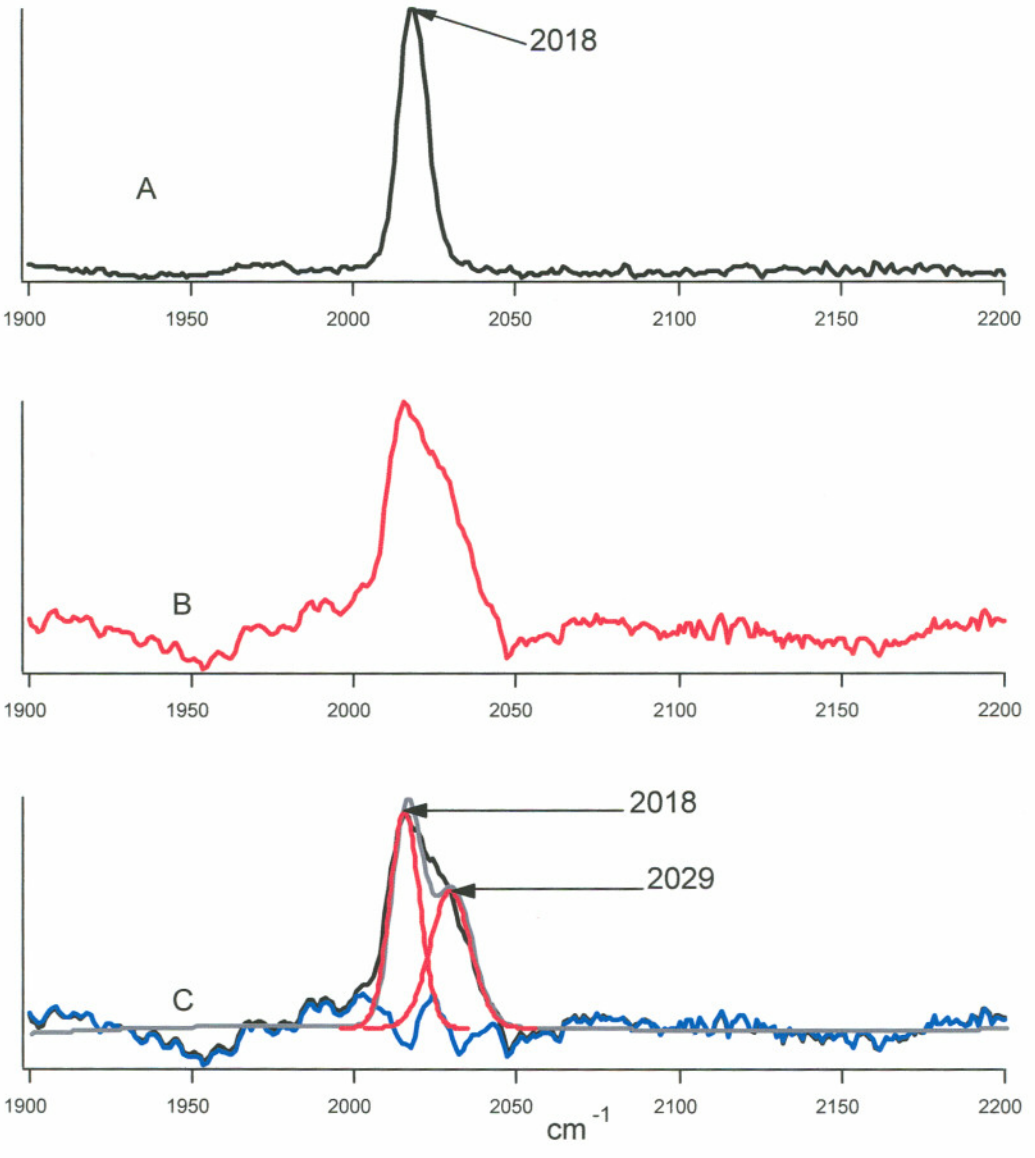


**Figure 5.5** IR spectra of $^{13}$CO-Hc complex (A). Spectrum of the half-apo $^{13}$CO-Hc complex (B). Spectral simulation of the half-apo $^{13}$CO-Hc complex (C). Black = actual spectrum; gray-dashed = simulated spectrum; red = fitted peak; blue = residual.

metallated CO stretching frequency [Fager and Alben, 1972]. If the CO bound to copper in the fully metallated protein is terminally coordinated and only interacting with one of the coppers, then removal of the non-ligating copper should not affect the observed $\nu_{CO}$ for hemocyanin. The appearance of the second $\nu_{CO}$ at 2074 $cm^{-1}$ in the half-apo complex is indicative of both coppers contributing to CO binding in the di copper protein (Scheme 5.1).

If both coppers are involved in the binding of CO, removal of one of the coppers should affect the $\nu_{CO}$ in one of two ways. The first would be an increase in the apparent width of the absorption peak associated with the CO frequency. This value would be expected to increase upon removal of one of the coppers only if the non-ligating copper was responsible for preventing line broadening by limiting the available rotational space of the bound CO–Cu complex. The observed width for $\nu_{CO}$ in hemocyanin from this study and previous studies is quite small $\sim$10–11 $cm^{-1}$ [Fager and Alben, 1972]. This has been attributed to an active site environment that does not allow for different binding conformations of the CO ligand, thus limiting the CO to one location in the active site.

The second effect that would be observed if both coppers are contributing to the ligation of CO is that upon removal of one of the coppers from the active site, a new $\nu_{CO}$ is observed. This would indicate a modified coordination environment for the CO–Cu(I) center and a new species being present in the active site of Hc. The appearance of the second $\nu_{CO}$ in the half-apo complex that is 14 $cm^{-1}$ higher in energy than the fully metallated $\nu_{CO}$ suggests this latter possibility. The second peak is also 8 $cm^{-1}$ broader than the $\nu_{CO}$ for the fully metallated system, indicating more freedom of movement of the CO bound to the Cu in the half-apo complex. The upshift in energy of the second band indicates a decrease in the strength of the Cu–C bond and an increase in the carbon–oxygen bond of CO. This is an indication that in the half-apo complex the degree of backbonding of the CO ligand to the copper centers is less than in the fully metallated protein. This could be due to loss of interaction from the second copper center and a less basic metal center. Therefore, it appears that a better description of the ligation of CO to the active site of fully metallated Hc would be of a bridging CO (Scheme 5.1). In this model, the carbon of the CO forms a semi-

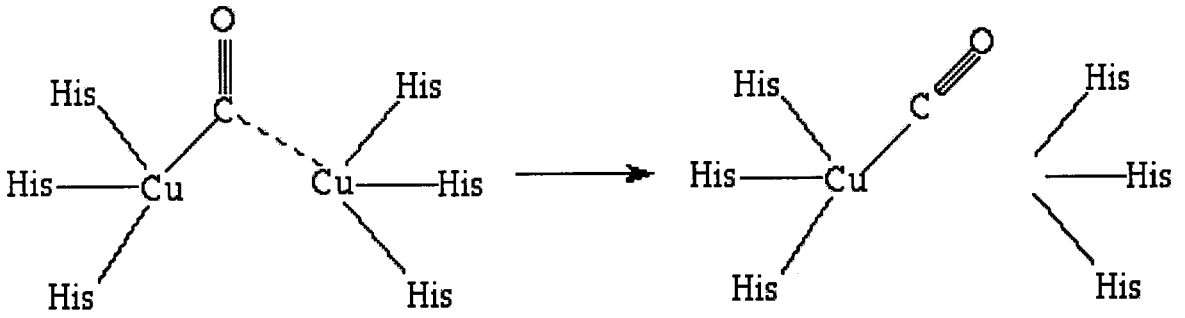


**Scheme 5.1** Proposed ligation of CO to Hc before (A) and after (B) cyanide dialysis.

bridging structure between the two copper atoms where it interacts more strongly to one copper than the other. Upon removal of the second copper, this bridging interaction is disrupted and the CO now ligates to a single copper atom.

### 5.3.6 Half-Apo $^{13}$CO–Hc IR Spectrum

Cu(CN)x complexes exhibit stretching frequencies in the 2090 to 2070 $cm^{-1}$ IR region due to the $^{12}C \equiv N$ intraligand stretches, with $Cu(CN)^{-3}_4$ being at 2075 $cm^{-1}$. To rule out the possibility of a Cu(CN)x being the observed stretch at 2073 $cm^{-1}$, $^{13}CO$ was used to ligate the half-apo Hc, thus shifting the IR stretching frequencies of CO to a region below that of the Cu(CN)x. Since the half-apo $^{13}$CO–Hc band was still present at 2030 $cm^{-1}$, it was evident that the 2070 band was also due to the half-apo $^{12}$CO–Hc.

## 5.4 CONCLUSIONS

Earlier research points to the idea that removal of one of the two coppers in Hc affects the CO–Cu complex. These studies indicated that upon generation of a half-apo protein and ligation of CO to the remaining copper atom, the observed emission spectrum of CO–Cu was lost [Finazzi-Agrò et al., 1982; Zolla et al., 1984]. Here we have shown, through IR analysis of half-apo CO–Hc, that the frequency of the CO–Hc complex also changes. This suggests that both coppers may be responsible for the ligation of CO in hemocyanin, possibly as a bridging ligand between the two metal centers.

# CHAPTER 6
# CONCLUSIONS

In studying the PHMcc enzyme, the major goal was to better understand the role each copper center played in relationship to the catalytic mechanism of the enzyme. Previous research had developed the belief that only one of the copper centers ($Cu_B$) was responsible for $O_2$ activation and substrate catalysis. Therefore, it was assumed that the $Cu_A$ center functioned as an electron donating center and was not involved in oxygen ligation. Furthermore, experiments with ligation of small molecules to D$\beta$M seemed to demonstrate that the $Cu_A$ center was not designed to ligate $O_2$. The crystal structure of PHMcc showed that each center was essentially isolated from each other, residing on separated domains of the protein. Since an electron is needed from each copper center, it was critical to try and understand how the two metal centers communicated across this 11-Å gap seeing that no rearrangement of the protein structure was observed and no through bond network was seen.

Ligation of isocyanides to the copper centers in PHMcc has demonstrated that each individual center has an influence upon the second center and mutation at one center directly affects the remaining copper center. When both copper centers are present in the enzyme, it was shown that ligation of isocyanide occurs only at the $Cu_B$ center. However, removal of the $Cu_A$ center changes the binding ability of the $Cu_B$, enabling a new bis-isocyanide copper complex to form. Furthermore, influential effects from $Cu_B$ were seen with regard to the $Cu_A$ center. Removal of the $Cu_B$ metal center allowed isocyanide ligation to occur at the $Cu_A$ center. Finally, in the His172Ala mutant, where both copper centers are present, it appears that ligation of isocyanides may be occurring at both copper centers simultaneously. In conclusion, these are the first experiments that demonstrate the ability of the $Cu_A$ center to bind

exogenous ligands and demonstrate that the copper centers communicate with each other across the 11-Å gap.

If one is to believe the catalytic mechanism outlined in Chapter 1, where $O_2$ ligation initially occurs at the $Cu_A$ center, then travels to the $Cu_B$ center as superoxide, it is important to show that the $Cu_A$ center can bind oxygen analogues. While we have shown that the $Cu_A$ center is capable of ligating isocyanides, isocyanides are probably not the best $O_2$ analogue. However, continued research utilizing carbon monoxide, as an $O_2$ mimic, has also shown that this molecule will bind to the $Cu_A$ center. This ligation is accomplished only after the protein has bound pro-peptide substrate. Since it was previously shown that substrate binds to the protein before oxygen, it appears that this opens up a binding site on the $Cu_A$ center. This is then followed by CO ligation to the $Cu_A$ center. In the case of $O_2$, this strongly suggest that oxygen may initially bind to the $Cu_A$ center where the oxygen accepts an electron from the $Cu_A$ center, becomes reduced to superoxide, and migrates to the second copper center where catalysis occurs.

In conclusion, the isocyanide binding to PHM has conclusively shown that both centers are capable of ligating Cu(I) probes. This suggests that the $Cu_A$ center may play a different role in the overall catalytic mechanism than previously suggested. Furthermore, the two distant copper centers influence each other with regard to their binding properties, demonstrating that they are able to communicate with each other.

## LITERATURE CITED


Adman, E. T. (1991) Copper protein structures. *Adv. Protein Chem.* **42,** 145–197.

Ardizzoia, G. A., Angaroni, M. A., La Monica, G., Masciocchi, N. and Moret, M. (1990) Synthesis, X-ray crystal structure, and reactivity of the binuclear copper(I) complex [{Cu(3,5$Me_2$-pz)(CNR}$_2$] (R = cyclohexyl, 3,5$Me_2$pz = 3,5dimethylpyrazolate) toward RNCO (R = cyclohexyl), PhNCS, COS and $CS_2$. N,S co-ordination of the 3,5-dimethylpyrazolecarbodithioate anion in [Cu{3,5Me2-pz–C(S)–S}(CNR)$_2$]. *J. Chem. Soc. Dalton Trans.* 2277–2281.

Ardizzoia, G. A., Beccalli, E. M., La Monica, G., Masciocchi, N. and Moret, M. (1992) Synthesis of [Cu)dcmpz)]$_n$ and its reactions with carbon monoxide and cyclohexyl isocyanide. Crystal structures of [$Cu_2$(dcmpz)$_2$(py)$_2$(CO)] and [Cu(dcmpz)(RCN)]$_2$ (Hdcmpz = 3,5-dicarbomethoxypyrazole, R = cyclohexyl). *Inorg. Chem.* **31,** 2706–2711.

Binsted, N., Gurman, S. J. and Campbell, J. W. (1988) *EXCURV88 Program.* Daresbury Laboratory, Daresbury, Cheshire, UK.

Blackburn, N. J., Collison, D., Sutton, J. and Mabbs, F. E. (1984) Kinetic and EPR studies of cyanide and azide binding to the copper sites of dopamine (3,4-dihydroxyphenethylamine-$\beta$-mono-oxygenase. *Biochem. J.* **220,** 447–454.

Blackburn, N. J., Concannon, M., Shahiyan, S. K., Mabbs, F. E. and Collison, D. (1988) Active site of dopamine-$\beta$-hydroxylase. Comparison of derivatives containing four and eight coppers per tetramer using potentiometry and EPR spectroscopy. *Biochemistry* **27,** 6001–6008.

Blackburn, N. J., Hasnain, S. S., Pettingill, T. M. and Strange, R. W. (1991) Copper K-extended X-ray absorption fine structure studies of oxidized and reduced dopamine-$\beta$-hydroxylase: confirmation of a sulfur ligand to Cu(I) in the reduced enzyme. *J. Biol. Chem.* **266,** 23120–23127.

Blumberg, W. E., Desai, P. R., Powers, L., Freedman, J. H. and Villafranca, J. J. (1989) X-ray absorption spectroscopic study of the active copper sites in dopamine-$\beta$ hydroxylase. *J. Biol. Chem.* **264,** 6029–6032.

Boswell, J. S., Reedy, B. J., Kulathila, R., Merkler, D. J. and Blackburn, N. J. (1996) Structural investigations on the coordination environment of the active-site copper centers of recombinant bifunctional peptidylglycine α-amidating enzyme. *Biochemistry* **35,** 12241–12250.

Bradbury, A. F., Finnie, M. D. A. and Smyth, D. G. (1982) Mechanism of C-terminal amide formation by pituitary enzymes. *Nature* **298,** 686–688.

Brenner, M. C. and Klinman, J. P. (1989) Correlation of valency with product formation in single turnovers of dopamine-β-monooxygenase. *Biochemistry* **28,** 4664–4670.

Brenner, M. C., Murray, C. J. and Klinman, J. P. (1989) Rapid freeze- and chemical-quench studies of dopamine-β-monooxygenase: comparison of pre-steady-state and steady-state parameters. *Biochemistry* **28,** 4656–4664.

Brown, J. M., Powers, L., Kincaid, B., Larrabee, J. A. and Spiro, T. G. (1980) Structural studies of the hemocyanin active site. 1. Extended X-ray absorption fine structure (EXAFS) analysis. *J. Am. Chem. Soc.* **102,** 4210–4216.

Colman, P. M., Freeman, H. C., Guss, J. M., Murata, M., Norris, V. A., Ramshaw, J. A. M., Venkatappa, M. P., and Vickery, L. E. (1977) Preliminary crystallographic data for a basic copper-containing protein from cucumber seedlings. *J. Mol. Biol.***112**, 649–650.

Cuff, M. E., Miller, K. I., van Holde, K. E. and Hendrickson, W. A. (1998) Crystal structure of a functional unit from Octopus hemocyanin. *J. Mol. Biol.* **278,** 855–870.

Dooley, D. M., Scott, R. A., Ellinghaus, J., Solomon, E. I. and Gray, H. B. (1978) Magnetic susceptibility of laccase and oxyhemocyanin. *Proc. Natl. Acad. Sci. U.S.A.* **75,** 3019–3022.

Eickman, N. C., Himmelwright, R. S. and Solomon, E. I. (1979) Geometric and electronic structure of oxyhemocyanin: spectral and chemical correlations to met apo, half met, met, and dimer active sites. *Proc. Natl. Acad. Sci U.S.A.* **76,** 2094–2098.

Eipper, B. A., Perkins, S. N., Husten, E. J., Johnson, R. C., Keutmann, H. T. and Mains, R. E. (1991) Peptidyl-α-hydroxyglycine α-amidating lyase. Purification, characterization, and expression. *J. Biol. Chem.* **266,** 7827–7833.

Eipper, B. A., Green, C. B. R., Campbell, T. A., Stoffers, D. A., Keutmann, H. T., Mains, R. E. and Ouafik, L. H. (1992a) Alternative splicing and endoproteolytic processing generate tissue-specific forms of pituitary peptidylglycine α-amidating monooxygenase (PAM) *J. Biol. Chem.* **267,** 4008–4015.

Eipper, B. A., Stoffers, D. A. and Mains, R. E. (1992b) The biosynthesis of neuropeptides: peptide α-amidation. *Annu. Rev. Neurosci.* **15,** 57–85.

Eipper, B. A., Quon, A. S. W., Mains, R. E., Boswell, J. S. and Blackburn, N. J. (1995) The catalytic core of peptidylglycine α-hydroxylating monooxygenase: investigation by site-directed mutagenesis, Cu X-ray absorption spectroscopy, and electron paramagnetic resonance. *Biochemistry* **34,** 2857–2865.

Fager, L. Y. and Alben, J. O. (1972) Structure of the carbon monoxide binding site of hemocyanins studied by Fourier transform infrared spectroscopy. *Biochemistry* **11,** 4786–4792.

Ferrari, M., Hanley, D. F., Wilson, D. A. and Traystman, R. J. (1990) Cerebral cytochrome-*c*-oxidase copper band quantification in perfluorocarbon exchange transfused cats. *Adv. Exp. Med. Biol.* **277,** 85–93.

Fiaschi, P., Floriani, C., Pasquali, M., Chiesi-Villa, A. and Gaustini, C. (1984) Monomeric alkoxo complexes of copper(I): syntheses and structures of di(p-tolyl isocyanide)(2,6-di-t-butylphenoxo)copper(I) and a di(2,6-dimethylphenoxo)cuprate(I). *J. Chem. Soc., Chem. Commun.* 888–890.

Finazzi-Agrò, A., Zolla, L., Flamigni, L., Kuiper, H. A. and Brunori, M. (1982) Spectroscopy of (carbon monoxy)hemocyanins. Phosphorescence of the binuclear carbonylated copper centers. *Biochemistry* **21,** 415–418.

Francisco, W. A., Merkler, D. J., Blackburn, N. J. and Klinman, J. P. (1998) Kinetic mechanism and intrinsic isotope effects for the peptidylglycine α-amidationg enzyme reaction. *Biochemistry* **37,** 8244–8252.

Freedman, T. B., Loehr, J. S. and Loehr, T. M. (1976) A resonance Raman study of the copper protein, hemocyanin. New evidence for the structure of the oxygen-binding site. *J. Am. Chem. Soc.* **98,** 2809–2815.

Frieden, E. (1981) The evolution of copper proteins. In *Copper Proteins* (Sigel, H., Ed.), Marcel Dekker, New York, pp. 1–14.

George, G. N. (1990) *EXAFSPAK*, Stanford Synchrotron Radiation Laboratory, Stanford, CA.

Guckert, J. A., Lowery, M. D. and Solomon, E. I. (1995) Electronic structure of the reduced blue copper active site: contributions to reduction potentials and geometry. *J. Am. Chem. Soc.* **117,** 2817–2844.

Gurman, S. J. (1989) Review on curved wave EXAFS simulation. In *Synchrotron Radiation and Biophysics* (Hasnain, S. S., Ed.), Ellis Horwood Ltd., Chichester, U.K., pp. 9–42.

Gurman, S. J., Binsted, N. and Ross, I. (1984) EXCURV Phys Rev Paper. *J. Phys. C* **17,** 143–151.

Gurman, S. J., Binsted, N. and Ross, I. (1986) EXCURV Phys Paper. *J. Phys. C* **19,** 1845–1861.

Guss, J. M. and Freeman, H. C. (1983) Structure of oxidized popular plastocyanin at 1.6 Å resolution. *J. Mol. Biol.* **169,** 521–563.

Hazes, B., Magnus, K. A., Bonaventura, C., Bonaventura, J., Dauter, Z., Kalk, K. H. and Hol, W. G. J. (1993) Crystal structure of deoxygenated *Limulus polyphemus* subunit II hemocyanin at 2.18 Å resolution: clues for a mechanism of allosteric interaction. *Protein Sci.* **2,** 597–619.

Ho, R. Y. N., Liebman, J. F. and Valentine, J. S. (1995) Biological reactions of dioxygen: an introduction. In *Active Oxygen in Biochemistry* (Valentine, J. S., Foote, C. S., Greenberg, A. and Liebman, J. F., Eds.), Blackie Academic & Professional, New York, pp. 1–37.

Holm, R. H., Kennepohl, P. and Solomon, E. I. (1996) Structural and functional aspects of metal sites in biology. *Chem. Rev.* **96,** 2239–2314.

Husten, E. J. and Eipper, B. A. (1991) The membrane-bound bifunctional peptidylglycine α-amidating monooxygenase protein. Exploration of its domain structure through limited proteolysis. *J. Biol. Chem.* **266,** 17004–17010.

Husten, E. J., Tausk, F. A., Keutmann, H. T. and Eipper, B. A. (1993) Use of endoproteases to identify catalytic domains, linker regions, and functional interactions in soluble peptidylglycine α-amidating monooxygenase. *J. Biol. Chem.* **268,** 9709–9717.

Ito, N., Phillips, S. E. V., Stevens, C., Ogel, Z. B., McPherson, M. J., Keen, J. N., Yadav, K. D. S. and Knowles, P. F. (1991) Novel thioether bond revealed by a 1.7 Å crystal structure of galactose oxidase. *Nature* **350,** 87–90.

Jaron, S. and Blackburn, N. J. (1999) Does superoxide channel between the copper centers in peptidylglycine monooxygenase? A new mechanism based on carbon monoxide reactivity. *Biochemistry* **38,** 15086–15096.

Kitajima, N., Fujisawa, K., Fujimoto, C., Moro-oka, Y., Hashimoto, S., Kitagawa, T., Toriumi, K., Tatsumi, K. and Nakamura, A. (1992a) A new model for dioxygen binding in hemocyanin. Synthesis, characterization, and molecular structure of the $\mu$-$\eta^2$:$\eta^2$ peroxo dinuclear copper(II) complexes, [Cu(HB(3,5-$R_2$pz)$_3$)](O$_2$) (R = *i*-Pr and Ph). *J. Am. Chem. Soc.* **114,** 1277–1291.

Kitajima, N., Fujisawa, K., Tanaka, M. and Moro-oka, Y. (1992b) X-ray structure of thiolatocopper(II) complexes bearing close spectroscopic similarities to blue copper proteins. *J. Am. Chem. Soc.* **114,** 9232–9233.

Klinman, J. P. (1996) Mechanisms whereby mononuclear copper proteins functionalize organic substrates. *Chem. Rev.* **1996,** 2541–2561.

Klinman, J. P., Krueger, M., Brenner, M. and Edmondson, D. E. (1984) Evidence for two copper atoms/subunit in dopamine-$\beta$-monooxygenase catalysis. *J. Biol. Chem.* **259,** 3399–3402.

Kolhekar, A. S., Keutman, H. T., Mains, R. E., Quon, A. S. W. and Eipper, B. A. (1997) Peptidylglycine $\alpha$-hydroxylating monooxygenase: active site residues, disulfide linkages, and a two-domain model of the catalytuc core. *Biochemistry* **36,** 10901–10909.

Kuiper, H. A., Lerch, K., Brunori, M. and Finazzi Agrò, A. (1980) Luminescence of the copper–carbon monoxide complex of *Neurospora* tyrosinase. *FEBS Lett.* **111,** 232–234.

Lerch, K., Longoni, C. and Jordi, E. (1982) Primary structure of tyrosinase from *Neurospora crassa*. I. Purification and amino acid sequence of the cyanogen bromide fragments. *J. Biol. Chem.* **257,** 6408–6413.

Ling, J., Nestor, L. P., Czernuszewicz, R. S., Spiro, T. G., Fraczkiewicz, R., Sharma, K. D., Loehr, T. M. and Sanders-Loehr, J. (1994) Common oxygen binding site in hemocyanins from arthropods and mollusks. Evidence from Raman spectroscopy and normal coordinate analysis. *J. Am. Chem. Soc.* **116,** 7682–7691.

Magnus, K. A., Ton-That, H. and Carpenter, J. E. (1994) Three-dimensional structure of the oxygenated form of the hemocyanin subunit II of *Limulus polyphemus* at atomic resolution. In *Bioinorganic Chemistry of Copper* (Karlin, K. D. and Tyeklár, Z., Eds.), Chapman & Hall, New York, pp. 143–150.

McCracken, J., Peisach, J., Cote, C. E., McGuirl, M. A. and Dooley, D. M. (1992) Pulsed EPR studies of the semiquinone state of copper-containing amine oxidases. *J. Am. Chem. Soc.* **114,** 3715–3720.

McKee, V., Dagdigian, J. V., Bau, R. and Reed, C. A. (1981) Copper(II) hemocyanin models. *J. Am. Chem. Soc.* **103,** 7000–7001.

Milgram, S. L., Johnson, R. C. and Mains, R. E. (1992) Expression of individual forms of peptidylglycine $\alpha$-amidating monooxygenase in AtT-20 cells: endoproteolytic processing and routing to secretory granules. *J. Cell Biol.* **117,** 717–728.

Ouafik, L., May, V., Keutman, H. T. and Eipper, B. A. (1984) Developmental regulation of peptidylglycine $\alpha$-amidating monooxygenase (PAM) in rat heart atrium and ventricle. *J. Biol. Chem.* **264,** 5839–5845.

Pasquali, M., Fiaschi, P., Floriani, C. and Gaetani-Manfredotti, A. (1983) Bridging phenoxo-ligands in dicopper(I) complexes: synthesis and structure of tetrakis(isocyanide)-bis($\mu$-phenoxo)-dicopper(I) complexes. *J. Chem. Soc., Chem. Commun.* 197–199.

Pettingill, T. M., Strange, R. W. and Blackburn, N. J. (1991) Carbonmonoxy dopamine-$\beta$-hydroxylase. Structural characterization by Fourier transform infrared, fluorescence, and X-ray absorption spectroscopy. *J. Biol. Chem.* **266,** 16996–17003.

Prigge, S. T., Kolhekar, A. S., Eipper, B. A., Mains, R. E. and Amzel, L. M. (1997) Amidation of bioactive peptides: the structure of peptidylglycine $\alpha$-hydroxylating monooxygenase. *Science* **278,** 1300–1305.

Reedy, B. J. and Blackburn, N. J. (1994) Preparation and characterization of half-apo dopamine-$\beta$-hydroxylase by selective removal of $Cu_A$. Identification of a sulfur ligand at the dioxygen binding site by EXAFS and FTIR spectroscopy. *J. Am. Chem. Soc.* **116,** 1924–1931.

Reedy, B. J., Murthy, N. N., Karlin, K. D. and Blackburn, N. J. (1995) Isocyanides as ligand-directed indicators of Cu(I) coordination in copper proteins. Probing the inequivalence of the Cu(I) centers in reduced dopamine $\beta$-monooxygenase. *J. Am. Chem. Soc.* **117,** 9826–9831.

Robertson, J. G., Adams, G. W., Medzihradszky, K. F., Burlingame, A. L. and Villafranca, J. J. (1994) Complete assignmant of disulfide bonds in bovine dopamine $\beta$-hydroxylase. *Biochemistry* **33,** 11563–11575.

Sanyal, I., Karlin, K. D., Strange, R. W. and Blackburn, N. J. (1993) Chemistry and structural studies on the dioxygen-binding copper–1,2 dimethylimidazole system. *J. Am. Chem. Soc.* **115,** 11259–11270.

Sawyer, D. T. (1991) *Oxygen Chemistry*. Oxford University Press, New York.

Solomon, E. I., Dooley, D. M., Wang, R. H., Gray, H. B., Cerdonio, M., Mogno, F. and Romani, G. L. (1976) Susceptibility studies of laccase and hemocyanin using an ultrasensitive magnetometer. Antiferromagnetic behavior of the T3 copper in *Rhus* laccase. *J. Am. Chem. Soc.* **98,** 1029–1031.

Southan, C. and Kruse, L. I. (1989) Sequence similarity between dopamine-$\beta$-hydroxylase and peptide $\alpha$-amidating enzyme: evidence for a conserved catalytic domain. *FEBS. Lett.* **255,** 116–120.

Stewart, L. C. and Klinman, J. P. (1987) Characterization of alternate reductant binding and electron transfer in the dopamine-$\beta$-monooxygenase reaction. *Biochemistry* **26,** 5302–5309.

Stewart, L. C. and Klinman, J. P. (1988) Dopamine-$\beta$-hydroxylase of adrenal chromaffin granules: structure and function. *Annu. Rev. Biochem.* **57,** 551–592.

Stoffers, D. A., Green, C. B. and Eipper, B. A. (1989) Alternative m-RNA splicing generates multiple forms of peptidyl-glycine $\alpha$-amidating monooxygenase in rat atrium. *Proc. Natl. Acad. Sci. U.S.A.* **86,** 735–739.

Stoffers, D. A., Ouafik, L. H. and Eipper, B. A. (1991) Characterization of novel mRNAs encoding enzymes involved in peptide $\alpha$-amidation. *J. Biol. Chem.* **266,** 1701–1707.

Strange, R. W., Blackburn, N. J., Knowles, P. F. and Hasnain, S. S. (1987) X-ray absorption spectroscopy of metal–histidine coordination in metalloproteins. Exact simulation of the EXAFS of tetrakis(imidazole)copper(II) nitrate and other copper–imidazole complexes by the use of a multiple-scattering treatment. *J. Am. Chem. Soc.* **109,** 7157–7162.

Tian, G. and Klinman, J. P. (1993) Discrimination between $^{16}O$ and $^{18}O$ in oxygen binding to the reversible oxygen carriers hemoglobin, myoglobin, hemerythrin, and hemocyanin: a new probe for oxygen binding and reductive activation by proteins. *J. Am. Chem. Soc.* **115,** 8891–8897.

Tian, G., Berry, J. A. and Klinman, J. P. (1994) Oxygen-18 kinetic isotope effects in the dopamine $\beta$-monooxygenase reaction: evidence for a new chemical mechanism in non-heme metallomonooxygenases. *Biochemistry* **33,** 226–234.

Toth, A., Floriani, C., Pasquali, M., Chiesi-Villa, A., Gaetani-Manfredotti, A. and Gaustini, C. (1985) Reaction of copper(I)-*N,N'*-ethylenebis(benzaldimine) complexes with carbon monoxide and isocyanides. *Inorg. Chem.* **24,** 648–653.

Toth, A., Floriani, C., Chiesi-Villa, A. and Gaustini, C. (1987) Dinucler copper(I) benzoato complexes binding isocyanides and azo compounds. *Inorg. Chem.* **26,** 236–241.

Toth, A., Floriani, C., Chiesi-Villa, A. and Gaustini, C. (1988) Structurally diversified neutral copper(I) isocyanide complexes: mono- and bi-nuclear complexes from the reaction of copper(I) halides with *p*-tolyl isocyanides. *J. Chem. Soc. Dalton Trans.* 1599–1605.

van der Deen, H. and Hoving, H. (1979) The binuclear cupric center of cancer magistrate methemocyanin. *Biophys. Chem.* **9,** 169–179.

Villafranca, J. J. (1981) Dopamine-$\beta$-hydroxylase. In *Metal Ions in Biology* (Spiro, T. G., Ed.), John Wiley & Sons, New York, pp. 263–289.

Volbeda, A. and Hol, W. G. J. (1989) Crystal structure of hexameric hemocyanin from *Panulirus interruptus* refined at 3.2 Å resolution. *J. Mol. Biol.* **209,** 249–279.

Woolery, G. L., Powers, L., Winkler, M., Solomon, E. I., Lerch, K. and Spiro, T. G. (1984) Extended X-ray absorption fine structure study of the coupled binuclear copper active site of tyrosinase from *Neurospora crassa*. *Biochim. Biophys. Acta* **788,** 155–161.

Yonekura, H., Anzai, T., Kato, I., Furuya, Y., Shizuta, S., Takasawa, S. and Okamoto, H. (1996) Identification of the five essential histidine residues for peptidylglycine monooxygenase. *Biochem. Biophys. Res. Commun.* **218,** 495–499.

Zabriskie, T. M., Cheng, H. and Vederas, J. C. (1991) Incorporation of aerobic oxygen into the hydroxyglycyl intermediate during formation of C-terminal peptide amides by peptidylglycine $\alpha$-amidating monooxygenase (PAM). *J. Chem. Soc. Chem. Commun.* 571–572.

Zolla, L. and Brunori, M. (1983) A spectrophotometric method to determine the amount of CO bound to hemocyanin. *Anal. Biochem.* **133,** 465–469.

Zolla, L., Calabrese, L. and Brunori, M. (1984) Distribution of copper atoms and binding of carbon monoxide in partially copper-depleted hemocyanin. *Biochim. Biophys. Acta* **788,** 206–213.

## BIOGRAPHICAL SKETCH

Francis C. Rhames was born on July 17, 1970, in Pontiac, Michigan. He received his Bachelor of Arts degree in Chemistry from Kalamazoo College in 1992. In September of 1992, he began work on his Ph.D. at the Oregon Graduate Institute of Science and Technology under the direction of Dr. Ninian J. Blackburn. Following successful defense of his dissertation in 1999, he accepted a position as Research Fellow in the Department of Biological Chemistry, University of Michigan, Ann Arbor.